Development of Small Scale Alcohol Biofuel Cells using Enzymes as Catalyst

A Thesis

Submitted by

PRIYANKI DAS

For the award of the degree

of

Doctor of Philosophy

School of Energy Science and Engineering

Indian Institute of Technology Guwahati

Guwahati-781039, Assam, India

November, 2021

Dedicated to my most precious possession-
My family

INDIAN INSTITUTE OF TECHNOLOGY GUWAHATI
School of Energy Science and Engineering
Guwahati – 781039

STATEMENT

I do hereby declare that the matter embodied in this thesis entitled "**Development of Small Scale Alcohol Biofuel Cells using Enzymes as Catalyst**" is the result of investigations carried out by me in the School of Energy Science and Engineering, Indian Institute of Technology Guwahati, Assam, India, under the guidance of **Prof. Pranab Goswami**.

In keeping with the general practice of reporting scientific observations, due acknowledgements have been made wherever the work described is based on the findings of other investigators.

November, 2021 Priyanki Das

INDIAN INSTITUTE OF TECHNOLOGY GUWAHATI
School of Energy Science and Engineering
Guwahati – 781039, Assam, India

Dr. Pranab Goswami
Professor (Higher academic grade)

Tel: +91-(0)361 2582202
Fax: +91-(0)361 2582249/2690762
Email: pgoswami@iitg.ac.in

CERTIFICATE

It is certified that the work described in this thesis, entitled "**Development of Small Scale Alcohol Biofuel Cells using Enzymes as Catalyst**", done by **Ms. Priyanki Das (**Roll No. 14651005**)** for the award of degree of Doctor of Philosophy is an authentic record of the results obtained from the research work carried out under my supervision in the School of Energy Science and Engineering, Indian Institute of Technology Guwahati, India.

The results embodied in this thesis have not been submitted to any other University or Institute for the award of any degree.

November, 2021

Prof Pranab Goswami

(Thesis supervisor)

Acknowledgement

Taking the opportunity of this column, I would like to express my sincere gratitude to all those who directly or indirectly helped me in successful completion of my PhD. First of all, I am thankful to Indian Institute of Technology Guwahati for giving me the opportunity to carry out Ph.D. in this esteemed Institute and providing me the financial support.

With immense pleasure, I would like to extend my deepest gratitude and indebtedness towards my PhD supervisor ***Prof. Pranab Goswami,*** *Department of Biosciences and Bioengineering and School of Energy Science and Engineering, IIT Guwahati for his enthusiastic guidance, constant encouragement and countless help throughout the period of my research work and preparation of the thesis. I would also like to thank him for the well-equipped laboratory, vast resources and dedicated work culture that has made working in this laboratory a pleasant experience.*

I would also like to extend my gratitude towards my doctoral committee members, ***Prof. K. Pakshiranjan (Chairperson)****,* ***Prof. Amaresh Dalal*** *and* ***Dr. S.P. Kanaujia*** *for their critical assessments and valuable suggestions during the course of my thesis work.*

I would like to express my sincere gratitude to former and present HoC of the School of Energy Science and Engineering, IIT Guwahati. I also would like to extend my appreciation towards ***Dr. Lepakshi Barbora*** *for her valuable suggestions,* ***Prof. Eduardo Corton*** *for his thoughtful active discussions during his visit as guest faculty to School of Energy Science and Engineering, IITG, from Argentina and also grateful to all the faculty members, office staff of School of Energy Science and Engineering for their inestimable support and help.*

I would like to thank Centre for excellence facility of Department of Biosciences and Bioengineering, Central Instruments Facility, Chemical Engineering, Physics, IIT Guwahati for providing the access to various instruments without which this study would not be feasible.

I would like to give my warm thanks to my seniors ***Dr. Madhuri Das****,* ***Dr Santhosh M****,* ***Dr. Seraj Ahmed****,* ***Dr. S.S Reddy****,* ***Dr. Mitun Chakraborty, Dr. Mrinal Sarma,, Dr. Ankana***

***Kakoty**, **Dr. Priyamvada Jain**, **Dr. Babina Chakma**, **Dr. Sharbani Kaushik**, **Dr. Naveen Singh**, **Dr Lightson**, **Dr. Sudarshan**, **Dr. Bahaa El-Din Ahmed Mohamed Hemdan** for their inspired support at the time of my acclimatization in the lab and guidance in learning various experimental techniques. I would like to mention my special thanks to my amazing fellow lab members **Phurpa**, **Arup**, **Vinay**, **Abdul**, **Smita**, **Aparupa**, **Priyalakshmi**, **Caraline**, **Pooja**, **Nabajyoti**, **Malaya**, **Rashmi ba**, **Rupam**, **Sanjay**, **Lekhashree**, **Roshika**, **Reshmi**, **Nishu**, **Ankit**, **Sunandan, Torsha** who have shared their struggles so intimately and trusted my assistance in their various endeavors.*

*Most of all, I express my profound debt to my family members, my late father, my mother and my sister who kept on encouraging me to pursue this path. Special thanks to my husband **Mr. Biman Das** and my in-laws for supporting and showing great patience while I pursued my PhD. Their unconditional love, encouragement, sacrifices, and faith in my capabilities had always kept me going and made me fulfil this journey.*

Above all, I thank God for his blessings bestowed upon me to complete this thesis.

Priyanki Das

November, 2021

Table of Contents

Abstract i

List of Abbreviations iv

List of Symbols viii

List of Figures and Schemes ix

List of Tables xv

CHAPTER I

1. Introduction and Literature Review 1

1.1. Enzymatic fuel cell: a highlight on the basic principle and operation 4

1.1.1. Electron transfer mechanism in enzyme-based bioelectrode 11

1.1.2. Techniques to characterize electron transfer in enzyme-bioelectrode 13

1.1.3. Challenges on electron transfer in enzyme-bioelectrode 15

1.2. Materials, platforms and techniques for developing EFC bioelectrode 16

1.2.1. Material for developing bioelectrode 16

1.2.2. Enzymes for bioelectrode development 19

1.2.3. Techniques for enzyme immobilization on electrodes 22

1.3. Fuel for EFC 25

1.4. Development of small scale EFC 27

1.5. Approach for the improving EFC voltage 34

1.5.1. Stacking of EFC 34

1.5.2 Employment of external boost converter 35

1.6. Self- powered EFC 35

1.7. Key areas and scope 36

1.8. Objectives of the present study 39

CHAPTER II

2. Development of Conductive Ink for Fabrication of Enzyme Electrodes 42

2.1. Overview 42

2.2. Experimental approaches 45

2.2.1. Reagents and stock solutions 45

2.2.2. Extraction of silk fibroin and silk sericin 45

2.2.3. Preparation of conductive ink 46

2.2.4. Characterization of the prepared inks 46

2.2.5. Characterization of the secondary structure of protein 48

2.3. Results and discussion 48

2.3.1. Characterization of the ink 48

2.3.1.1 Conductivity measurement 48

2.3.1.2. Aqueous stability of the conductive inks 49

2.3.1.3. Thermal characterization of conductive ink 50

2.3.1.4. Crystallinity of the conductive ink 50

2.3.1.5. Viscosity of the graphite-PEG-sericin ink 51

2.3.2. Secondary structures of the protein 51

2.4. Conclusions 52

Figures 53

Table 59

CHAPTER III

3. Fabrication and Characterization of Laccase-based Bioelectrode

3.1. Overview 60

3.2 Experimental approaches 63

3.2.1. Reagents and stock solutions 63

3.2.2. Apparatus and measurements 63

3.2.3. Preparation of bioelectrode 64

3.3. Results and discussion 65

3.3.1. Morphological characterization of the bioelectrode 65
3.3.2. Electrochemical characterization of the bioelectrode 65
3.3.3. Electrochemical response of laccase bioelectrode to pyrocatechol 69
3.3.4. Analytical performance of the laccase bioelectrode for pyrocatechol determination 70
3.3.5. Operational stability, storage stability and reproducibility of the bioelectrode 71
3.3.6. Interference study 72
3.4. Conclusions 73
Figures 74
Table 82

CHAPTER IV

4. Development of a Paper-based Enzymatic Biofuel Cell for Alcohol Sensing Application

4.1. Overview 83
4.2. Experimental approaches 85
4.2.1. Reagents 85
4.2.2. Fabrication of paper-based EFC (pEFC) device 86
4.2.3. Apparatus and measurements 88
4.2.4. Operating principle of the pEFC device in sensing methanol 89
4.3. Results and Discussions 90
4.3.1. Morphological characterization of pEFC 90
4.3.2. Response analysis of the pEFC 90
4.3.3. Interference study 91
4.4. Conclusions 92
Figures 92

CHAPTER V

5. Development of Methanol Biofuel Cell through Passive Fuel Delivery Facility in the Anode chamber

5.1. Overview 96
5.2. Experimental approaches 101

5.2.1. Reagents 101
5.2.2. Enzyme assay 101
5.2.3. Spectroscopic measurement 102
5.2.4. Synthesis of Fe_3O_4 (magnetite) nanoparticles (MNps) 102
5.2.5. Characterization of MNp 102
5.2.6. Fabrication of bioelectrodes for EFC 103
5.2.7. Characterization of Bioelectrodes 104
5.2.8. Fabrication of self-pumping EFC 105
5.2.9. Operation of self-pumping EFC 106
5.2.10. Docking study 107
5.2.11 Statistical analysis of data 108
5.3. Results and discussion 108
5.3.1. Development of enzyme bioelectrodes for EFC 108
5.3.2. Development of EFC with fuel self-pumping facility 110
5.3.3. Power and stability of the stacked EFCs 113
5.3.4. Role of AOx on the operational stability of the EFC 114
5.4. Conclusions 116
Figures 118
Tables 129
Conclusions and Scope for Future Research 131
Bibliography 135
List of Publications and Award 159

Abstract

The major objective of the present study is to develop small-scale alcohol fuel-based enzymatic biofuel cells (EFCs) for power generation and alcohol biosensing applications using alcohol oxidase (AOx) as anodic catalyst. One of the key approaches we propose to develop the small-scale EFCs is to exclude external pumping system from fabricating the devices. To make the idea effective, we introduce natural cellulosic materials (cotton or papers) in the device fabrications to deliver the fuel to the bioanode through passive diffusion activity. An additional important objective of the present work is to develop a biocompatible conductive ink with high aqueous stability for fabrication of the bioelectrodes, as these are vital properties of an ink to harvest stable bioelectrocatalytic function of the redox enzymes on the electrode surfaces. We studied some biopolymers and eventually identified silk-sericin and polyethylene glycol (PEG) as suitable materials for developing a graphite-based conductive ink in a ratio of 0.03:2.0:1.0 for sericin:PEG:graphite. Interestingly, sericin facilitates transformation of amorphous graphite powder to a crystalline form in PEG environment that improved the conductivity of the ink (11.2 $mS.cm^{-1}$) by 5.6-folds from the ink devoid of sericin. The viscosity and shear rate values of the ink were calculated as 0.11 Pa.s and $100s^{-1}$, respectively, thermos-stability up to 100 ^{0}C, and heat of formation (ΔH_f) -4.204 KJ/g. In addition, the ink coated over paper surface retains high aqueous stability and the reason being recognized as the enhancement of β–sheets content of sericin by 2.8% upon mixing it with PEG. Then we moved towards the selection of a cathodic enzyme and used laccase for the same. The laccase enzyme, which is extracted from *Tramates versicolor* fungi, can oxidize phenolic compounds with concomitant reduction of molecular oxygen to water. Laccase was immobilized on a glassy carbon electrode using a nanocomposite matrix comprising of osmium tetroxide on poly 4-vinylpyridine, multiwalled carbon nanotubes,

nafion and carbon black. SEM images revealed that the nanocomposite matrix provides a porous structure for easy immobilization of the enzyme. Whereas cyclic voltammetry studies explained that, the nanocomposite matrix offers a highly electroactive surface for facile diffusion-free electron transfer kinetics. The response of the bioelectrode for oxygen substrate at the determined formal potential of laccase was established. The heterogeneous electron transfer rate constant (k_s) and surface concentration of the ionic species (Γ) of the bioelectrode were discerned as $0.67 s^{-1}$ and 1.32×10^{-8} mol.cm^{-2}, respectively. The results infer the potential application of the constructed bioelectrode as oxygen breathed biocathode for EFC application. This bioelectrode also offers a reliable electrochemical response towards pyrocatechol in a biocatalytic mode. The response of the fabricated biosensor was generated at a potential of 0.14 V from the electrocatalyzed reduction of 1, 2-benzoquinone formed from the biocatalyzed oxidation of pyrocatechol. The bioelectrode showed a linear range of output current against pyrocatechol in the concentration range of 3.98 nM-16.71 nM with a minimum detection limit of 2.82 nM and a sensitivity of 3.82 ± 0.31 nA nM^{-1}. After working on cathodic enzyme, we focus on developing a small sized EFC utilizing paper (pEFC) as support material for methanol biosensing application. We used the as prepared Graphite-PEG-Sericin conductive ink for making support electrode for enzymes on chromatographic paper surface. To this end, we immobilized AOx on anode, and bilirubin oxidase (BOx) instead of laccase on cathode. It may be mentioned that due to incompatibility of laccase in physiological pH, we later replaced this enzyme with BOx, which exhibits high activity in the pH value. The sensor showed a linear range of output current of 0.03125μM -0.5μM (R^2 = 0.9988), sensitivity of 0.66245 μAμM^{-1} and a detection limit of 0.022 μM for methanol validating the potential of the pEFC for methanol biosensing application. Next, we report a methanol-fueled pure EFC fabricated by using AOx and BOx as anodic and cathodic catalysts, respectively with a focus on power generation. Here, we have fabricated EFC with

a new design strategy comprising a passive fuel pumping facility to the anode, efficient anoxic conditions in the anodic chamber and adequate airflow to the cathode for enhancing oxygen reduction reactions, and a connected storage tank for fuel. A bio-nanocomposite paste comprising of the as prepared Graphite-PEG-Sericin ink with magnetic nanoparticle over the supporting carbon cloth electrode was used as the biocompatible enzyme immobilization matrix for harvesting electron in the EFC through direct electron transfer mechanism. The open circuit potential of the device increased to 4.3-fold (3.1V) upon stacking six units of the EFCs in series. The device also rested at a stable state under a light emitting diode as load with a half-life of 372 days (w.r.t voltage) and a coulombic efficiency of 60%. This exceptional high operational stability has been accredited to the efficient anoxic setup in the anodic chamber that supported the stability of AOx, the activity of which was intact even after 49 days of the operation. This work also validated that the prolonged interaction of molecular oxygen with AOx significantly inactivates it without affecting the structural integrity of the enzyme protein. This EFC with improved design and functions is a step forward for achieving practical application as a standalone power supply to small-scale devices.

List of Abbreviations

AAO	Aromatic alcohol oxidase
ADH	Alcohol dehydrogenase
ADP	Adenosine diphosphate
$AgNO_3$	Silver nitrate
AgNP	Silver nanoparticle
AKD	Alkyl ketene dimer
ANOVA	Analysis of variance
AOx	Alcohol oxidase
AuNP	Gold nanoparticle
BET	Brunauer Emmett Teller
BFC	Biological fuel cell
BOx	Bilirubin oxidase
CB	Carbon black
CC	Carbon cloth
CD	Circular Dichroism
CE	Coulombic efficiency
CLEA	Cross-linked enzyme aggregate
CNT	Carbon nanotube
CS	Chitosan
CV	Cyclic voltammetry
DC	Direct current
DET	Direct electron transfer
DL	Detection limit
DPV	Differential pulse voltammetry

DSC	Differential scanning calorimetry
EFC	Enzymatic fuel cell
ET	Electron-transfer
EPR	Electron paramagnetic resonance
ETM	Electron transfer mediators
FAD	Flavin adenine dinucleotide
FESEM	Field emission scanning electron microscope
FETEM	Field emission transmission electron microscope
GCE	Glassy carbon electrode
GDH	Glucose dehydrogenase
GMC	Glucose-methanol-choline
GO	Graphene oxide
GOx	Glucose oxidase
H_2O_2	Hydrogen peroxide
HPLC	High Performance Liquid Chromatography
HRP	Horseradish peroxidase
HRTEM	High-resolution transmission electron microscopy
IUPAC	International Union of Pure and Applied Chemistry
LCAO	Long chain alcohol oxidase
LED	Light emitting diode
LiBr	Lithium bromide
MEA	Membrane electrode assembly
MET	Mediated electron transfer
MFC	Microbial fuel cells
$MgSO_4$	Magnesium sulphate

MNP	Magnetic nanoparticles
MWCNT	Multiwalled carbon nanotube
NADH	Nicotinamide adenine dinucleotide hydrogen
NADPH	Nicotinamide adenine dinucleotide phosphate
NaF	Sodium fluoride
NaN_3	Sodium azide
NP	Nanocomposite paste
Np	Nanoparticles
Nf	Nafion
OCP	Open-circuit potential
OsO_4 on P4VP	Osmium tetroxide on poly-4(vinyl pyridine)
OTFT	Organic thin film transistor
PANI	Polyaniline
PDMS	Polydimethylsiloxane
PEG	Polyethylene glycol
PoC	Point of care
PoN	Point of need
PTFE	Polytetrafluoroethylene
PtNP	Platinum nanoparticle
PVA	Polyvinyl alcohol
PVP	Poly (vinyl pyrrolidone)
rGO	Reduced graphene oxide
RT	Room temperature
SAM	Self-assembled monolayer
SAO	Secondary alcohol oxidase

SC	Selectivity coefficient
SCAO	Short chain alcohol oxidase
SD	Standard deviation
SEM	Scanning electron microscope
TGA	Thermo-gravimetric analysis
TTF	Tetrathiafulvalene
VSM	Vibrating Sample Magnetometer
XRD	X-ray powder diffractometer
$ZnSO_4$	Zinc sulphate

List of Symbols

E_{emf}	Electromotive force
ΔG_r	Gibbs free energy
η_{act}	Activation overpotential
λ	Reorganization energy
η_{conc}	Concentration overpotential
ΔH_f	Heat of formation
K_m	Michaelis-Menten constant
$t_{1/2}$	Half life
R	Thermodynamic gas constant
E_E	Energy efficiency
n	Number of electron
E_{pa}	Anodic peak potential
E_{pc}	Cathodic peak potential
F	Faraday constant
I_{SC}	Short circuit current
V_{OC}	Open circuit potential
F_f	Fill factor
I_{pa}	Anodic peak current
I_{pc}	Cathodic peak current
υ	Potential scan rate
Γ	Surface concentration of the ionic species
α	Charge transfer coefficient
k_s	Heterogenous electron transfer rate constant
V_{max}	Maximum velocity
Ω	Ohm
σ	Conductivity
ρ	Resistivity
S	Siemens

List of Figures and Schemes

Figure/Scheme No	Figure/Scheme caption	Page No.
Scheme 1.1:	General configuration of the typical biosensor (Kuri et al., 2021)	**4**
Figure 1.1:	Schematic diagram of a typical EFC consisting of a bioanode, a biocathode, and a partitioning membrane	**5**
Figure 1.2	Typical variations of the cell voltage and power of an operating fuel cell with current density. The major losses of cell voltage and the approximate ranges of current density in which they occur are indicated	**7**
Figure 1.3	Tafel plot for calculation of current density	**10**
Figure 1.4	EFCs based on paper material. (A) Anodes and cathodes are separated by a dialysis membrane (Jenkins et al., 2012), (B) electrodes are screen-printed on both side of a Japanese paper (Shitanda et al., 2013), (C) electrodes are screen-printed on the same side of the paper with a hydrophilic channel acting as membrane (Wu et al., 2013a), (D) air-breathing cathode (Ciniciato et al., 2012) and (Ea) single or (Eb) stacked fan-like biofuel cell painted on two-face of a Whatman paper (Villarrubia et al., 2014).	**32**
Scheme 2.1	Schematic of the silk fibroin and silk sericin extraction procedure	**46**
Figure 2.1	Conductivity versus time graph of various graphite conductive inks	**53**

Figure 2.2	Images of the conductive traces over paper substrate made from Graphite-PEG, Graphite-PEG-Chitosan, Graphite-PEG-Sericin and Graphite-PEG-Fibroin conductive inks before and after incubation with water.	**54**
Figure 2.3	Differential scanning calorimetry (DSC) and thermo-gravimetric analysis (TGA)	**54**
Figure 2.4	First derivative of DSC	**55**
Figure 2.5	Complex peak graph of DSC of GPS	**56**
Figure 2.6	X-ray powder diffractometer (XRD) pattern of (A) graphite, sericin and graphite-sericin composite powder and (B) PEG, graphite-PEG and graphite-PEG-sericin composite powder.	**57**
Figure 2.7	Viscosity of the GPS ink as a function of time	**58**
Figure 2.8	The Far-UV CD spectra of silk sericin (0.01 %), sericin-PEG composite	**58**
Scheme. 3.1	Schematic representation of laccase catalyzed oxidation of pyrocatechol with its subsequent electrochemical reduction on the bioelectrode.	**71**
Figure 3.1	SEM images of (A) GCE, (B) GCE/MWCNT–CB–Nf, (C) GCE/MWCNT–CB–Nf–OsO4–P4VP and (D) GCE/MWCNT–CB–Nf–OsO4–P4VP–laccase	**74**
Figure 3.2	(A) CV of (a) GCE (—), (b) GCE/MWCNT–CB–Nf (- -), (c) GCE/MWCNT–CB–Nf–OsO4–P4VP (–··–··), (d) GCE/MWCNT–CB–Nf–OsO4–P4VP–laccase (····), in oxygen gas purged solution of 0.1 M sodium citrate buffer (pH 4.7) at a scan rate of 50 mV/s.	**75**

	(B) CV of GCE/MWCNT–CB–Nf–OsO_4–P4VP–laccase electrode with (a) argon (—), (b) oxygen (–··–··–), and (c) pyrocatechol (- - -) in 0.1 M sodium citrate buffer (pH 4.7).	**76**
Figure 3.3	CV of laccase electrode with increasing scan rates viz. 30, 50, 70, 100, 200, 300, 400, 500, 600, 700 mV/s in 0.1 M sodium citrate buffer (pH 4.7) purged with O_2 (a) Plot of anodic (I_{pa}) and cathodic (I_{pc}) peak currents vs. scan rate (b) Plot of anodic (E_{pa}) and cathodic (E_{pc}) peak potentials vs. log(scan rate).	**77**
Figure 3.4	DPV of (a) GCE (····), (b) GCE–laccase (- - -), (c) GCE/MWCNT–CB–laccase (–··–··–), (d) GCE/OsO4P4VP–laccase (–·–·–) and (e) GCE/MWCNT–CB–Nf–OsO4–P4VP–laccase (—) in 16 nM pyrocatechol in 0.1 M sodium citrate buffer solution (pH 4.7). Inset: cathodic peak current values for bare GCE and different laccase bioelectrodes.	**78**
Figure 3.5	(A) DPV of laccase biosensor with increasing substrate concentration (nM): (a) 0, (b) 3.98, (c) 7.93, (d) 14.77, (e) 15.74, (f)16.71. (B) Response curve obtained for laccase biosensor for different concentrations of pyrocatechol in 0.1 M sodium citrate buffer (pH 4.7).	**79**
Figure 3.6	Operational stability of the laccase biosensor for substrate pyrocatechol	**80**
Figure 3.7	Effect of potential interfering agents on the laccase-based biosensor response.	**81**
Scheme 4.1	Fabrication process for alcohol/air EFC on paper	**88**

Scheme 4.2	Schematic diagram of operating principle of EFC-based alcohol sensor on paper platform	**89**
Figure 4.1	Schematic diagram of pEFC configuration, where 1 is Anode, 2 is Cathode; Surface area of Anode / Cathode: 1.13 cm^2	**92**
Figure 4.2	The reaction of alkyl and alkenyl ketene dimers with cellulose. Adapted From Li et al., (2009).	**93**
Figure 4.3	FESEM image of (A) blank filter paper; (B) AKD printed filter paper	**93**
Figure 4.4	A sessile drop of MQ water (2µl) applied to the surface of AKD coated filter paper	**93**
Figure 4.5	FESEM image of (A) blank filter paper (hydrophilic zone/channel); (B) graphite-PEG-sericin ink over filter paper; (C) AOx over graphite-PEG-sericin ink on filter paper (D) BOx over graphite-PEG-sericin ink on chromatography paper.	**94**
Figure 4.6	(A) Polarization curve with 0.5 µM methanol (B) Calibration curve for methanol detection plotted as output current vs. the concentration of methanol with a 150 kΩ resistor.	**95**
Scheme 5.1	Schematic diagram of central reactions of anode and cathode	**99**
Scheme 5.2	Schematic diagram of fabrication of CC-NP-AOx-CS bioanode and CC-NP-BOx-CS biocathode.	**104**
Figure 5.1.	Hysteresis loop of MNp by VSM	**118**

Figure 5.2.	TGA curve of MNp	**118**
Figure 5.3	Nitrogen adsorption-desorption isotherm for MNp	**119**
Figure 5.4	(A) TEM images of MNp (B) HRTEM of MNp (C) SAED (D) size distribution of MNp	**120**
Figure 5.5	FESEM image of (A) blank CC electrode (5 kX) with inset at 200X, (B) CC with hydrophilic paste (5 kX), (C) MNp-Nf layer over the hydrophilic paste on CC (5kX) with inset at 50 kX (D) AOx enzyme entrapped with chitosan over NP on CC (5 kX), (E) BOx enzyme entrapped with chitosan over NP on CC (5kX).	**121**
Figure 5.6.	CV of (a) CC-NP-AOx-CS bioanode without methanol, (b) CC-NP-AOx-CS bioanode with 2 µM methanol, (c) CC blank electrode in 0.1 M KPBS, pH 7.5.	**122**
Figure 5.7	Schematic diagram of the EFC set up fabricated with acrylic glass (lateral view).	**123**
Figure 5.8.	(A) Polarization curve of an EFC unit. (B) OCP of EFC with and without MNp	**124**
Figure 5.9.	(A) Picture of the series connected six EFC setup operated by using an LED (B) Voltage with respect to time of the stacked EFC after connecting to LED (C) Current with respect to time of the stacked EFC after connecting to LED (D) Power with respect to time of the stacked EFC after connecting to LED.	**125-127**
Figure 5.10	CD studies of AOx in aerobic and anoxic conditions	**128**

Figure 5.11 (A) Docked pdb structure obtained from Pymol, AOx with oxygen molecule (inset: Dimensions of the Docking area). (B) PLIP results window screen shot. (C) Tabulation of different binding poses obtained with their respective binding affinities **129**

List of Tables

Table No.	Table caption	Page No.
Table 2.1	Resistivity of conductive traces made by different inks	59
Table 3.1	Electron transfer kinetics and response characteristics of GCE/MWCNT-CB-Nf-MWCNT-OsO_4P4VP-laccase electrode	82
Table 5.1	Comparative account on the fill factors of some EFCs reported in the literature	129
Table 5.2	Enzyme activity study of AOx in aerobic and anoxic conditions	130

CHAPTER I

Introduction and Literature Review

CHAPTER I

Introduction and Literature Review

Currently, the global fuel demand is met mostly with the fossil fuels. These conventional fossil fuels are however, not environment friendly, as the process of their conversion to energy through the conventional technology has been contributing to the green house effect, elevating the atmospheric CO_2 levels steadily at an average pace of 2.3% (Coyle and Simmons, 2014). The International Energy Agency has issued certain directives to neutralize the detrimental effect to the globe, among which exploring energy efficient technology to generate clean energy from the renewable sources is a key recommendation (Mohtasham, 2015). Biological fuel cell (BFC)-based energy technology, in principle, has the potential to addresses the above-mentioned issue. The fuel cells, in general, are regarded as environmentally friendly technology that directly convert chemical energy into electrical one (Xiao et al., 2019). Normally, the conventional fuel

cells are energy efficient devices that utilize noble metals like platinum, palladium, ruthenium etc or their alloys as catalysts for the oxidation of fuels like hydrogen, methanol at the anode and the reduction of the oxidant like oxygen at the cathode. These noble metals are usually expensive and non-renewable. Moreover, most of the chemical fuel cells require electrolytes at extremes of pH and temperature, which poses a challenge to maintain a non-hazardous environment during their operation.

BFCs are a variant of chemical fuel cells employing renewable biological catalysts as well as renewable (mostly) fuel. These bioelectrochemical devices are normally operable at near-neutral pH and ambient temperature. In the broadest sense, BFCs can be defined as a device that are capable of converting chemical to electrical energy via electrochemical reactions involving biochemical pathways. Electrons produced by the enzymatic reactions from supplied fuel substrates are transferred to the anode (negative terminal) and flow to the cathode (positive terminal) linked by a conductive material containing a resistor, or operated under a load (i.e., producing electricity that runs a device). By convention, positive current flows from the positive to the negative terminal, a direction opposite to that of electron flow. The electrons that reach the cathode combine with protons that diffuse from the anode through a separator (or proton exchange membrane) and oxygen provided from the air and resulted in the production of water.

BFCs can be categorized mainly into Microbial fuel cells (MFCs) and Enzymatic BFCs (EFCs) depending on the types of biocatalysts being used to perform the catalysis. MFCs utilize whole living organisms as the source of complete enzyme pathways (Bullen et al., 2006). These cells are fabricated using a variety of materials, and involve diverse design configurations. A wide range of conditions such as differences in pH, temperature, electrode surface areas, electron acceptor, reactor size, and operation time are involved in

their operation (Logan et al., 2006). The microbial catalysts based BFCs normally have a long lifetime and are capable to oxidize the whole fuel organic matter into carbon dioxide. Conversely, they are limited by low power densities due to slow electron transfer across microbial cell membranes. On the other hand, EFCs use isolated enzyme proteins to perform specific reaction catalysis (Bullen et al., 2006). EFC typically possesses higher power densities (although still lower than conventional fuel cells), but can only partially oxidize the fuel and have limited lifetimes (typically 7–10 days) due to the fragile nature of the enzyme (Minteer et al., 2007). The third category of BFCs utilizes cellular organelles as electrode catalysts that, however, are still in a budding stage.

On the other hand, EFC as a biosensor device has certain advantages. The fuel cell-based biosensor is a stand-alone system, as unlike other electrochemical devices it does not require external power sources to drive the bioelectrocatalytic reaction to generate the electrical signal. In general, a biosensor is an analytical tool consisting of biologically active material used in close conjunction with a device that converts the biochemical signal into a quantifiable electrical signal (IUPAC definition). It consists of a bio-recognition element such as enzymes, antibodies, and whole cells for the specific detection of the target analyte in spatial contact to a transducer for converting the biochemical signal into an electrically manageable format through a signal processing unit (Scheme 1.1).

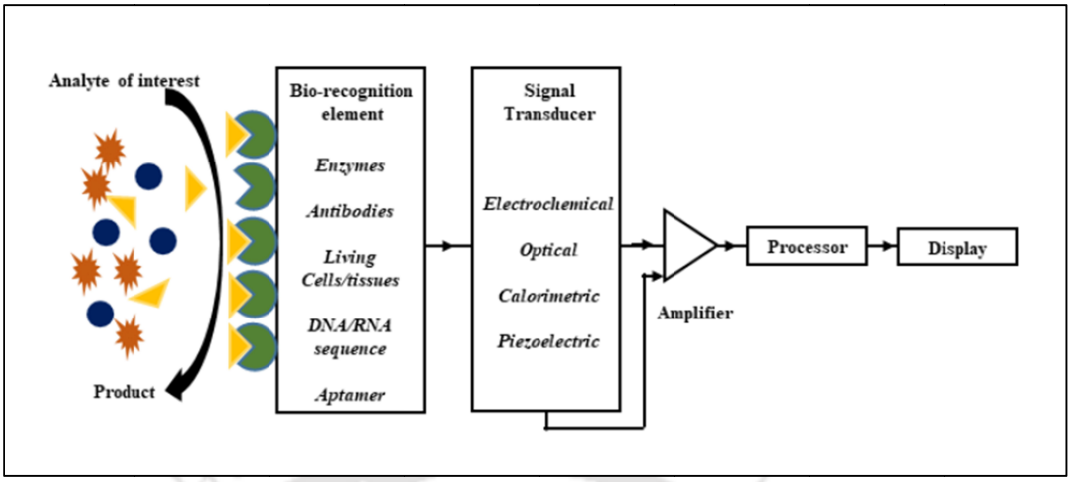

Scheme 1.1: General configuration of the typical biosensor (Kuri et al., 2021)

1.1. Enzymatic fuel cell: a highlight on the basic principle and operation:

EFC is emerging as a promising power source for powering micro-scale electronic devices in the field of biomedical, telecommunications, space, and environmental research (Das et al., 2014). Following the first EFC report by Yahiro and coworkers in 1964 (Yahiro et al., 1964), the progress in the field of EFC was however, not very encouraging until 1990s. The research interest on the EFCs however, resurrected since the beginning of the 1990s due to the growing demand for implantable medical devices in the field of healthcare such as continuous glucose monitoring, and pacemakers (Barton et al., 2004; Heller, 2004). The interest was also then fueled by the parallel growth of electronics, communication, and material sciences owing to their enormous impact on transforming these bio-based products to potential modern consumer technology. As an example, Sony had developed an enzymatic biobattery using sugar as the fuel to power a Walkman®, an mp3 player with speakers or a small remote-controlled car (Sakai et al., 2009).

EFCs have numerous advantages such as the catalysts are renewable (redox enzymes), which can be extracted from a wide range of living organisms. Further, a wide

range of renewable substrates such as sugars, hydrogen, alcohols, organic acids, and mixtures of these materials which can be digested by living organisms, can be used as fuels for EFCs. The operational conditions are very mild as the EFCs can be operated at room temperature, physiological pH, and ambient pressure. Additionally, the redox enzymes provide specificity towards their natural fuel substrates. Finally, the EFCs could be developed as a disposable device as most of its components could be constructed by using biodegradable, non-hazardous and non-toxic materials (Xiao et al., 2019). A typical scheme on EFC is shown in figure 1.1

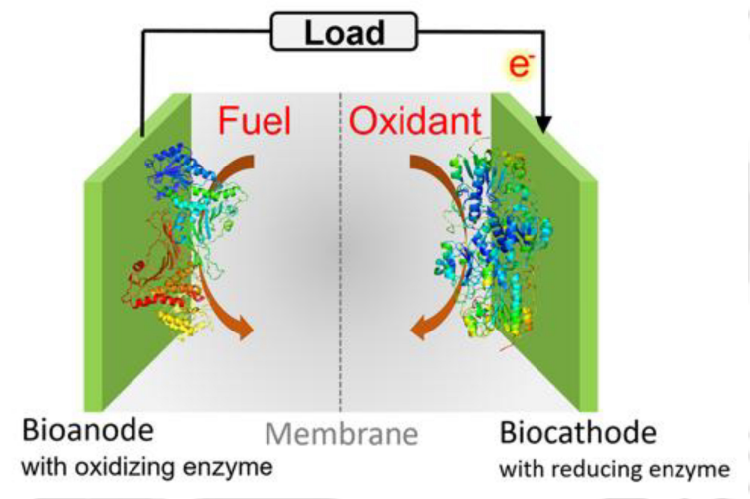

Figure 1.1: Schematic diagram of a typical EFC consisting of a bioanode, a biocathode, and a partitioning membrane (optional), (Xiao et al., 2019), Copyright 2019, reprinted with permission from ACS Publications.

Nevertheless, the EFCs also possess many shortcomings among which poor lifetime and low power density are widely described. The poor lifetime has been attributed to the low stability of the redox enzymes in a foreign environment, while the low power densities are mainly caused by a sluggish electron transfer rate between the enzyme and electrode (Kim

et al., 2006). The research over the last several decades could, however, made a significant stride in increasing the lifetime of enzymes by adapting their different immobilization strategies on solid surfaces (Minteer et al., 2007).

The fundamentals of the fuel cell can be protracted to EFC to evaluate its performance. As guided by the general principle, an EFC generates electricity when the electrode reactions are thermodynamically favorable (Logan et al., 2006). The concept may be defined by the following equation:

$$\Delta G_r = -E_{emf} \times nF \quad \text{.....1.1}$$

Where, ΔG_r (J) is the Gibbs free energy, nF is the charge transferred in the reaction with n representing the number of electrons per reaction mol, and F is Faraday's constant (9.64853×10^4 C.mol^{-1}). The electromotive force (E_{emf}) generated in the fuel cell is due to the difference between the cathodic (E_{cat}) and anodic (E_{an}) potential as shown below (Logan *et al*., 2006) and can be calculated from the Gibbs free energy change for the anodic and cathodic reactions (Osman et al., 2011).

$$E_{emf} = E_{cat} - E_{an} \quad \text{.....1.2}$$

Ideally, the cell voltage should be independent of the current drawn. However, in reality, this reversible cell voltage (E_{cell}) is not realized even under zero current conditions due to internal losses and fuel cross over during the operation of the cells. The cell voltage at zero current is termed as open-circuit potential (OCP). As current is drawn from the fuel cell (at varying load), the E_{cell} deviates from OCP as a result of the losses which are known as overpotential as depicted by the following equation (Logan *et al*., 2006).

$$E_{cell} = E_{emf} - (\Sigma_{\eta act} + \Sigma_{\eta conc} + IR_{\Omega}) \quad \text{.....1.3}$$

Where η_{act} is the activation overpotential, η_{conc} is concentration overpotential; I and R_{Ω} represent current and resistance (load), respectively.

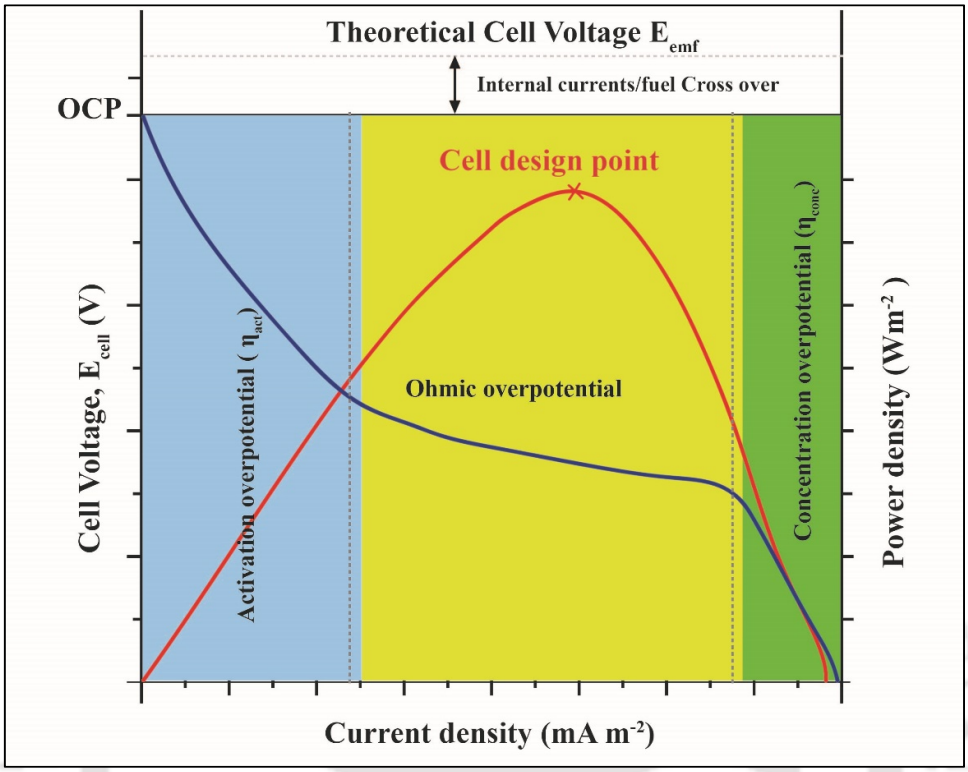

Figure 1.2: Typical variations of the cell voltage and power of an operating fuel cell with current density. The major losses of cell voltage and the approximate ranges of current density in which they occur are indicated.

The current generation pattern with respect to the external resistance can be explained by the polarization curve, which is plotted by considering the change in current density versus voltage (Mohan et al., 2014). Polarization graphs offer critical information about the influence of external and internal resistances involved in the functioning of the fuel cells. There are three distinctive regions at different current ranges (Figure 1.2):

a) At low currents, the dominating parameter is the activation (charge transfer) overpotential (η_{act}). These arise from the energy barrier to charge transfer, from the mediator or enzyme to the electrodes, and vise-versa. The charge transfer

overpotentials depend on the nature of the electrode materials and structure, reactant activities, performance of catalysts, electrochemical mediators, and operational conditions (Zhao et al., 2009). Activation losses can be reduced by improving the electrode catalysis, increasing the electrode surface area, and optimising the operating conditions (e.g. temperature and pH).

b) The ohmic overpotential (IR_{Ω}) is observed at the intermediate current regions. Ohmic losses are due to the resistance to charge transport through the various components in the cell, including contact resistances. They include both ionic and electronic resistances through the current collectors, electrolytes, membrane and electrodes, as well as the interfaces between these components (Osman et al., 2011). These overpotentials (separate for the two electrodes) can be approximated if expressions for the reaction rates are known, e.g. a Tafel's or Butler–Volmer's relation. To keep ohmic losses to a minimum, the membrane must possess a low resistance, the gap between the electrodes should be optimal and the components in the cells ought to be well contacted.

c) Concentration overpotential (η_{con}) is caused by resistance to mass transport, leading to large concentration gradients, at the interface between electrode surface region and bulk electrolyte prevalent at high current densities. They can be lowered by proper reactor design, mixing/aeration and hence reducing diffusion gradients.

The extractable power of a fuel cell (P_{cell}) is the product of the cell voltage (V_{cell}) and the cell current (I_{cell}), $P = V_{cell}$ (V) × I (A). The power density can be determined by normalizing the power with respect to the electrode cross-sectional area, electrode volume or the working volume of the anodic chamber. The resistance at which both the current and

voltage are optimum for the highest power output is called the cell design point (Mohan et al., 2014).

The overpotentials as discussed above can be analyzed separately for the two electrodes if the expressions for the reaction rates are known with the help of Butler–Volmer's and Tafel's relation. The charge transfer overpotentials are controlled by the rate of heterogeneous electron transfer, and the kinetics of this process is described by the Butler–Volmer equation (Zhao et al., 2009) when the reactants are abundant and the current is small enough that the ohmic and concentration overpotentials are negligible:

$$I = Ai_0\{e^{\left(\frac{\alpha nF\eta_{act,c}}{RT}\right)} - e^{\left(\frac{(1-\alpha)nF\eta_{act,a}}{RT}\right)}\} \quad \text{.....1.4}$$

Where I is the current, A is the electrode active surface area, a is the charge transfer barrier (symmetry coefficient), i_o is the exchange current density, n is the number of electrons involved in the electrode reaction, and η_{act} is the charge transfer overpotential (Zhao et al., 2009). The Butler–Volmer equation can be simplified in the high overpotential region (>118/n mV), yielding the Tafel equation (Zhao et al., 2009):

$$\eta_{act} = blog_{10}\left(\frac{i}{i_0}\right) \quad \text{.....1.5}$$

Where i is the current density and b is the Tafel slope, which is an important experimental parameter commonly used to probe the mechanism of an electrode reaction. Plots of overpotential against $log_{10}i$ are known as Tafel Plots (Figure 2.3); i_o and b are obtained by extrapolation of the linear region of the curve to η_{act} = 0 (Zhao et al., 2009). The activation overpotential can be limited by facilitating direct electron transfer to anode, increasing the reaction sites by increasing the surface area (Zhao et al., 2009).

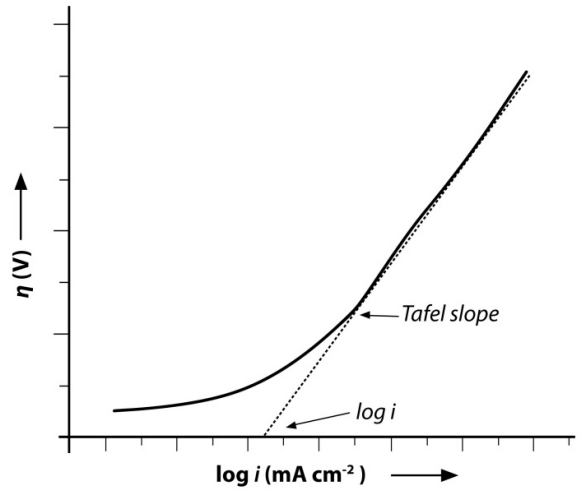

Figure 1.3: Tafel plot for calculation of current density

One of the most important performance parameters of an EFC is the coulombic efficiency, which is defined as the ratio of coulombs transferred from the substrate to the anode, to the theoretical maximum coulombs produced if all of the substrate is oxidized (×100%) (Liu et al., 2005). The coulombic efficiency (*CE*) of an EFC can be determined by integration of the area under the current–time curve (Liu et al., 2005) using the following equation:

$$CE = \frac{C_p}{C_{Ti}} \times 100\% \quad \text{.....1.6}$$

Where C_p is the total coulombs calculated by integrating the current over time.

Again, $C_{Ti} = \frac{Fb_iS_iv}{M_i}$, where, F is Faraday's constant (96,485 C/mol.electrons), b_i is the number of moles of electrons produced per mole of the substrate, S_i is the substrate concentration, v is the volume of substrate used and M_i is the molecular weight of the substrate. The major causes of reduced coulombic efficiency are (a) the occurrence of alternative reactions that do not result in current production; (b) build-up of biomass; and (c) crossover of the substrate or mixing of the anodic and cathodic reagents, a particular

problem in membrane-less systems (Clauwaert et al., 2008). Another important parameter to assess the performance of an EFC is the overall energy recovery or energy efficiency (E_E). E_E can be calculated using the following equation:

$$E_E = \frac{E_P}{E_{Ti}} \times 100\% \quad \text{.....1.7}$$

Where, E_p (J), is the total energy calculated by integrating the power over time. E_{Ti} (J) is the theoretical amount of energy that can be produced from the substrate, calculated as, $E_{Ti} = \frac{\Delta H S_i v}{M_i}$; where ΔH is the enthalpy change of oxidation of the substrate (Liu et al., 2005).

1.1.1. Electron transfer mechanism in enzyme-based bioelectrode

The exchange of electrons between electrochemically active redox enzymes and the electrode is mostly dependent on the specific properties of the enzyme, such as accessibility of the active site, distance of the redox center from the protein surface, the nature of the redox cofactor, the innate protein stability and the mode of its immobilization on the electrode surface (Schmidt and Schuhmann, 1996). So, according to the type of electrical communication, redox enzymes can be categorized into three groups. The enzymes with their active site cofactors are poorly or weakly bound to the protein e.g. NADH, NADP-based enzymes, come under the first group. In these enzymes, the active site cofactors can diffuse out of the enzymes during the electron transfer processes. The next group comprises the enzymes (mostly peroxidase) where the active center is located at the periphery of the enzyme's protein matrix. These permit easy exchange of electrons with electrode due to the short electron tunneling distances. The third group of enzymes contains deeply buried active sites in the protein matrix, e.g. flavin adenine dinucleotide

(FAD) based enzymes (Heller, 1992). So, the transfer of electrons between redox enzyme and electrode is known to take place through either of the two mechanisms: mediated electron transfer (MET) or direct electron transfer (DET) (Barton et al., 2004). In MET, paring of electrons between the redox active centers of the enzyme and the electrode takes place through some specialized small electroactive molecules. These specialized molecules are termed as 'electron transfer mediators' (ETM), which shuttles electrons between the redox center of the enzyme and the electrode. Conversely, the DET mechanism involves direct electrical communication between the redox centre of the enzyme and the electrode.

The feasibility of electron exchange between the redox centers of proteins and the electrodes may be elucidated by the electron-transfer (ET) theory of Marcus (Marcus and Sutin, 1985). The ET rate constant (K_{ET}) between a donor and acceptor couple is given by Eq. (2.8), where, d and $d°$ are the distance separating the electron and donor, and the van der Waals distance, respectively, β is the electron-coupling constant and $\Delta G°$ and λ are the free energy change and the reorganization energy associated with the electron-transfer process, respectively

$$K_{ET}\ \alpha \exp[-\beta(d-d^0)]\,.\exp[-\frac{(\Delta G^0+\lambda)^2}{4RT\lambda}] \quad \text{.....1.8}$$

Hence, the electron exchange between two redox sites depends basically on three factors: the reorganization energy qualitatively signifying the conformational rigidity of the redox compound in its oxidized and reduced form, the potential difference between the involved redox entities (as, $\Delta G^0 = \sim -nF\eta$, where, overpotential $\eta = E - E^0$, E and E^0 are applied and standard potential, respectively), and separation between the redox sites (Das et al., 2016).

1.1.2. Techniques to characterize electron transfer in enzyme-bioelectrode

The formal redox potentials, detection of chemical reactions that precede or follow the electrochemical reaction, and evaluation of electron transfer (*ET*) kinetics are usually measured by a powerful electrochemical technique, known as cyclic voltammetry (CV). CV is usually carried out with working electrodes at different potential scan rates (υ) to obtain *ET* parameters. At first, the redox potentials, anodic potential (E_{pa}) and cathodic potential (E_{pc}) of the fabricated working bioelectrode are determined in an argon-saturated buffer solution at a fixed scan rate (for example: υ = 50 mVs^{-1}). If the peak separation (ΔE_P) is > 59 mV, which is more than the peak separation of a reversible process (59 mV), represents a quasi-reversible redox process (Scott and Lukehart 2007). Additionally, with the increase in scan rate, if the anodic (E_{pa}) and cathodic (E_{pc}) peak potentials shift to more positive and more negative values respectively increasing the ΔE_p, further suggests a quasi-reversible process. Besides this, if the magnitudes of anodic (I_{pa}) and cathodic (I_{pc}) peak currents increased linearly with increasing scan rate the phenomenon is described as a surface confined redox process and indicates a thin-layer electrochemical behavior (Scott and Lukehart 2007). For a quasi-reversible wave, the relationship between peak potential and scan rate conforms to the following equation (Laviron, 1974):

$$E_P = E^0 + \frac{RT}{\alpha nf} - \frac{RT ln\vartheta}{\alpha nf} \quad \text{.....1.9}$$

Where E_p is the peak potential (cathodic or anodic), E^0 is the apparent standard potential, R is the thermodynamic gas constant (8.314 $J\ K^{-1}\ mol^{-1}$), F is the Faraday constant (96,500 $C\ mol^{-1}$) and T is the temperature (298 K). The symbols n and υ are the electron transfer number and scan rate, respectively. The value of charge transfer coefficient (α) can be

determined from equation 2.10 by using the slopes from the linear plots of E_{pa} and E_{pc} versus log υ.

$$\alpha = \frac{\delta_{pa}}{\delta_{pa} - \delta_{pc}} \quad \text{.....1.10}$$

Where, δ_{pa} and δ_{pc} are the anodic and cathodic slopes of linear region of the plot. Again, slopes for the anodic and cathodic peaks can be calculated by using the following equations:

$$Anodic\ slope\ (\delta_{pa}) = \frac{2.3RT}{(1-\alpha)nF} \quad \text{.....1.11}$$

$$Cathodic\ slope\ (\delta_{pc}) = \frac{-2.3RT}{\alpha nf} \quad \text{.....1.12}$$

The symbols *F, R, T* have their usual meanings.

The surface concentration of the ionic species (Γ) (mol cm^{-2}) on working bioelectrode can be estimated from the plot of peak current versus scan rate (υ) using the Brown-Anson model that is based on the following equation (Laviron, 1979):

$$I_p = \frac{n^2F^2\Gamma A\vartheta}{4RT} \quad \text{.....1.13}$$

Where n is the number of electrons transferred, and A is the surface area of the electrode. The symbols *F, R* and *T* have their usual meanings. The heterogeneous electron transfer constant (k_s) of the bioelectrode could be obtained by the following equation (Laviron 1979):

$$\log(k_s) = \alpha\log(1-\alpha) + (1-\alpha)log\alpha - \log\left(\frac{RT}{nF\vartheta}\right) - \alpha(1-\alpha)\frac{nF\Delta E_p}{2.3RT} \quad \text{.....1.14}$$

Where (α) is the charge transfer coefficient and (k_s) is the heterogeneous electron transfer rate constant and *R, T, F* and *n* having their usual meaning. The magnitude of k_s designates the efficacy of the DET between the immobilized enzymes and the electronic unit. In CV the increasing height of the redox peak with increasing concentration of substrate entails the involvement of the DET principle in sensing the substrate of interest by the fabricated enzyme electrode (Kuri et al., 2021).

1.1.3. Challenges on electron transfer in enzyme-bioelectrode

The slow heterogeneous electron transfer in the enzyme–electrode interface and denaturation of enzymes outside their native environment are regarded as the major obstacles in developing enzyme-based bioelectrode. Marcus' theory (Marcus and Sutin, 1985) proposed that the kinetics of electron transfer between the electrode and the redox species is determined by the distance between them as revealed from the above elaborations. Due to the large gap between the prosthetic group of redox enzyme and the electrode surface and due to the shielding effect of a protein shell, the electron transfer through tunneling mechanism is rarely encountered (Gorton et al., 1999). Although the different fabrication strategies have been utilized for direct transfer of electrons as discussed in the following sections, the electrical contact efficiency (turn over rate of electrons) is usually significantly lower than the electron exchange rate between the redox center of the enzymes and their native electron acceptor or donors. Hence, there has been a constant effort made to improve the electrical communications between the enzyme and the base-electrode through different strategies and techniques that subsumed a major research activity on this enzyme-based electrochemical technology.

1.2. Materials, plateforms and techniques for developing EFC bioelectrode:

1.2.1. Material for developing bioelectrode:

The efficiency of the electrodes in terms of electron transfer kinetics, mass transport, stability and reproducibility is governed by the enzyme-electrode interactions, which in turn is influenced by the materials being used for fabricating the bioelectrode such as solid support, enzyme, electron transport mediator, and conductive support matrix (Osman et al., 2011). The immobilization of enzymes on the electro sensing surface is the vital step for fabricating enzyme bioelectrode. It is done with the help of an immobilizing matrix whose function is to hold the enzyme molecules on the electrode. The support matrix should possess good mechanical stability, rigidity and good flow properties for enzyme activity, and storage stability (Park et al., 2010). Further, it should be flexible to different pH, temperature, and chemical composition of the solvent, non-degradable and biocompatible (De Poulpiquet et al., 2014; Kim et al., 2006).

Incorporation of appropriate nanomaterials in the bioelectrode fabrication is known to enhance electron transfer kinetics between enzymes and the base electrodes (Zhang et al., 2021). Due to their high surface area, favorable electronic properties and electrocatalytic effect, the incorporation of nanomaterials in bioelectrodes generates larger electroactive surface area and linked bioelectrocatalytically active enzyme loading on the electrodes (Asefa et al. 2009; Kim et al. 2008). Moreover, many of these nanomaterials help in maintaining bioactivity of the biomolecules on their surface owing to their biocompatibility nature (Pingarron 2008). These properties of nanomaterials make them an attractive immobilization matrix for the fabrication of bioelectrode for EFCs. Carbon

nanotubes, graphene, metal nanoparticles (gold and platinum), composite material are among the most widely used nanomaterials in the area of biofuel cells. Nanoparticles (Np) alter the electrode surface and generate a microenvironment that may maintain the innate conformation of the redox proteins. Again, the conductive tunnels of many inorganic Np help to overcome the shielding effect of the protein shell on the charges (Das et al., 2016). The frequently used metal nanoparticles are gold Np (AuNp) (Gai et al., 2017); silver Np (AgNp) (Christwardana et al., 2018), and platinum Np (PtNp) (Sun et al., 2015). For the electrical wiring of the redox center and aligning the enzyme on the electrode surface, the AuNp acts as an electrical nano plug (Das et al., 2016). The condensation reaction between the amino group of enzymes and the carboxyl group of AuNps could be exploited for immobilization of the enzyme, which may significantly improve the electron transfer rate of the bioelectrode (Zhang et al., 2021). One more class of Nps worth mentioning for their applications in EFCs is the magnetic nanoparticles (MNps) such as hematite, ilmenite, and magnetite. MNps have required characteristics like high coercivity, super paramagnetism, a low level of toxicity and a low curie temperature (Sarma et al., 2018). Smaller sizes with an ideal particle size distribution are desirable for better catalytic activity of MNps for their utilization in EFC applications. Additionally, the MNps may be repeatedly used and applied to concentrate the conjugated enzymes (Safarıkova and Safarik 1999).

Recently, graphite and graphene have been extensively used as the substrate material for developing enzyme electrodes and using the former, a self-powered DET-based ethanol biosensor was constructed (Zhang et al., 2021). Graphene has high thermal conductivity (5000 $W.mK^{-1}$), high surface-to-volume ratio (2630 m^2g^{-1}), excellent electrical conductivity (1738 $Siemens.m^{-1}$), and biocompatibility. Low cost, ease of processing, high surface area, and safety are some of the benefits of graphene over CNTs.

The sensor devices with graphene materials possess better sensitivity and signal-to-noise ratio (Kaushik et al., 2021). A partially modified graphene, known as reduced graphene oxide (rGO) is also commonly used for the fabrication of electrode materials. This reduced form is normally prepared by the reduction of graphene oxide (GO). Owing to incomplete reduction, the rGO contains oxygen-containing functional groups, which offers the strong hydrophilic properties to the material. This property is suitable for the immobilization of biocatalysts over the rGO materials (Erickson et al., 2010; Kong et al., 2020) through various interactions, which is beneficial to improve the efficiency of electron transfer between biocatalyst and electrode surface (Zhang et al., 2021).

Two or more kinds of materials with different physical and chemical properties may be combined by physical or chemical methods resulting in the formation of composite materials. Recently, composite materials have been increasingly used in the construction of EFC. Among the composite materials, carbon materials with metal particles are extensively used. Zhang and his colleagues prepared a 3-D rGO/AuNps/nitrogen-doped carbon nanotube composite material with foamed nickel as the carrier to fabricate the anode of EFC (Zhang et al., 2017). Again, Campbell and his group (Campbell et al., 2015) prepared 3D graphene and CNTs gel composites, and immobilized glucose oxidase (GOx) and bilirubin oxidase (BOx) on the electrode surface to develop a membrane-less EFC. DET could be realized at both cathode and anode (Zhang et al., 2021)

Apart from the nanomaterials, conductive polymers are also widely used for the fabrication of enzyme electrodes. The conducting polymers are also termed “synthetic metals” since they mimic the electrical, electronic, magnetic and optical properties of metals. They are the resonance stabilized –conjugated organic polymers. The delocalized π

electrons, which furnish the highway for charge mobility along the backbone of the polymer chain, are the key factors for conductivity in conducting polymer. In addition to conductivity, these conductive polymers also possess controllable electrochemical properties, optical transparency, and flexibility in chemical structure, biocompatibility, and ion selectivity. Nafion (Nf), chitosan (CS), polypyrrole, polyaniline (PANI), polyphenol, polythiophene, poly-1,3-phenylenediamine, polyvinyl pyridine, polyvinyl alcohol, polycarbonate, osmium redox polymers, nylon are some of the examples of polymer (Sarma et al., 2009).

Conductive ink that can be patterned by screen-printing, inkjet printing, or direct writing method to form conductive tracks is a critical component for making printed electronic technology or paper electronics suitable for developing chip-based EFCs. Researchers are also paying more attention to direct writing methods, which can be applicable to most substrates where printing can't be achieved. Inks or pastes, consisting of solid conductive particles such as graphite powder, carbon nanotubes, metal particles and nanoparticles suspended in mixtures of solvents and additives, such as polymeric stabilizers, wetting agents and adhesion promoters, were profitably adopted for this purpose. Inks based on the use of organo-metal compounds or metal precursors were also proposed, but they require additional heat-treatment to achieve reduction to metallic species, to achieve the conductivity (Perelaer et al., 2010).

1.2.2. Enzymes for bioelectrode development:

The number of different redox enzymes reported so far, for developing EFCs is limited. Among the reports, GOx (Ivnitski, 2006; Mano 2008; Yahiro et al., 1964), glucose dehydrogenase (GDH) (Togo et al., 2007), alcohol dehydrogenase (ADH) (Davis et al.,

1983; Topcagic and Minteer, 2006), fructose dehydrogenase (Murata et al., 2009a), aldehyde dehydrogenase (Neto et al., 2013), and lactate dehydrogenase, are widely used as the anodic catalyst. There is enough scope to explore new redox enzymes as catalysts for EFCs. One of the focuses in our lab is to search for a stable alcohol oxidizing enzyme whose co-factor is avidly bound to the protein matrix for EFC and other electrochemical sensor applications. In this context, AOx has attracted intensive research interest in our lab for the last decade. These are flavoenzymes belonging to the group of glucose-methanol-choline (GMC) family. It catalyzes the oxidation of alcohols to the corresponding aldehyde or ketone with a consequent release of hydrogen peroxide. Based on substrate specificity, AOx may be broadly classified into four different groups namely, (a) short chain alcohol oxidase (SCAO), (b) long chain alcohol oxidase (LCAO), (c) aromatic alcohol oxidase (AAO), and (d) secondary alcohol oxidase (SAO) (Goswami et al., 2013). SCAO enzymes produced mainly by the methylotrophic yeast (mostly *Pichia pastoris*) are also known as methanol oxidase or ethanol oxidase (Alcohol: O_2 oxidoreductase EC 1.1.3.13). It is an oligomeric enzyme that consists of eight identical subunits arranged in a quasi-cubic arrangement, each containing an avidly bound cofactor, flavin adenine dinucleotide (FAD) molecule (Ozimek et al., 2005). The FAD is the main acceptor of hydride ion from alcohol. Upon oxidation of the substrate, the FAD is reduced to $FADH_2$; the reduced FAD then transfers the redox equivalents to dioxygen as the final acceptor. Along with the three major domains namely a FAD binding domain, a substrate-binding domain and a flavin attachment loop, AOx also possesses two minor domains, viz a FAD-covering loop and an extended FAD-binding domain. The FAD-binding domain is the most conserved region, which comprises an ADP-binding motif (βαβ) and a specific nucleotide-binding site GXGXXG (amino acids 13-18 of AOx) (Ozimek et al., 2005). The

structure of AOx is irreversibly altered following the dissociation of FAD, which is deeply buried inside the protein matrix (Zlateva et al. 2001). On account of the strongly bound co-factor to the redox center of the enzyme, the substrate specificity and irreversible catalytic oxidation of alcohols, AOx has emerged as a potential biorecognition element for developing alcohol biosensors (Goswami et al., 2013) as well as alcohol based EFCs.

The cathodic catalysts widely used in EFCs are BOx (Topcagic and Minteer 2006), laccase (Barton et al., 2001; Barriere et al., 2006) with copper ions as cofactors, horseradish peroxidase (HRP) (Gomez et al., 2010; Ramanavicius and Ramanaviciene 2009) with iron ions as cofactors, and microperoxidase (Ramanavicius et al., 2008). The use of oxygenase enzymes such as laccase as O_2 reducing catalyst is advantageous over the chemical catalyst platinum (Pt) as the latter is expensive and requires high overpotential for the reduction (Schaetzle et al., 2009). Laccase (*p*-diphenol: oxygen oxidoreductase, EC 1.10.3.2) is a copper-containing oxidase that catalyzes reduction of molecular oxygen to water, accompanied by the oxidation of a phenolic substrate. The majority of laccases reported in the literature were extracted from fungi and less frequently found in higher plants and bacteria (Morozova et al., 2007). Yoshida first described Laccase in 1883 making the enzyme one of the oldest reported enzymes so far. Later it was characterized by Bertrand as a metal containing oxidase in 1985. The active site of laccases possess four copper ions: a mononuclear “blue” copper ion (T1 site) and a three- nuclear copper cluster (T2/T3 site) comprising of one T2 copper ion and two T3 copper ions; which are categorized by their spectral and EPR characteristics (Morozova et al., 2007). T1, the substrate binding site of the enzyme is involved in the oxidation of substrate and transfer of electron to T2/T3 cluster, while T3 is responsible for oxygen uptake and as a whole, this T2/T3 site is responsible for the reduction of O_2 to water (Solomon et al., 1996). The

copper ions in the active site of laccase facilitate electron transfer by switching their oxidation states between Cu (II) and Cu (I). The function of the T1 center is to provide a long-range intramolecular electron transfer from the substrate to the T2/T3 redox copper center. The T2/T3 copper center plays a key role in the reduction of oxygen. The fully reduced trinuclear copper center reacts with dioxygen to generate a peroxide level intermediate and finally, molecular oxygen is reduced to water (Ivnitski and Attanasov, 2007).

1.2.3. Techniques for enzyme immobilization on electrodes

The foremost consideration given for enzyme immobilization on the electrode is to avoid its detachment and cofactors from the electrode surface. Once immobilized, enzymes usually exhibit an extended lifetime compared to those in solution. In EFCs, enzymes can be immobilized onto solid electrode surfaces by a range of approaches that include physical adsorption, covalent binding, entrapment and cross-linking (Kuri et al., 2021).

Adsorption refers to the simplest technique of immobilization of the bioreceptor onto a surface by reversible surface interaction between the bioreceptor and the surface. Weak forces like van der Waals, hydrogen bonds, hydrophobic interactions and ionic bonds are involved in this interaction. In this method, the solid support onto which the immobilization is chosen is placed in contact with a solution containing the dissolved bioreceptor at optimum pH, ionic concentration, etc., for an appropriate period to allow the adsorption to take place. The unbound bioreceptor molecules are removed from the surface by washing with a suitable buffer.

The covalent binding involves covalent bonds between the bioreceptor and the transducer surface. The side chains of cysteine (thiol group), lysine (e-amino group), aspartic and glutamic acids (carboxylic group), imidazole and phenolic groups, which are not essential for the catalytic activity of the enzyme, are utilized in the binding processes (Mohamad et al., 2015). The covalent bindings are though stronger than the adsorption-based immobilization, its preparation procedure is tedious and the enzyme activity may be reduced. However, one of the very useful covalent techniques known as Self-assembled monolayers (SAMs) finds enormous importance in developing enzyme based bioelectrodes. Owing to the well-defined structure of SAMs and simplified protein–SAMs system, it is possible to systematically study the influence of experimental parameters on the electron transfer kinetics of redox protein (Behera and Raj, 2007; Yue et al., 2006). SAMs are formed by chemisorptions of organothiols on an appropriate support like gold or silver. The ordered SAM on the surface is hold by Metal–sulfur bonds and as per requirement; the electron transfer distance can be altered by varying the SAM alkyl chain length (Cooney et al., 2008). On account of the selective and strong interaction of sulfur groups for gold, SAMs are very suitable systems for immobilizing biomolecules (Davis and Higson, 2005). SAM (Chaki and Vijayamohanan, 2002), permits the enzyme to adhere in the right conformation on the electrode surface, resulting in a decreased distance between the active site and electrode surface leading to effective DET (Freire et al., 2003).

In the entrapment method, the enzyme molecules are confined within the interstitial spaces of a crosslinked and water-insoluble polymer matrix or semi-permeable membranes. This localization is independent of the formation of bonds or chemical coupling between the enzyme and gel matrix or membranes. Matrix pore size is such that the enzyme is entrapped while the substrate and product molecules can pass through it

(Aehle 2007; Costa et al., 2005). The matrices used for entrapping enzymes include polyacrylamide gel, gelatin, collagen, cellulose, starch, silicone and rubber. The advantages of the technique include an extremely large surface area for contact between substrate and enzyme within a relatively small volume and the possibility of co-immobilizing different types of enzymes physically separated from each other in a single step. The technique does not alter the conformation of the enzyme where only aqueous solvents are used (Park et al. 2010).

Cross-linking is another irreversible method of enzyme immobilization, which is a carrier-free immobilization method (Sheldon et al., 2005). It does not involve a support matrix. The absence of a support matrix is the distinctive feature for enzyme immobilization by cross-linking. It is based on the formation of cross-links between enzyme molecules through poly-functional reagents. These reagents react with the enzyme molecules and create bridges. These bridges are the backbone to hold enzyme molecules and form cross-linked enzyme aggregate (CLEA). Glutaraldehyde, diazobenzidine, hexamethylene diisocyanate, and toluene di-isothiocyanate are generally used as cross-linking reagents. Glutaraldehyde is the most extensively used cross-linking reagent (Gorecka and Jastrzebska 2011; Sheldon et al., 2005). Quiocho and Richards first described the cross-linking of a crystalline enzyme by glutaraldehyde in 1964 (Quiocho and Richards 1964). Their main objective was to stabilize enzyme crystals for X-ray diffraction studies but they also found the integrity of the catalytic activity of the enzyme. Enzyme-glutaraldehyde crosslinks are irreversible. These can endure extreme pH and temperature. Such crosslinking method is used to immobilize enzymes like glucose isomerase, penicillin amidase. The crosslinking technique is though simple and cost-

effective, it suffers from a problem of denaturation of the enzyme by the poly-functional reagent (Chakraborty and Hashmi 2017).

1.3. Fuel for EFC

EFCs generally derive power from renewable sources. The diversity of fuel for EFCs has been greatly extended to accommodate many organic compounds that are common intermediates metabolized in living organisms. Hydrogen with its highest energy density value has been extensively used in traditional fuel cells. It can also be used in EFCs using hydrogenases as anodic catalysts (Mazurenko et al., 2017; Xia et al., 2016). However, difficulty in storage and transportation of this low dense fuel has seriously hampered its application in the field prompting rigorous research to facilitate its commercial use. A result of the studies has identified formic acid as a stable hydrogen carrier and has been used to power some EFCs because of its high volumetric capacity (53 g H_2L^{-1}), flammability under ambient conditions and low toxicity. On the other hand, methanol is an encouraging alternative to hydrogen as a fuel due to its easy transportation and storage, and volumetric energy density, nearly 3-fold higher than that of formic acid. However, it is toxic to human beings if ingested (Xiao et al., 2019). Moreover, the theoretical maximum voltage for a methanol/oxygen fuel cell (1.19 V) is nearby to that for a H_2/O_2 fuel cell (1.23 V) (Palmore et al., 1998). Another alcohol, ethanol as a fuel source for EFC has some advantages, such as low cost, non-toxic, wide availability and water solubility. Besides, ethanol is a renewable energy source that can be generated through the fermentation of agricultural products. Glycerol is another potential fuel easily acquired from many biobased fuel industries since it is a by-product of biodiesel production. High energy density, low toxicity, low flammability, extremely low vapor pressure (Arechederra

and Minteer 2009) are the other benefits of glycerol as fuel. Pyruvate, a key intermediate from the glycolysis pathway, has also been utilized as a fuel in EFCs (Sokic-Lazic and Minteer 2009). Finally, the most regularly studied fuels in EFCs are sugars as they are inexpensive, renewable, abundant, and safe to use. Sugars can be obtained from the naturally abundant lignocellulosic biomass (ca. 1×10^{11} tons/year globally), which are more uniformly distributed on earth than fossil fuels. Glucose-based EFCs are mainly suited for implantable applications due to their availability in human blood. Other sugars like fructose, xylose, sucrose, and maltodextrin have also been investigated for developing EFCs (Li et al., 2013; Zhu et al., 2011).

One of the parallel efforts to enhance the energy density in EFC is to extract the entire enthalpic energy stored in the organic fuel substrates. Theoretically, glucose possesses an energy density of 4,125 $Wh.L^{-1}$ releasing 24 electrons per molecule to produce carbon dioxide and water. Hence, with the complete enzymatic oxidation of the glucose units from a 15% maltodextrin solution the energy-storage density of the EFC could be enriched as high as 596 $Ah.kg^{-1}$, which is an order of magnitude higher than that of lithium-ion batteries and primary batteries (Zhu et al., 2014). Glycerol has even higher energy density (6,260 $Wh.L^{-1}$) compared to glucose, or ethanol (5,442 $Wh.L^{-1}$), methanol (4,047 $Wh.L^{-1}$), making it a very potential fuel. Nevertheless, pyruvate also has a high energy density (4,594 $Wh.L^{-1}$), and requires fewer enzymes than glucose for its complete oxidation.

The studies on alcohol based EFCs are limited. In these limited studies, ADH (NAD^+ dependent enzyme) has been widely used (Addo et al., 2011) as anodic catalyst due to its low redox potential, which supports the anode to function at low potential for

generating high cell voltage. However, the leaching susceptibility of the cofactor NAD^+ from the electrode surface and electrode fouling caused by the polymerization of oxidized products on the electrode surface eventually increases the overvoltage for oxidation of NADH (Bartlett et al., 2002). Hence, a redox enzyme with a strongly bound cofactor in the active center may be a better choice for developing operationally stable EFC. Considering the above fact, our research group has been focusing on the enzyme AOx, which contains strongly bound FAD cofactor, as a potential anodic biocatalyst for developing alcohol EFC (Goswami et al., 2013).

Using alcohols as fuels, the EFC with ADH as an anodic catalyst generated power densities between 32 and 1000 μWcm^{-2} (Kim et al., 2013; Neto et al., 2013). PQQ dependent ADH has also been used (Yakushi and Matsushita, 2010) in many EFCs. AOx based bioanode with air breathed laccase biocathode was utilized for generating power in fuel cell setup using methanol as substrate in our lab (Das et al., 2014). This fuel cell generated an OCP of 0.61 (± 0.02) V with a maximum power density of 46 (± 0.002) μWcm^{-2} at an optimum of 1M methanol, 25°C and an internal resistance of 0.024 μΩ. The operation and storage half-life ($t_{1/2}$) of the EFC were 17.22 hours and 52 days, respectively at a fixed load of 1.85 Ω.

1.4. Development of small scale EFC:

Explosive growth occurring recently on wireless consumer electronics and portable biomedical devices (including body integrated) has prompted intensive research for developing a stable power supply of smaller dimensions for powering these miniaturized utilities. In this aspect, small-scale EFCs are emerging as the latest addition to this modern field of microscale devices (Gellett et al., 2010). However, miniaturization of these bio-

based power-generating devices confronts several technical difficulties on their simple fabrication, operational stability, and efficient functions. These devices must provide similar performances to larger EFCs in terms of efficiency and power density while using fewer reagents, space and time consumption. Over the last decade, the questions that loomed over the technical and economic dimension on the miniaturization of EFCs have been significantly addressed by the emergence of advanced techniques like microfluidics, lithography, and allied engineering microfabrication tools. Fuel cell technologies often adopt microfluidic techniques for miniaturization of the devices (Kjeang et al., 2009). Microfluidics is the science and technology of systems that process or manipulate small (10^{-9} to 10^{-18} liters) amounts of fluids, using channels with dimensions of tens to hundreds of micrometres. In these devices, fuel and oxidant streams introduced into a microchannel proceed in parallel laminar flow without turbulent mixing. However, diffusion happens across the interface between the two streams transverse to the flow streams. Laminar flow occurs at low Reynolds numbers (*Re*) (equation 2.8), where viscous forces are dominant over inertia forces.

$$Re = \frac{\rho UL}{\mu} \quad \text{.....1.8}$$

Where, ρ is the density of the fluid, μ represents viscosity of the fluid, L depicts the length of the channel, U is the mean velocity of the fluid.

Microchannels are commonly fabricated using soft lithography (Zhao et al., 1997) with T-shaped or Y-shaped geometry. Micro-fluidic fuel cells are typically made of polydimethylsiloxane (PDMS). Electrodes are either placed in the inner wall of the main channel or immersed in an electrolyte and placed in the main chamber. The performance of these cells can be influenced by the efficiency of chemical reactions as well as the size and geometry of the chamber. Smaller the chamber size efficient is the power density as

observed. This is due to the larger surface-to-volume ratio, which shortens energy production start-up time and allows for faster power generation recovery. It is demonstrated that a high aspect ratio (width/height) microchannel could improve the fuel utilization and consequently the power density of the fuel cells (Kjeang et al., 2007).

The research on developing small-scale EFCs is limited and among the reports glucose fuel-based systems have been intensively investigated following different strategies. Heller and co-workers successfully demonstrated the efficiency of a miniatured membraneless EFCs functioning under physiological conditions. They have developed the first handmade miniature device containing electrodes of seven micrometre diameter and two centimetre long carbon fibers, placed in a polycarbonate support. The anode and cathode were modified by GOx and either laccase or BOx within, and mediated by redox osmium-based hydrogels (Mao et al., 2003). The group developed the first miniature membraneless EFC that delivered a power density of 137μWcm^{-2} at 0.4V (Chen et al., 2001). This simple device validated the goal of a miniature autonomous sensor–transmitter system (Bullen et al., 2006; Heller, 2004). Following further modifications, the devices could deliver higher power densities of 431 μWcm^{-2} at 0.52 V (Mano et al., 2002) and 440 μWcm^{-2} at 0.52 V (Mano et al., 2003), in pH 7.2, 37° C and 15 mM glucose. The high power density delivered by these devices comes from the cylindrical mass transport at the carbon fibers and the use of efficient redox polymers to transport electrons. They also showed that this system produced a power density of 240μWcm^{-2} at 0.52V when implanted in a living organism, near the skin of a grape. Later, by replacing carbon fibers with engineered porous microwires made of oriented carbon nanotubes, the most efficient glucose/O_2 EFC ever designed was developed (Gao et al., 2010) and delivered a high power density of 740 μWcm^{-2} at a cell voltage of 0.57 V. The success of the experiment

achieved probably was due to an increase in the mass transfer of substrates to the bioelectrodes. Though this approach has made the device significantly simpler and more compact, external pumps and outlet systems were still required to maintain the fuel concentration and remove the by-product, respectively, thus indirectly increasing the overall dimensions of the device (Kjeang et al., 2009). As an alternative to the external pumping system, a self-pumping or passive pumping method is thought to be a good option to deliver the fluids in a micro-fuel cell. With the idea of a self-pumping mechanism, paper-based micro fuel cells may be much more attractive than the traditional ones. Paper-based microfluidics has been extensively investigated by researchers for various applications (such as disease diagnostics), in which transport may be sustained due to the capillary action of fluids through the cellulose fibers and pores in the paper (Martinez et al., 2010). The fluid flow rates have been found to be very low (2–3μl min^{-1}), so that a given small volume of fluid can be delivered for a long period of time in contrast to the syringe pump-based arrangement (Wang et al., 2013). Thus, with the use of paper, the power generating capacity of the small-scale EFCs may be enhanced significantly due to the constant laminar flow of fluids for a long time at low volume consumption.

Miniaturization may improve the performance of the EFC for sensor applications as this act lowers the internal resistance of the device, which makes them energy dense. Non-ohmic and ohmic resistances are the two components of the internal resistance. Resistance to the charge transfer and diffusion comprises the non-ohmic resistance. Electrode with high surface area and supporting good catalytic activity can lower the non-ohmic resistance. Contrarily, the ohmic resistance affects the output signal. Placing the electrodes in close vicinity and using electrolytes with high conductivity can reduce ohmic resistance. Ohmic resistance can be defined as:

$$\Delta V_{\Omega} = \frac{d \times I}{K \times A} \quad \text{.....1.9}$$

Where, ΔV_{Ω} is the voltage difference between the anode and cathode, d is the distance of electrode separation, I is the current, K is the solution conductivity, and A is the cross-sectional area (cm^2) through which ionic conduction occurs. The ohmic resistance can be calculated as, $R_{\Omega} = \frac{l}{(A \times K)}$, where l is electrode length in cm. Therefore, the ohmic resistance can be managed by reducing the d/A ratio, which can be addressed by microsystems (Kaushik et al., 2021).

Owing to the porous structure and fluid wicking ability of paper, biofuel (substrate) could be continuously supplied to the paper electrode without using an external pump. Enzyme can be easily adsorbed/immobilized on paper surface whereas the conductive ink and enzyme biocatalysts could be printed on paper using inkjet or screen-printing technology. It supports the integrity of the biocatalysts used in EFC. The first work on biofuel cells using paper-based electrodes is probably the work by Jenkins and his colleagues in 2012. In this work, both anode and cathode were printed on separate paper sheets and were separated by a dialysis membrane, which acted as the separator. CNT, enzymes (Laccases or PQQ-dependant aldose dehydrogenase) and mediators (osmium complexes) containing ink was printed onto Whatman paper. Anodes and cathodes were connected to the electrochemical device by direct contact with graphite plates and were separated by a dialysis membrane (Figure 1.4A). The cell could be supplied with 200 µL of glucose solution and could have an operation time of about 90–100 h (Jenkins et al., 2012).

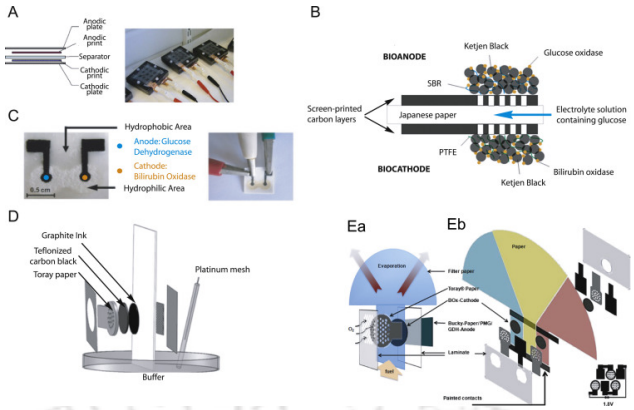

Figure 1.4. EFCs based on paper material. (A) Anodes and cathodes are separated by a dialysis membrane, (B) electrodes are screen-printed on both sides of a Japanese paper, (C) electrodes are screen-printed on the same side of the paper with a hydrophilic channel acting as a membrane, (D) air-breathing cathode and (Ea) single or (Eb) stacked fan-like biofuel cell painted on two-face of a Whatman paper (Desmet et al., 2016), Copyright 2016, reprinted with permission from Elsevier.

Shitanda and his group developed membraneless paper-based EFC (Figure 1.4B). They used Japanese paper and anode and cathode was screen-printed on each of the paper sheet to build a membrane-less EFC. The anode was composed of GOx and Tetrathiafulvalene (TTF) adsorbed at the surface of Ketjen black/styrene butadiene rubber polymer. Styrene butadiene rubber is replaced by PTFE at the cathode in order to create a water repelling electrode. Glucose is supplied by diffusion from a solution to the anode via the paper fluidic (Shitanda et al., 2013). Next Zhang and his group printed anodes and cathodes on the same side of the paper, where the hydrophilic channel (or region) between each electrode acts as a membrane (Figure 1.4C). GDH and BOx were immobilized together with chitosan onto screen-printed anode and cathode, respectively. In this system, oxygen from air is diffused to the enzyme in the cathode. The cell was operated with 30

µL of a glucose solution supplemented by NAD^+. The cell was operating for 0.75 h and the power was fully recovered by adding an additional 30 µL of biofuel to the EFC system (Zhang et al., 2012b). Ciniciato and his group developed different designs of air-breathing bio cathode and ink based biocathode. In this half-cell, the paper material is used as the electrolyte support. A carbon ink containing BOx was painted onto nitrocellulose and was further pressed onto a gas diffusion layer (teflonized carbon black) and a toray paper as connector (Ciniciato et al., 2012). Atanassov group developed a novel EFC design. They utilized paper-based quasi-2D microfluidic system to supply biofuel to the enzymatic layer. The anode was fabricated using GDH immobilized over bucky paper and cathode was fabricated using BOx immobilized on carbon black over toray paper. The Whatman filter paper was designed as a fan, anode and cathode being pressed on the handle of the fan. This geometry permits the improvement of the transport of fuel to the anode. The handle of the fan was plunged into the substrate solution that reached the anode by capillary forces but the solution in the fan was evaporated. The evaporation becomes the main driving force resulting in a quasi-steady-state flow. Power output could be increased by stacking three electrodes together using carbon yarn (Figure 2.4E) (Narváez et al., 2014).

Paper-based biofuel cells are still in their infancy in spite of these inspiring examples. The stability of the paper itself should be investigated once hydrated. Moreover, strategies are yet to be developed to improve electron transfer (electrode surface modification). Again, Atanassov group developed a paper-based biofuel cell with passive laminar flow to show the impact of flow on the performance of two different enzyme cascades – for methanol and ethanol substrates. To utilize substrates effectively, they used enzyme cascades to ensure complete oxidation of methanol. Both cascades demonstrated

enhanced electrochemical output as a consequence of the decreased diffusion path of the reaction intermediates. They identified the intermediates diffusion in between the enzym active sites as the rate-limiting step in cascade operating systems (Desmet et al., 2016; Lau et al., 2015).

1.5. Approach for the improving EFC voltage

1.5.1. Stacking of EFC:

EFCs may be stacked in series to increase the output voltage of the device, while cells stacked in parallel can increase the current density (Xu and Armstrong, 2015). Unlike microbial fuel cells, EFCs do not possess the problem of voltage reversal when stacked (Oh and Logan, 2007). Sakai and his group developed one glucose/O_2 EFC with GDH and BOx that generated a maximum power density of 1.45 ± 0.24 $mWcm^{-2}$ at 0.3 V and OCP of 0.8V in the presence of 400 mM glucose. A stacked cell of two individual EFCs connected in parallel functioned a radio-controlled car (16.5 g) and a memory-type Walkman uninterruptedly for more than 2 h (Sakai et al., 2009). Again, Xu and Armstrong fabricated one H_2/O_2 EFC composed of two stacks of four cells in parallel with OCP and P_{max} of 2.09 V and 7.84 mW, respectively. It delivered power to an electronic clock and red LEDs for 8 h with no fall in light intensity (Xu and Armstrong, 2015). A screen-printed paper-based circular-type EFC system was developed by Shitanda and his group. With single cell OCP of 0.57 V, five individual cells when serially connected, generated an OCV of 2.65 V and lightened an LED directly (Shitanda et al., 2017). However, the overall performance of stacked EFC in serial is limited by the weak EFC. Yet again, the individual EFCs in the serially connected system should be isolated properly to avoid short-circuits resulting from ion-conductive electrolytes (Xiao et al., 2019).

1.5.2. Employment of external boost converter:

The voltage generated by an EFC could be increased by externally connecting a charge pump as a DC-DC converter. A voltage-doubler operates by charging two capacitors in parallel separately followed by discharge in series. Southcott and his group fabricated a fluidic glucose/O_2 EFC with an OCP of 0.47 V in a serum solution that mimics the human blood circulatory system (Southcott et al., 2013). A single EFC was connected to a combination of a charge pump with a DC-DC converter, which increased the voltage from 0.3 to 2 V and from 2 to 3 V, respectively. The resultant device was able to operate a commercial pacemaker for a continuous period. Jia and his colleagues reported a wearable biofuel cell printed directly onto textile substrates. For the generation of electrical energy, the EFC utilized physiologically produced sweat lactate as the fuel. The cell generated OCV of 0.67V and when two EFCs parallelly connected, it generated 6 μW at 0.376 V, which was scaled up to 3.2 V with an EFC/voltage booster couple that can illuminate a blue LED bubble requiring 2.5 V and 0.5 mA (Jia et al., 2014).

1.6. Self powered EFC:

Owing to their high sensitivity, reliability, and simplicity, electrochemical biosensors are the most reliable candidate from commercial point of view. In addition to being electrochemical, some extra prominent features make EFCs more operational. Contrasting to electrochemical biosensors EFCs are power generating devices, the presence of the target analyte in a sample could be sensed directly from their electrical signal output, thus precluding the need for any external power source (Chouler et al., 2018). Depending on the effect of the target analyte on the enzyme of the EFCs, the output signal (current or voltage) may be higher (turn-on sensors) or lower (turn-off sensors) than

the control signal. For example, if the target analyte is an activator of the enzyme, the EFC works as a turn-on sensor; again, if the target analyte is an inhibitor of the enzyme, the EFC operates as a turn-off sensor (Kaushik et al., 2021). The self-powered biosensors have some advantages, these are (i) this type of sensor comprises of two electrodes, and there is no need for application of external voltage to the electrodes. (ii) As the system is self-powered by biological fluids, the sensor may function as an implanted invasive sensing device. (iii) No application of potential to the electrode makes the operation of the biosensor device specific, and hence there is no interference by contaminants. (vi) In absence of the substrate, the system does not generate voltage or current, so, one concentration of the substrate is sufficient to calibrate the system (Katz et al., 2001).

The first EFC-based self-powered biosensor was developed in 2001 by Willner and co-authors for sensing glucose and lactate (Katz et al., 2001). After that, Self- powered enzymatic biosensors for the detection of glucose (Fischer et al., 2016), cholesterol (Sekretaryova et al 2014), lactate (Hickey et al., 2016), acetaldehyde (Zhang et al., 2012a) ascorbic acid (Zloczewska et al., 2014), proteins (Wang et al., 2014), explosives (Germain et al., 2008) were reported. However literature on self powered alcohol biosensors is rare. Ruff and his group developed a self powered ethanol biosensor using ADH/ redox polymer based bioanode and AOx/HRP based biocathode (Ruff et al., 2017).

1.7. Key areas and scope

There are a plethora of reports on the development of EFCs. Efficiency, stability, and simple design are the key research issues on this energy-generating device. However, commercial EFC products for real-world applications are not yet widely known. The major hurdles for this sluggish development are generally attributed to their low power density

and poor operational stability, which is mainly caused by the short lifetime of enzymes being used as electrode catalysts in these devices.

EFCs of smaller sizes have several advantages among which portability and low production cost are prominent. For biosensor applications, chip-based devices offer many benefits in all functionality, handling and economic fronts. The fabrication of such devices commonly exploits microfluidic techniques, which made the device significantly simple, compact and enables multiplex analysis of microlitre sample volumes. However, proper fluid flow (fuel in the present case) in the microfluidic devices and in the macro-sized fuel cells is usually enacted by coupling an external pump, which eventually increases the overall dimensions and cost of the device. To mitigate the problem, we proposed to introduce materials that facilitate fluid flow to the devices through passive diffusion mode. Cellulose fibre-based materials present in paper and cotton allow the flow of aqueous liquids within its fibre matrix through capillary action. This property provides the basis for using paper to fabricate microfluidic systems (Stock and Rice 1974). Therefore, with the self-pumping mechanism, paper or cotton-based biofuel cells may be much more attractive than the traditional ones. These paper-based microfluidic platforms can be easily fabricated by creating hydrophilic channels by adapting various techniques including photolithography (Martinez et al., 2007).

The enzyme electrodes are the kingpin for the function of EFCs as it is largely accountable to the operational stability, coulombic efficiency and power density of the construct. The short lifetime of the redox enzymes is mainly responsible for the poor operational stability. Additionally, efficient electrical communication between the redox enzymes and the electrodes is a major challenge since the active centers of most of the

redox enzymes are buried inside the protein matrices. To overcome this obstacle, two approaches are widely used: mediated electron transfer (MET) and direct electron transfer (DET). The MET method even though offers high redox current, the leaching susceptibility of the mediating molecules from the enzyme–electrode interface discourages this approach to use for cases where operational stability is a critical task. On the other hand, the DET approach involves the direct transfer of electrons between the enzyme and the electrode (Das et al., 2016). To facilitate the DET, various highly conductive nanostructured materials are widely used. Over the past few years, the magnetic nanoparticles (Fe_3O_4 Nps) (MNps) have attracted attention for different applications due to their distinctive properties like good biocompatibility, high surface reactivity, strong super para-magnetism, low toxicity, and strong adsorption ability to immobilize enzymes. However, the use of MNps for improving the electrocatalytic performance of enzymes in EFC is limited.

Again, the research on EFC biosensors for the detection of alcohol is not yet adequately known. We envisage that with the aid of a passive diffusion facility for the target alcohol in a chip-based platform, and biocompatible electroactive advanced materials to realize the bioelectrocatalytic function of the redox enzyme with long-term stability, it would be possible to design a suitable EFC based alcohol biosensor for practical use.

Considering the enormous potential of EFCs as power generating as well as biosensing devices, the gaps and challenges to develop such devices as briefly discussed above, the following objectives have been set for the present investigation embodied in this thesis.

1.8. Objectives of the present study

The overall objective of the present investigation is to develop small-scale enzymatic biofuel cells for power generation application using alcohol as fuel substrate and for alcohol biosensing application using paper as support material.

The specific objectives of the work are:

- Fabrication of stable and bioelectrocatalytically efficient enzyme electrodes using highly conductive and biocompatible graphite paste ink with silk sericin as electrode material.
- Fabrication and characterization of a laccase-based biocathode for developing the biofuel cell and validate its performance using a suitable substrate.
- Construction of EFC using the enzyme electrodes for power generation application.
- Fabrication of small-scale paper-based EFC for alcohol sensing application.

The entire thesis has been outlined into five chapters as described below, followed by a short section covering the conclusions on the present work and the scope for future research.

Chapter I: Introduction and Literature review

This chapter furnishes a brief introduction, summarizes the status and progress in the area of EFC. It highlights the basic concept of the EFC, underlying electron transfer mechanism in enzyme based bioelectrode, electrode materials used in EFC, approaches for improving cell voltage and a brief review on the alcohol detection system with a special

emphasis on EFC based sensors. The chapter also defines the origin of the work that comprehends the motivation for pursuing the work, challenges involved and the objectives undertaken to address the challenges.

Chapter II: Development of Conductive Ink for Fabrication of Enzyme Electrodes

The study in the chapter includes the development of graphite-based conductive pastes with different biopolymers like chitosan, silk fibroin and silk sericine as stability and conductive enhancing additives. In particular, graphite pastes containing sericin as an additive showed better conductivity and stability.

Chapter III: Fabrication and Characterization of Laccase-based Bioelectrode

This chapter describes the fabrication of laccase-based biocathode for biofuel cell application. It also illustrates the development of an amperometric laccase-based biosensor for the detection of pyrocatechol to validate the function of the bioelectrodes for future EFC applications. The detection principle has been elucidated and the response against different common interfering agents has been evaluated.

Chapter IV: Development of a Paper-based Enzymatic Biofuel Cell for Alcohol Sensing Application

This chapter describes a low-cost, self-powered paper-based biosensor for monitoring of alcohol using an alcohol/oxygen EFC system. The device operating mechanism has been elucidated and the response against different common interfering agents has been evaluated.

Chapter V: Development of Methanol Biofuel Cell through Passive Fuel Delivery Facility in the Anode Chamber

This chapter describes a new design strategy to develop a methanol fueled EFC using alcohol oxidase (AOx) in anode and bilirubin oxidase (BOx) in cathode. The EFC operates through passive fuel delivery approach obviating the need of for an external pump for continuous and prolonged operation of the cell. The performance of the EFC was evaluated.

Conclusions and Scope for Future Research

This section recounts the significant conclusions on of the present work. Furthermore, a brief critical evaluation on of the work and the future scope to advance the work for a technologically viable device has been projected.

CHAPTER II

Development of Conductive Ink for Fabrication of Enzyme Electrodes

CHAPTER II

Development of Conductive Ink for Fabrication of Enzyme Electrodes

2.1. Overview

One of the major thrusts of current research in the field of biofuel cell–based biosensors is the development of portable and inexpensive point-of-care diagnostic devices. Among the various biocatalysts being used in these devices, enzymes are regarded as a benchmark due to the high selectivity and sensitivity offered by this protein-based recognition system in the detection of target analyte of interest. The enzyme electrodes are the kingpin for the proper functioning of these bioelectrochemical devices. For large-scale production of these small-scale or chip-based EFCs of commercial interest, conductive inks are explored for developing the electrodes (Kim et al., 2006; Komoda et al., 2012). The inks generally consist of solid conductive particles such as graphite powder, carbon nanotubes,

metal particles, organo-metallic compounds, and nanoparticles. These solid materials are usually suspended in a mixture of solvents and additives, such as polymeric stabilizers, wetting agents and adhesion promoters, for preparing the ink (Kamyshny and Magdassi, 2014; Perelaer et al., 2010). However, one of the major challenges of developing such ink is to maintain their combined properties of conductivity and biocompatibility, more importantly when these inks are intended to use for preparing enzyme-based bioelectrodes (Park et al., 2007).

Over the last many years, graphites have received intensive interest in developing conductive ink. Graphite consists of superimposed lamellae of 2D carbon-carbon covalent networks, referred to as graphene, that form layers as a result of strong van der Waals interactions (Singh et al 2021). In graphene, the carbon atoms are bonded by sp^2 hybridization and the single atomic layer character imparts its outstanding physical properties (Allen et al., 2010). Graphite powder is though, far less expensive than their processed form (through exfoliate or other elaborate techniques) graphene, the weak conductive properties due to the amorphous nature of the graphite hinders its application in developing conductive ink. Hence, the transformation of the powdered graphite to a higher conductive form through a simple process may greatly boost the application of these widely available materials in various fields including developing portable enzyme based electrochemical devices.

Glycols are generally employed as a binder/drying retarding agent in the preparation of conducting inks for maintaining cohesion among the conductive particles such as the graphite within the water-based conductive ink composition and to slow down the drying process so as to permit manipulation of the conductive ink, such as by direct writing before it has a chance to dry. Polyethylene glycol (PEG) has been widely used as a binder for various ink formulations (El-Molla, 2007). PEG are water-soluble polymer/oligomer made from the monomer of ethylene oxide, have excellent wetting properties.

Herein, we explored various biocompatible materials like silk sericin, silk fibroin and chitosan for developing a conductive ink using graphite powder as the core conductive material. They were used in the preparation process of ink as a stability enhancer. Stability enhancer's role is to enhance the adherence between graphite particles in the composition and to prevent the leaching out of the conductive particle when it is applied over substrate once incubated with water. Silk, a mass-producible natural polymer is of two kinds: one is fibroin, which is fibrous in nature. The other one is sericin. Sericin is a gum like protein present in silk-cocoon associated with silk-fibroin. Sericin and fibroin both are biocompatible materials (Pal et al., 2016). Sericin is progressively used in the cosmetic industry, as an antibacterial agent and as a biocompatible biomaterial (Zhang 2002). The incorporation of sericin in hydrogel or poly (vinyl alcohol) (PVA) / poly (vinyl pyrrolidone) (PVP) composites also enhances their electrical properties (Cheong et al., 2014; Ramesan et al., 2016). Sericin was found applicable as an enzyme stabilizer (Kishimoto et al. 2009), which is an important trait for developing enzyme electrode. Chitosan (β-1, 4-poly-D-glucosamine), one of the naturally occurring biopolymers from deacetylation of natural chitin, is another biocompatible material. It exhibits good film forming capacity, good adhesion to various supports, high mechanical strengths, and high water permeability. The presence of the reactive amino and hydroxyl functional groups allows chitosan to be easily modified by covalent functionalization, making the resulting composites more stable and with tuned properties (Diaconu et al., 2010).

We report here the development of a conductive ink with graphite powder as a particulate conductive material using PEG as a binder or as dispersant along with silk sericin or silk fibroin or chitosan as stability as well as conductivity enhancer. The as-prepared inks were then characterized and the most conductive and stable ink was used for making carbon based enzyme electrodes in research work described in the next chapters.

2.2. Experimental approaches

2.2.1. Reagents and stock solutions

Graphite powder (<20 µm, synthetic), Polyethylene glycol (PEG) and chitosan were purchased from Sigma-Aldrich. Chitosan was dissolved in 1% acetic acid by ultra-sonication at 15 Hz for 1 h. Silk fibroin and sericin were extracted in the lab from *Bombyx mori* cocoons following a reported method (Rockwood et al., 2011). Whatman chromatographic papers grade 3 mm Chr (20 cm x 20 cm) were procured from GE health care. All other chemicals were of analytical grade and used without further purification. The entire experiment was performed using Elix Millipore water (with resistivity of 15 MΩ cm at 25 ^{0}C).

2.2.2. Extraction of silk fibroin and silk sericin

Cocoons of *Bombyx mori* used for the extraction of silk fibroin and silk sericin (Rockwood et al., 2011) were cut and boiled for 30 min, in 0.02 M of sodium carbonate to remove sericin. After a thorough rinse with water, the fibroin was removed, squeezed and placed on aluminium foil to dry in a laminar hood overnight. A total of 9.3 M of LiBr was used for dissolving the silk fibroin in potassium phosphate buffer for 4 h at 60 ºC. The amber colored fibroin solution was dialyzed against the water until $AgNO_3$ test detects no bromide ion in the silk solution. The final solution with the silk fibroin concentration of 5-6 % (w/v) was stored at 4 °C until use. For isolation of sericin, the solution remained after separation of the fibroins was filtered, dialyzed for 48 hours, and then lyophilized. This resultant lyophilized sericin powder was stored at 4 ^{0}C until use. The whole process of extraction of silk fibroin and silk sericin is described in scheme 2.1.

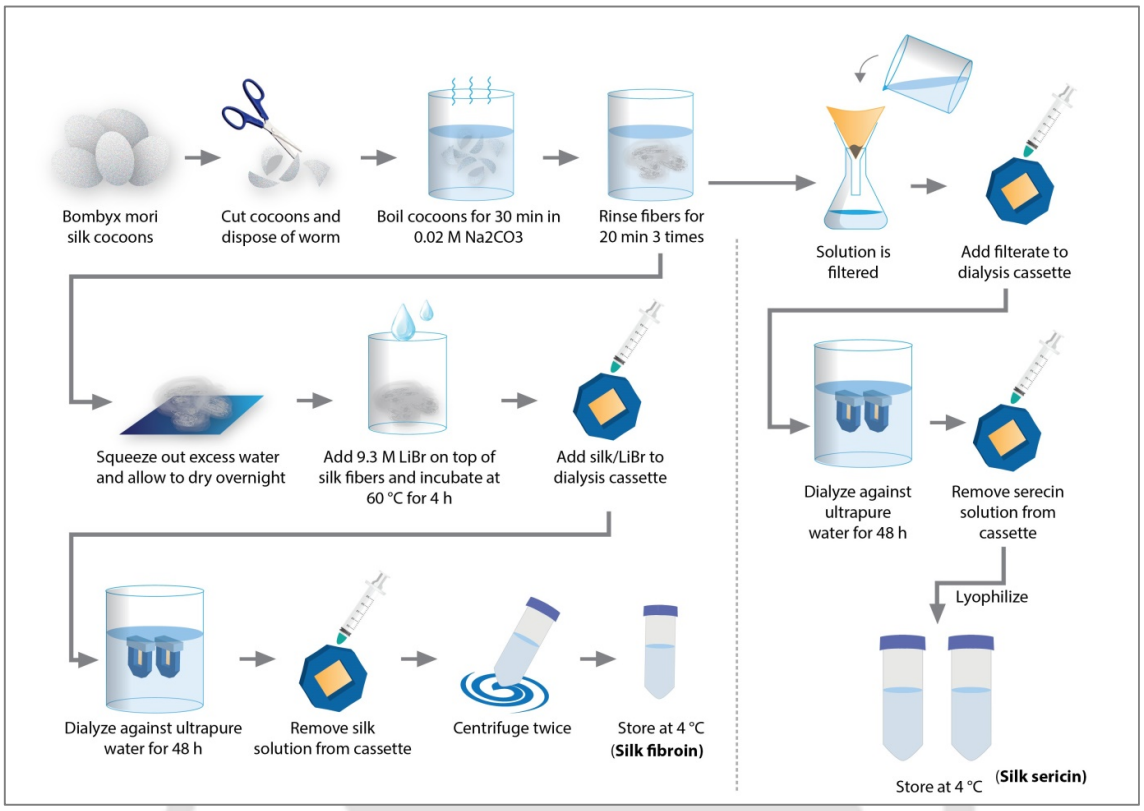

Scheme 2.1: Schematic of the silk fibroin and silk sericin extraction procedure (adapted from Rockwood et al., 2011)

2.2.3. Preparation of conductive ink:

The conductive inks were prepared by mixing 30% (w/v) graphite powder and 60% (w/v) PEG with about 1% (w/v) water-soluble biopolymers selected from the group consisting of chitosan, silk fibroin, and silk sericin. The mixing was done by ultra-sonicating for about 30 mins.

2.2.4. Characterization of the prepared inks:

The prepared inks were characterized for conductivity by using two-electrode data acquisition system (Agilent 34972A LXI, USA). First, all the three types of inks are hand brushed over chromatographic paper and allowed to dry. The resistance between two points

(of equal distance) on the ink painted papers was measured through a data acquisition system. After that, resistivity (ρ) was calculated using the equation 2.1

$$\boldsymbol{\rho} = \frac{\boldsymbol{RA}}{\boldsymbol{l}} \quad \text{.....2.1}$$

where '*R'* is resistance, '*A*' and '*l*' are cross sectional area and distance between the two specified points on the paper respectively. Then conductivity can be calculated using the following equation 2.2

$$\boldsymbol{\sigma} = \frac{\boldsymbol{1}}{\boldsymbol{\rho}} \quad \text{.....2.2}$$

Where σ is conductivity and ρ is resistivity.

For aqueous solubility study, the conducting inks painted dried chromatographic papers were incubated in water for three minutes and were observed the traces visually in water for each conducting inks. This experiment was done to study the aqueous stability of the inks on paper. Thermal stability of the highest conductive ink was monitored by thermo-gravimetric analysis (TGA) and differential scanning calorimetry (DSC) analysis that were performed simultaneously in the thermal analyzer (*NETZSCH STA*-449 F3 Jupiter®, Germany) from RT to 400°C at a rate of 10° C min^{-1} under dry nitrogen. Again, the degree of crystallinity of all the individual components of the highest conductive ink and their composites was analyzed using an X-ray powder diffractometer (XRD) (Rigaku X-Ray Diffractometer TTRAX III, Japan) equipped with CuKα radiation (λ = 1.54178 Å) in a continuous scanning mode. The viscosity of the ink was recorded using a rheometer (Anton Paar Physica MCR 301 rheometer, USA) with 1ml ink loading at RT.

2.2.5. Characterization of the secondary structure of protein

The Circular Dichroism (CD) spectra of sericin and sericin-PEG composites were recorded in a Jasco J-815 spectropolarimeter (Japan) calibrated with (±)–10- camphorsulfonic acid for optical rotation. The spectra were determined within 250-190 nm, in 2 mm path length suprasil quartz cuvette, at a scan rate of 50 nm min^{-1}, 0.1 nm intervals, a time constant of 1s, and the average of three scans. The temperature of the cell in the range of 25˚C was controlled by using a peltier temperature control unit. The baseline spectrum was subtracted from the sample and the resultant spectra were smoothed by Savitsky-Golay filter using Jasco spectral analysis. The secondary structure analysis was performed using the online server DICROWEB structure estimation program which utilizes the CONTIN program to evaluate the structure (Yang et al., 1986).

2.3. Results and discussion

2.3.1. Characterization of the ink

2.3.1.1 Conductivity measurement:

Different conductive graphite inks were prepared by combining various biocompatible polymers that were characterized by measuring resistance using two electrode systems as discussed in the experimental section. The conductivity values of the inks for the corresponding graphite inks containing sericin, chitosan, and silk fibroin were 11.2±0.104 $mS.cm^{-1}$, 6±0.036 $mS.cm^{-1}$, and 1.1±0.0116 $mS.cm^{-1}$ indicating the conductivity of the ink containing sericin is 1.86- and 10.18-fold higher than the ink containing chitosan and silk fibroin, respectively. For each case, the conductivity values did not change much (< 5%) over the time up to 600 s measured at a regular interval of time (Figure 2.1). Sericin is a highly charged molecule (Cheong et al., 2014). The well-ordered charged residues across the protein chains of sericin may facilitate its charge transfer property in the ink. Again, Patent

application no. US2011/0291078A discloses the invention of silk fibroin as an insulating material in the manufacturing of organic thin film transistor (OTFT), where fibroin is used as a dielectric material of the gate insulating layer. It is in accordance with our result that graphite ink containing silk fibroin ($1.1 mS.cm^{-1}$) exhibits less conductivity than ink containing silk sericin.

Conducting traces made from higher conductive ink leads to preparation of higher sensing platform for biosensor or biofuel cell application.

2.3.1.2. Aqueous stability of the conductive inks

The ink prepared only with graphite-PEG mixture was not significantly stable in an aqueous environment as the inks were easily dissolved following their incubation in water for three minutes as tested on a filter paper surface. This is due to the high solubility of PEG in water. In contrast, the inks prepared by mixing graphite and PEG with other biomaterials were significantly stable as the level of dissolution of the ink particles in the incubating aqueous environment was practically nil (Figure 2.2**)**. This infers that the selected biopolymers could strongly stabilize the graphite particles in the PEG environment preventing their dissolution into aqueous surroundings. This property is an important requirement for a conductive ink for their deployment to construct stable enzyme electrodes to catalyze substrate in an aqueous solution. The reason is attributed to the less solubility of chitosan at neutral pH, highly ordered β structure of silk fibroin and glue like properties of silk sericin. Moreover, the introduction of PEG into the sericin induces the change of secondary structure from random coils to β sheets that decrease sericin solubility in water (Cho et al., 2003).

2.3.1.3. Thermal characterization of conductive ink:

Considering the better aqueous stability and conductivity, Graphite-PEG-Sericin ink was considered for further study. The thermal stability of the ink was analyzed by using TGA techniques (Figure 2.3 black trace). A reduction in mass of 25 % was observed at ~ 100 ºC, which could be due to the evaporation of residual water from the ink. There was no drastic change in the mass of the sample during treatment up to 320 ºC indicating that the polymer binders do not degrade within this temperature range. DSC measurement of the ink (Figure 2.3 blue trace) indicates the presence of doublet endothermic peaks, one at 91.5 °C and a shoulder peak at 62.5 °C. These peaks can be attributed to the melting of the PEG binder (Pielichowski and Flejtuch 2002). The appearance of another endothermic broad peak at ~275 °C was suggested to be caused by the melting of sericin in the ink (Zhang et al., 2011).

Again, the first derivative curve of DSC was recorded from RT to 600°C at a rate of 10° C min^{-1} under dry nitrogen (Figure 2.4). The complex peak area from this curve was analyzed (Figure 2.5) to deduce the enthalpy of heat of formation (ΔH_f), which was found to be -4204 J/g indicating high thermal stability of the graphite-PEG-sericin ink. Highly thermally stable conductive is very much required for the fabrication of stable electrode surface for the preparation of biosensor and biofuel cell.

2.3.1.4. Crystallinity of the conductive ink

The degree of crystallinity of conductive ink was analyzed using an X-ray powder diffractometer (Figure 2.6 A and B). The 2θ range is dominated by peaks at 26.54º which correspond to graphite crystal plane (0 0 2) lattice spacing distance (Wojtoniszak et al., 2012) while sericin exhibits two weak intensity peaks at 23.26º and 19.06º (Figure 2.6 A). During the interaction of graphite with sericin, the peak intensity corresponds to the original (002) peak of the graphite increases and the peak shifts slightly to the lower angle. Based on Bragg

formula $\lambda=2d \sin\theta$, the d (0 0 2) interlayer spacing calculated for graphite and graphite-sericin were 0.3358 nm and 0.3359 nm, respectively. This can be directly attributed to an interactive role of sericin that transformed amorphous graphite to a crystalline form, which in turn enhanced the electrical conductivity of the graphite in the Graphite-PEG-Sericin nanocomposite ink. Figure 2.6B shows the XRD pattern of PEG, Graphite-PEG and Graphite-PEG-Sericin. PEG exhibits distinct two peaks at 23.29º and 19.12º (Barron et al., 2003). The crystallinity of both PEG and graphite decreases in the respective composite mixture, as evident from the decrease in intensity of the peak corresponds to PEG and graphite. While the incorporation of sericin to the PEG-graphite composite increases the intensity of (002) graphite peak at 26.5º. There is a strong positive correlation between improved electrical conductivity and increased crystallinity through the reduction of crystalline defects or by increase in ordered structure (Matsumoto et al., 2020). Hence increased crystallinity results in increased conductivity of the prepared ink, resulting in improved electrical conducting surface prepared through the ink through coating of paper/variety of substrate for biosensor/biofuel cell surface.

2.3.1.5. Viscosity of the graphite-PEG-sericin ink

The conductivity of the ink depends on the fluid rate and the composition of the ink. The fluid rate of ink is related to the ink viscosity. The viscosity of the ink was found to be around 0.11 Pa.s with respect to time (s) with the corresponding shear rate of $100s^{-1}$ (Figure 2.7) which is found to be suitable for producing uniform ink film traces on paper/variety of substrate either through hand written or via discretionarily coating (Chen et al., 2021).

2.3.2. Secondary structures of the protein

Analysis of secondary structures showed that sericin mostly contains *β*–sheets (35.4%) and random coils (37.1%) (Figure 2.8), which is in agreement with other reports

(Teramoto and Miyazawa, 2003). Interestingly, the *β*–sheets content of sericin was increased up to 38.2% upon the addition of PEG in the system. The increase in the *β*–sheets component reduces the aqueous solubility of the sericin protein, a phenomenon common to other proteins as well (Cho et al., 2003; Teramoto and Miyazawa, 2003). This fact highlights the aqueous stability of the nanocomposite ink prepared by mixing sericin in Graphite-PEG system as discussed above.

In a nutshell, the conducting inks of the present study can be applied over wide range of platform like human skin, paper, plant leaves etc, since it is made of biocompatible materials; through direct writing/ brushing technique. Again, it requires less amount of ink since direct writing/ brushing technique needs less amount of ink as compared to screen printing or other printing techniques (Bandodkar et al., 2015).

2.4. Conclusions

This work demonstrated for the first time the conductivity enhancement of graphite powder through material manipulation in a composite polymer matrix system. The reason for the enhancement has been ascribed to the transformation of the graphite powder to a crystalline form facilitated by a natural polymer, sericin in a microenvironment supported by PEG under ambient condition. The exact molecular mechanism for this transformation, however, needs further investigation to understand. The work also witnessed a significant improvement in the aqueous stability of the developed ink in the cellulosic paper surface. A substantial increase in *β*–sheets content of sericin under the influence of PEG in the nanocomposite matrix along with its increased viscosity has been attributed to the resulting aqueous stability of the ink. The prepared ink is particularly useful for preparing conducting traces through direct writing/ brushing technique. This has an advantage over screen printing or inkjet printing as it requires fewer amounts of ink and is also applicable over a wide range

of platforms. Again, the pastes are made from biocompatible polymers. This is particularly an important trait while preparing enzyme electrodes for the development of biosensor and biofuel cell. Some of the similar biocompatible conductive ink developed by previous worker has resistivity of their ink around~15 kΩ/cm (Bandodkar et al., 2015) which is equivalent to the conductivity of 0.05 mS/cm. Our developed ink exhibit conductivity of 11.2 mS/cm equivalent resistivity of 100 Ω/cm. Table 2.1 compares the resistivity of conductive traces made by different inks.

Figures

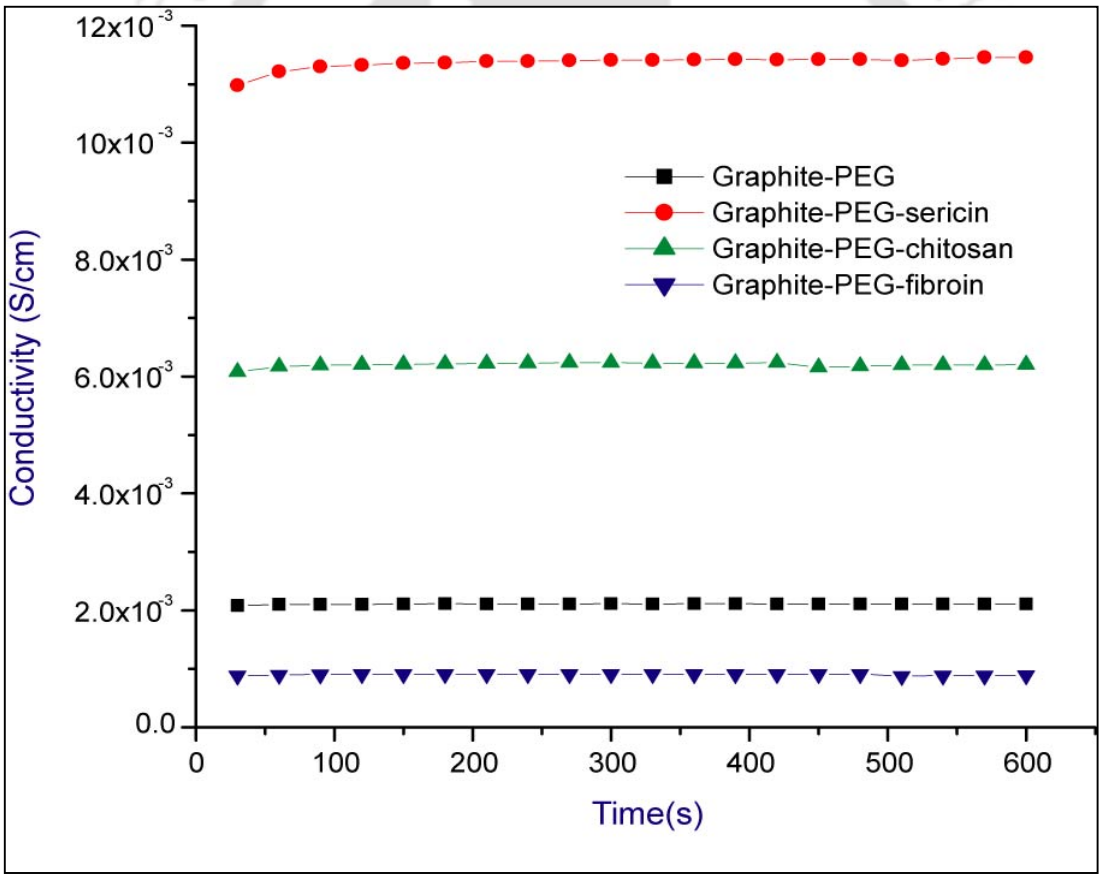

Figure 2.1: Conductivity versus time graph of various graphite conductive inks

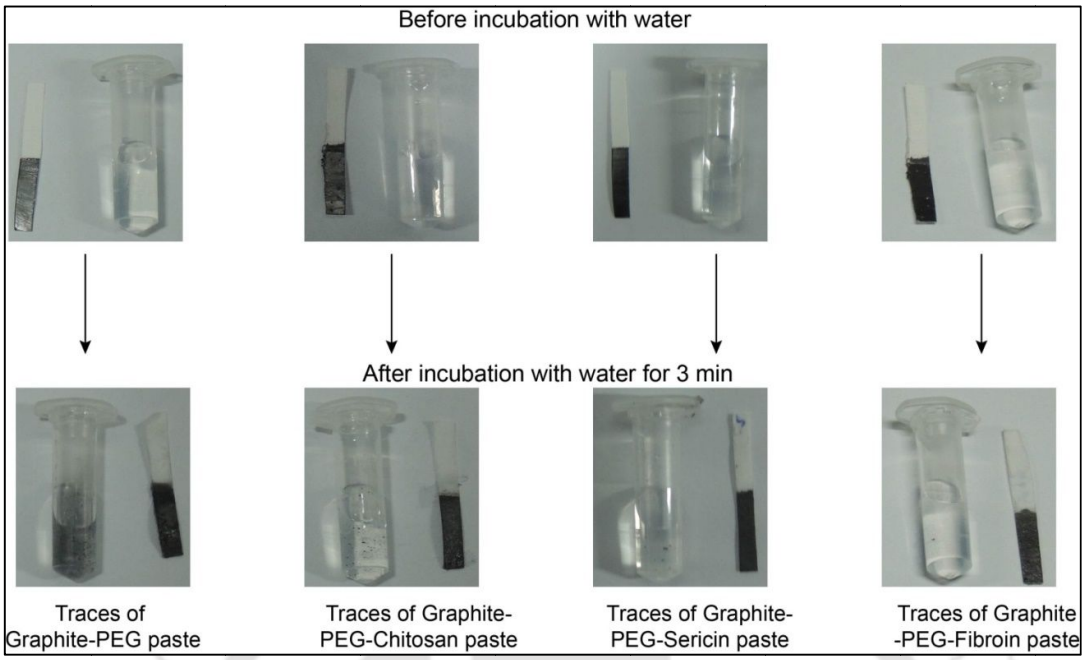

Figure 2.2: Images of the conductive traces over paper substrate made from Graphite-PEG, Graphite-PEG-Chitosan, Graphite-PEG-Sericin and Graphite-PEG-Fibroin conductive inks before and after incubation with water.

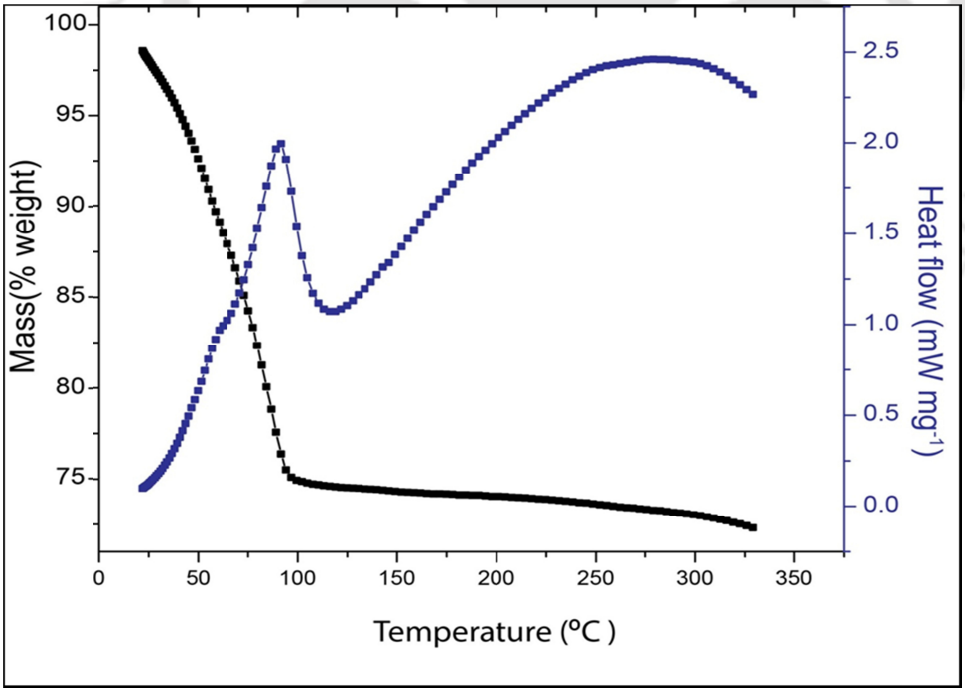

Figure 2.3: Differential scanning calorimetry (DSC) and thermo-gravimetric analysis (TGA) studies

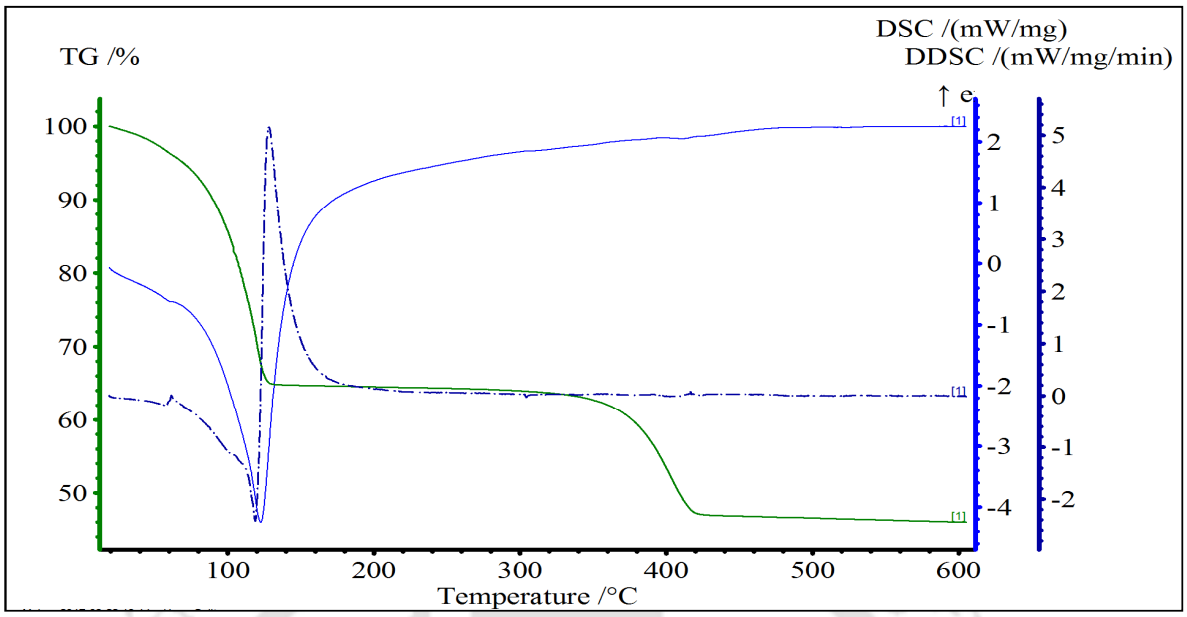

Figure 2.4: First derivative of DSC

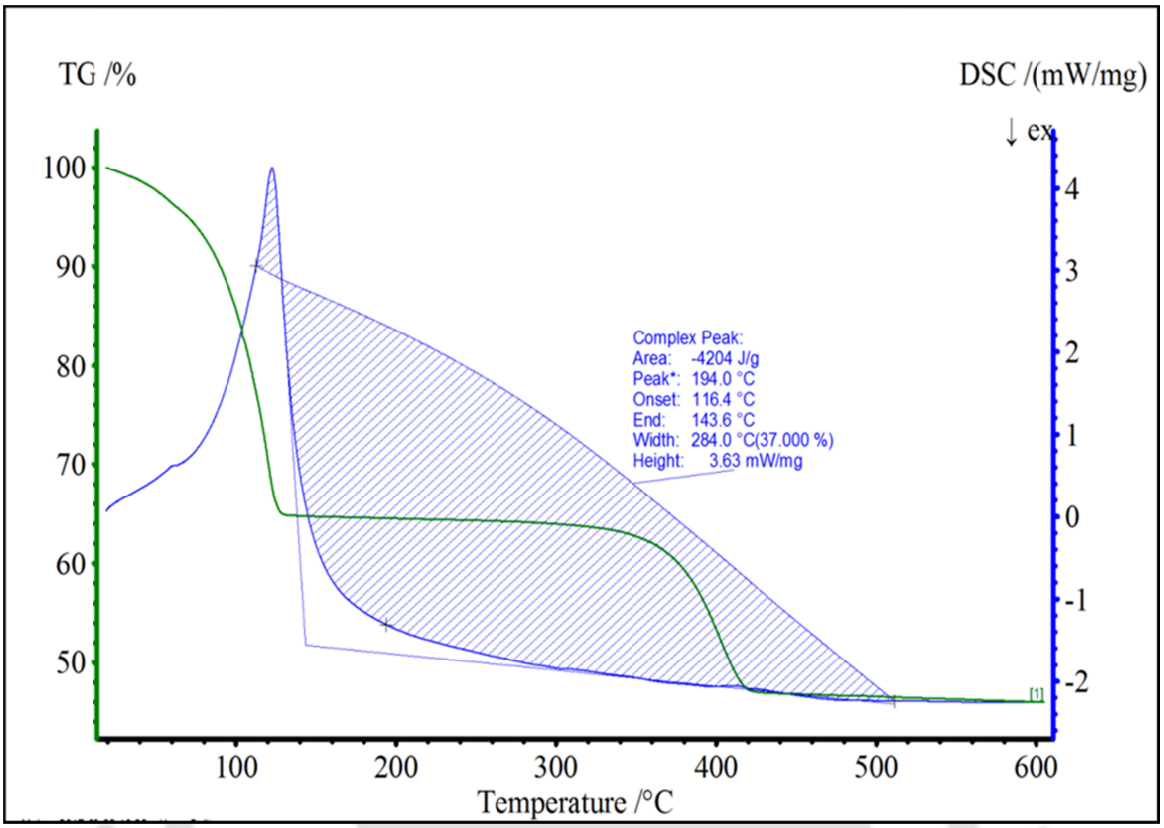

Figure 2.5: Complex peak graph of DSC of Graphite-PEG-Sericin

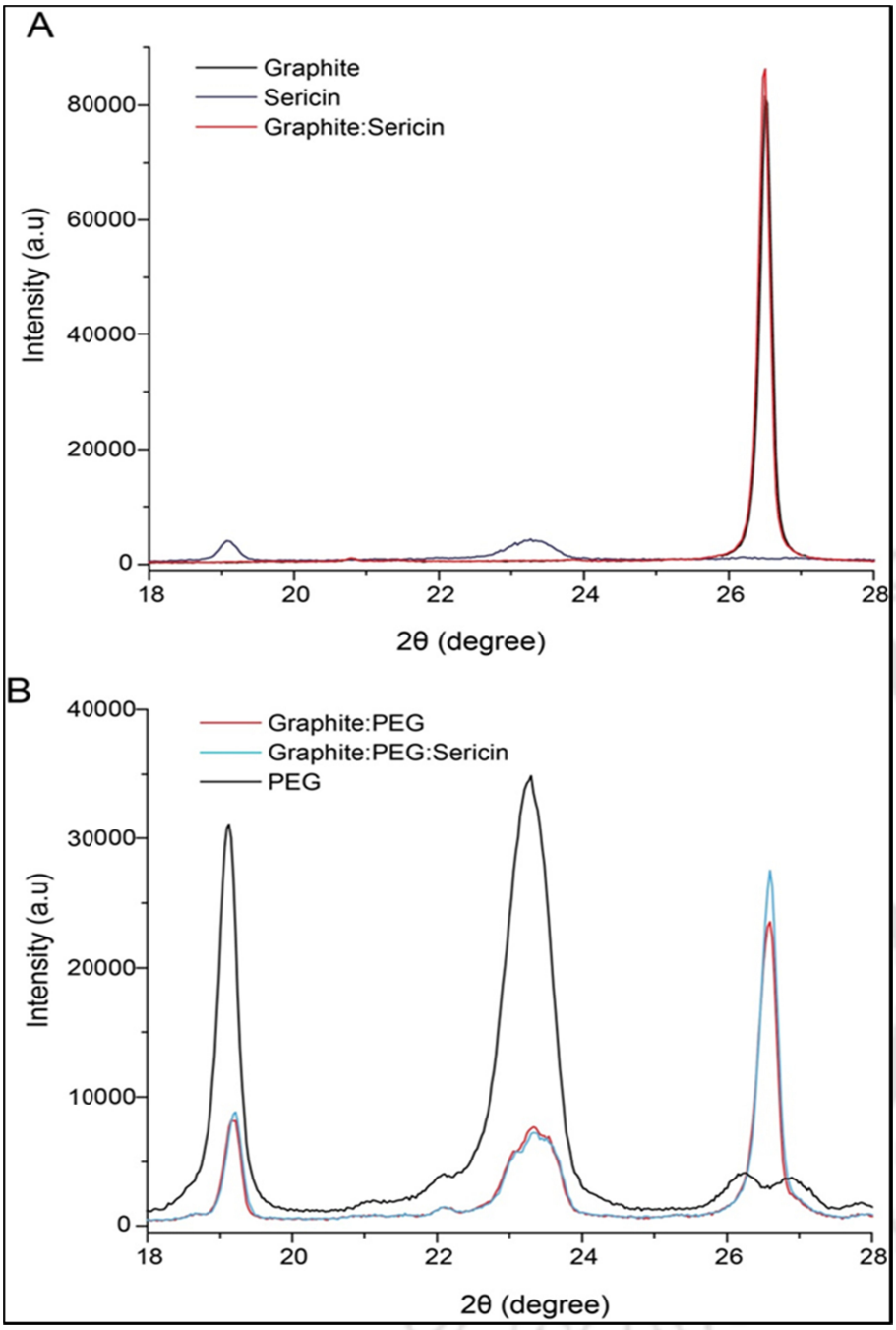

Figure 2.6: X-ray powder diffractometer (XRD) pattern of (A) Graphite, Sericin and Graphite-Sericin composite powder and (B) PEG, Graphite-PEG and Graphite-PEG-Sericin composite powder

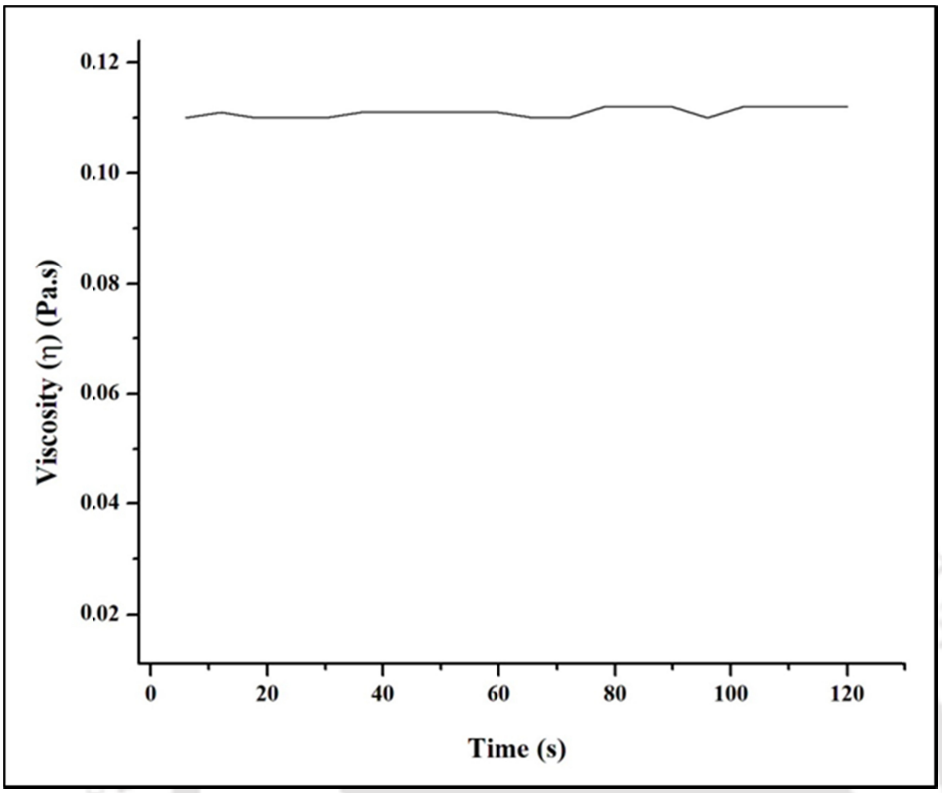

Figure 2.7: Viscosity of the Graphite-PEG-Sericin ink as a function of time

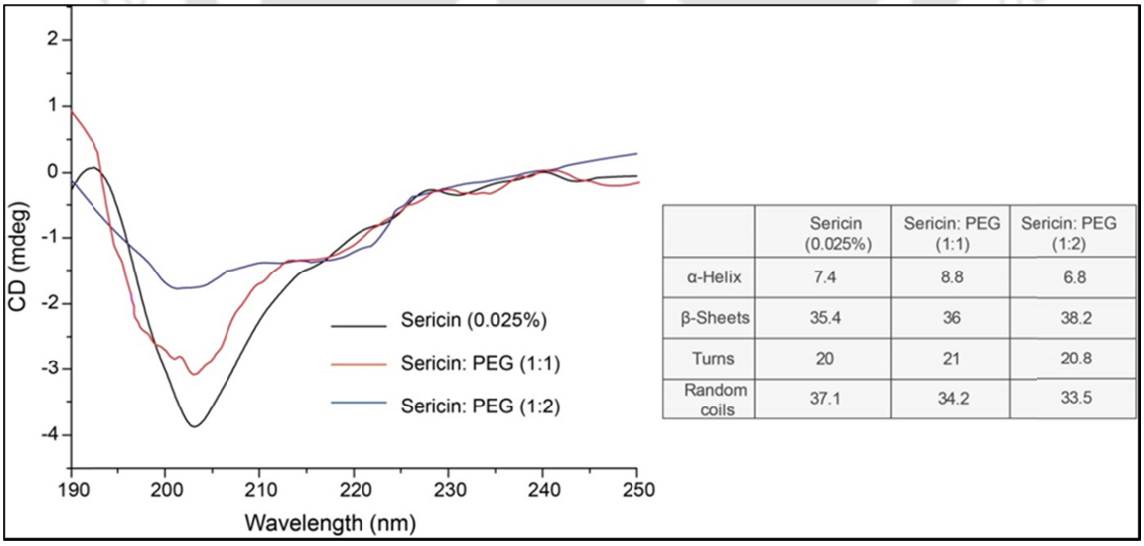

	Sericin (0.025%)	Sericin: PEG (1:1)	Sericin: PEG (1:2)
α-Helix	7.4	8.8	6.8
β-Sheets	35.4	36	38.2
Turns	20	21	20.8
Random coils	37.1	34.2	33.5

Figure 2.8: The Far-UV CD spectra of silk sericin (0.01 %), sericin-PEG composite

Tables

Method	Ink composition	Substrate	Resistivity	Reference
Roller pen	Graphite, PEG, water, chitosan, xylitol, methylene green	Office paper, alumina, skin, plant leaves	~15 kΩ/cm	Bandodkar et al., 2015
Fountain pen	SWCNT, water, sodium dodecyl benzene sulfonate	Office paper	Below 20 kΩ/cm	Han et al., 2014
Fountain pen	Carbon nanofibers, gellan gum water solution	Photo paper	97±20 kΩ/cm (for 1 layer) 3.4±0.1 kΩ/cm (for 10 layer)	Warren et al., 2013
brushing	Graphite, PEG, sericin, water	Chromatography paper	~100 Ω/cm	Present study

Table 2.1: Resistivity of conductive traces made by different inks

CHAPTER III

Fabrication and Characterization of Laccase-based Bioelectrode

CHAPTER III

Fabrication and Characterization of Laccase-based Bioelectrode

3.1. Overview

Laccase (EC 1.10.3.2) multi-copper redox enzyme, widely occurring in fungi and less frequently in higher plants and bacteria (Mayer and Staples, 2002), catalyzes the four-electron reduction of dioxygen to water along with the oxidation of substrate molecules (Thurston 1994) without forming toxic H_2O_2 molecule. Phenolic compounds act as the substrate for the enzyme laccase. The construction of laccase bioelectrode is simple as laccase does not require H_2O_2 as a co-substrate and any other external co-factor for its catalysis (Roy et al., 2005). Moreover, thermal tolerance is also a positive feature of laccase for bioelectrode applications (Kulys and Vidziunaite, 2003). Generally, laccase contains four copper atoms classified into type 1 (T1), type 2 (T2), and type 3 (T3), according to their spectroscopic and magnetic properties. T1, the substrate binding site of the enzyme is

involved in the oxidation of substrate and transfer of electron to T2/T3 cluster, while T3 is responsible for oxygen uptake and as a whole, this T2/T3 site is responsible for the reduction of O_2 to water (Solomon et al., 1996; Morozova et al., 2007).

To initiate proper electrical communications between the redox enzymes and the conductive electrode support, various conductive nanomaterials and polymers are used to develop enzyme bioelectrodes. Among the various nanomaterials and polymers, Multiwalled carbon nanotubes (MWCNT) and Osmium polymers are widely used for fabricating bioelectrodes (Agui et al., 2008; Gooding, 2005). MWCNTs offer many advantages such as their similarity in length scales with proteins, good electronic communication with the active site of redox proteins and their high surface areas for higher enzyme loading on the electrode surface (Gooding, 2005). Further, MWCNTs exhibit good electrical conductivity, have high mechanical strength and antifouling property that may contribute to improve sensitivity and stability of a biosensor (Vatsyayan et al., 2010). Osmium polymer is known as a potential electron transfer mediator between many redox enzymes and electrodes. Due to the hydrophobic nature MWCNTs are generally dispersed on the surface of the electrode using hydrophobic polymer chain of Nafion (Nf) (Wang et al., 2003).

Phenolic compounds constitute a large group of organic pollutants, which are widely distributed throughout the environment. These compounds are used in the large scale manufacture of plastics, resins, pesticides, explosives, detergents etc. Phenols are also breakdown products of natural organic compounds like humic substances, lignins and tannins (Wollenberger et al., 2008). Certain phenols are highly toxic, allergenic, carcinogenic and hepatotoxic. Several of these compounds are highly resistant to biotic and abiotic degradation and therefore, remain in the environment at toxic levels. These phenolic compounds are highly toxic for humans and animals, as they are rapidly absorbed through the skin and mucous membrane. Hence, there is a continuously increasing demand for selective and

sensitive detection of phenols like pyrocatechol and their determination is very important for evaluating the total toxicity of an environmental sample.

Again, pyrocatechol (1, 2-dihydroxybenzene) or catechol is one of the most important phenolic compounds and may be released to the environment during its manufacture and use (Mersal 2009). It has some applications, like, as reagent for photography, dyeing fur, rubber and plastic production and in the pharmaceutical industry. Although pyrocatechol is utilized in many industrial applications, they are highly toxic compounds. In living organisms, it may react with different biomolecules like DNA, protein, membranes and leads to non-repairable damage (Schweigert et al., 2001). Pyrocatechol in combination with heavy metals (e.g. Cu^{2+}, Fe^{3+}) and in presence of molecular oxygen can cause breakage of DNA strands (Li and Trush 1994).

Hence, for the above reasons, in the present study, pyrocatechol has been used as the model compound for developing laccase biosensor. Again, it has been used as the model compound to study the reductive catalytic property of the laccase-based bioelectrode to explore the efficiency of the enzyme as a catalyst for the development of biofuel cell cathode. Here, the pyrocatechol has been proposed to use as a reductive equivalent in the reaction for conveniently monitoring the catalytic reduction of molecular oxygen on the bioelectrode surface. The laccase from *Trametes versicolor* was immobilized in a nano-composite matrix including osmium redox polymer on the surface of a glassy carbon electrode (GCE). A detailed account of the characterization of the fabricated laccase electrode, its kinetic parameters and response of the bioelectrode for the substrate pyrocatechol are presented here.

3.2 Experimental approaches

3.2.1. Reagents and stock solutions

Laccase (p-diphenol: dioxygen oxidoreductase) from *Trametes versicolor* (0.5 U / mg solid), Nafion 117 (Nf) (5% w/v in isopropanol), MWCNT with 95% purity (10–15 nm outer diameter, 2-6 nm inner diameter and 0.1-10 μm length), osmium tetroxide on poly-4(vinyl pyridine) (OsO_4 on P4VP) and ethylbenzene were bought from Sigma-Aldrich (India). Tri-sodium citrate from Qualigens (India), monohydrate citric acid from Rankem (India) and pyrocatechol from Spectrochem (India) were purchased. VULCAN XC 72 grade carbon black (CB) was purchased from Cabot India Pvt. Ltd. GCE (3.0 mm diameter) was purchased from Bioanalytical Systems Inc., USA. The stock solution of laccase (10 $mg.ml^{-1}$) was freshly prepared in 0.1M sodium citrate buffer (pH 4.7), prior to being used. 0.1 M sodium citrate buffer solution (pH 4.7) prepared with tri-sodium citrate and monohydrate citric acid was employed as the supporting electrolyte. Again, a working solution of pyrocatechol (1μM) was freshly prepared in 0.1 M sodium citrate buffer (pH 4.7) prior to being used. The entire experiment was performed using Elix Millipore water with resistivity of 15 MΩ cm at 25 ^{0}C.

3.2.2. Apparatus and measurements

Electrochemical measurements like CV and differential pulse voltammetry (DPV) were performed with a potentiostat (Autolab PGSTAT 1212, Eco Chemie, Netherland). The measurements were done in a three-electrode system containing platinum rod as the counter electrode, Ag/AgCl (saturated KCl) as reference electrode, and GCE or modified GCE as the working electrode. All potentials were measured and reported relative to the Ag/AgCl reference electrode. All experiments were performed at room temperature (RT). The images

of the morphological characteristics of the bioelectrode were obtained on a scanning electron microscope (SEM) (Leo 1430vp, Germany).

3.2.3. Preparation of bioelectrode

A GCE (diameter, 3 mm) was cleaned first by polishing with alumina slurry, then washed ultrasonically with 70 % ethanol and deionized water separately for 5 min each and finally allowed to dry under clean air at RT. A total of 2 mg MWCNTs and 6 mg CB was added in 4 ml Nf and the mixture was sonicated for 30 mins to form a homogeneous mixture. 5µl of the mixture was dropped onto the GCE and then allowed to dry under clean air to make GCE/MWCNT-CB-Nf electrode. Thereafter, 10 mg OsO_4-P4VP in 1 ml ethylbenzene was sonicated for 1 hour and then 1mg MWCNT was added to it. The mixture was sonicated again for 1 hour and then 8 µl of the homogeneous mixture was dropped onto MWCNT-CB-Nf coated GCE to make the GCE/MWCNT-CB-Nf-OsO_4–P4VP electrode. When the nano-composite mixture on the electrode surface was in semi-dry condition, a total of 10 µl of a freshly prepared laccase enzyme stock solution was dropped onto it that resulted in the GCE/MWCNT-CB-Nf-OsO_4–P4VP-laccase bioelectrode. The fabricated bioelectrode was then dried under clean air in the laminar hood at RT. The bioelectrode was immersed in 0.1M sodium citrate buffer (pH 4.7) for 15 min prior to being used. The bioelectrode was stored in 0.1 M sodium citrate buffer (pH 4.7) at 4 °C when not in use.

Here, in this system, laccase was immobilized by simple electrostatic interaction between the enzyme and OsO_4-P4VP. Laccase is negatively charged in pH 4.7 and osmium polymer is positively charged, hence there existed electrostatic interaction between laccase and osmium polymer.

3.3. Results and discussion

3.3.1. Morphological characterization of the bioelectrode

The surface morphology of laccase immobilized on GCE/MWCNT-CB-Nf-OsO_4–P4VP was performed using SEM. Figure 3.1 shows the SEM images of the electrode at different fabrication steps. Blank GCE shows a plain homogenous surface (Figure 3.1A) which reveals GCE is devoid of any immobilized chemical; whereas the GCE/MWCNT-CB-Nf electrode shows porous morphology (Figure 3.1B), where intertwined thread-like structure of MWCNTs is clearly visible in the image with higher magnification (inset, Figure 3.1B). When solution of OsO_4–P4VP-MWCNT was added on the surface of GCE/MWCNT-CB-Nf electrode, the surface turned into patchy morphology indicating the OsO_4–P4VP polymer set in a pattern on the surface of the MWCNT-CB-Nf layer (Figure 3.1C). Now, when laccase was added to the MWCNT-CB-Nf-OsO_4–P4VP film, the surface morphology of the generated bioelectrode changed markedly (Figure 3.1D). The patchy surface was filled up and small globular structures could be seen at many places. This indicates the adsorption of the laccase in the supporting nano-composite polymer matrix on the electrode surface.

3.3.2. Electrochemical characterization of the bioelectrode

CV was carried out in sodium citrate buffer (pH 4.7) separately purged with argon and oxygen gas for bare GCE and different modified GCE at major steps of bioelectrode fabrication to identify the redox potentials of the fabricated working bioelectrodes (Figure 3.2). No clear redox peaks except at around -0.70 V were observed for bare GCE (Figure 3.2A, curve a) and GCE-MWCNT-CB-Nf (Figure 3.2A curve b), suggesting that both the MWCNT and Nf are electro-inactive in this potential window. The cathodic peak at -0.70 V indicates O_2 is electrochemically reduced at the electrode surface. After the adsorption of

MWCNT-CB-Nf on the GCE surface, an increase in the background current intensity was observed which is attributed to the increased electroactive surface area of MWCNTs (Figure 3.2A curve b). When OsO_4–P4VP is adsorbed on MWCNT-CB-Nf, the magnitude of the background current decreases with a pair of weak redox peaks appearing at -0.08 V (anodic) and at -0.12 V (cathodic) (Figure 3.2A curve c), which are attributed to the redox potential of osmium complex. The laccase enzyme when adsorbed in the nano-composite matrix on the electrode surface, two sharp quasi reversible peaks at 0.34 V (anodic) and at 0.23 V (cathodic) were observed (Figure 3.2A curve d). The formal potential of the redox couple calculated from the average value of anodic and cathodic peak potentials [$(E_{pa}+E_{pc})/2$] was 0.28 V. The present value is in agreement with redox potential values previously determined for laccase which fall in the range from 0.23 V to 0.59 V (vs Ag/AgCl) for laccase from different species (Ivnitski et al., 2010; Shleev et al., 2006). The result implies that at a cathodic potential of about 0.23 V molecular oxygen gets reduced in the redox centre of laccase. The oxidized redox centre of the laccase is regenerated at an anodic potential of 0.34 V. The result is supported by the fact that when oxygen was expelled from the buffer solution by purging with argon gas for 15 min, the magnitude of current of the redox pair at 0.34 V and 0.23 V was significantly decreased (Figure 3.2B curve a) and the current in the redox pair was regenerated again upon passing the oxygen gas through the buffer solution (Figure 3.2B curve b). Analysis of the copper centres of multicopper oxidases in the presence of a chelating agent specific for T2 copper centre has shown that a potential area between 0.0 V and +0.4 V (vs Ag/AgCl) belongs to O_2 reducing site for the trinuclear copper center of the enzyme (Ivnitski et al., 2009).

In absence of oxygen, a clear second redox pair at -0.03 V (anodic) and -0.15 V (cathodic) was also observed (Figure 3.2B curve a). The result is attributed to the existence of electrical communication of two copper based redox centres in the laccase enzyme with the

electrode. When pyrocatechol was added to the buffer, purged with O_2, a cathodic current of the bioelectrode in a broad potential range encompassing both the cathodic potentials obtained in absence of oxygen was recorded (Figure 3.2B curve c). Contrary to the high cathodic current, only a negligible increase in anodic current was detected. The result implies that the oxidation of the substrate pyrocatechol on the electrode surface proceeds biocatalytically and reduction proceeds electro-catalytically as shown in the scheme 3.1. The broad reduction potential is ascribed to the cumulative electrocatalytic reduction of the redox centre (~0.23 V) of a fraction of the enzymes and 1, 2-benzoquinone (~0.14 V), which is generated by the biocatalytic oxidation of pyrocatechol. The 1, 2-benzoquinone generated on the electrode surface thus entered in a redox recycled process between biocatalytic oxidation of pyrocatechol and electrocatalytic reduction of the quinone.

Again, to obtain the various electron transfer parameters of the bioelectrode, CV was carried out with GCE/MWCNT-CB-Nf/OsO_4-P4VP/laccase bioelectrode in sodium citrate buffer (0.1 M, pH 4.7) at different potential scan rates (υ) (30 to 700 mV/s). At υ = 50 mV/s, the peak separation (ΔE_p) was about 106 mV (Figure 3.3), which is more than the peak separation of a reversible process (59 mV), indicating a quasi-reversible redox process (Scott and Lukehart 2007). Moreover, as the scan rate increases, the anodic (E_{pa}) and cathodic (E_{pc}) peak potentials shift to more positive and more negative values, respectively, increasing the ΔE_p further suggesting a quasi-reversible process. Besides this, the magnitude of anodic (I_{pa}) and cathodic (I_{pc}) peak currents increase linearly with increasing scan rate in the range of 30 to 700 mV/s (Figure 3.3a) as expected for a surface-confined redox process and indicating a thin layer electrochemical behavior (Scott and Lukehart 2007). For a quasi-reversible wave, the relationship between peak potential and scan rate conforms to the following equation (Laviron equation):

$$E_p = E^0 + \frac{RT}{\alpha nf} - \frac{RTln\vartheta}{\alpha nf} \quad \text{.....3.1}$$

Where E_p is the peak potential (cathodic or anodic), E^0 is the apparent standard potential. R is the thermodynamic gas constant ($8.314 JK^{-1}mol^{-1}$), F is the Faraday constant ($96500 C.mol^{-1}$), T is the temperature (298K). The symbols n and υ are the electron transfer number and scan rate, respectively.

The value of charge transfer coefficient (α) can be determined from equation (3.2) by using the slopes from the linear plots of E_{pa} and E_{pc} versus log υ (Fig. 3.3b).

$$\alpha = \frac{\delta_{pa}}{\delta_{pa} - \delta_{pc}} \quad \text{.....3.2}$$

Where, δ_{pa} and δ_{pc} are the anodic and cathodic slopes of linear region of the plot, respectively. Again, slopes for the anodic and cathodic peaks can be calculated following these equations:

$$Anodic\ slope\ (\delta_{pa}) = \frac{2.3RT}{(1-\alpha)nF} \quad \text{.....3.3}$$

$$Cathodic\ slope\ (\delta_{pc}) = \frac{-2.3RT}{\alpha nf} \quad \text{.....3.4}$$

The symbols F, R, T have their usual meanings. From the above equations, α is calculated to be 0.52. From Figure 3.3b, anodic slope δ_{pa} was found to be 0.11. By using equation (3.3), the value of n was found to be 1. Thus, this result revealed that the redox reaction of laccase in MWCNT-CB-Nf-OsO_4-P4VP film was a single electron transfer process. The surface concentration of the ionic species (Γ) ($mol.cm^{-2}$) onto GCE/MWCNTs–CB-Nf-OsO_4-P4VP/laccase bioelectrode can be estimated from the plot of peak current versus scan rate (υ) (Figure 3.3a) using Brown-Anson model that is based on the following equation (3.5) (Laviron 1979):

$$I_p = \frac{n^2F^2\Gamma A\vartheta}{4RT} \quad \text{.....3.5}$$

Where, n is the number of electrons transferred, which is 1, and A is the surface area of the electrode (0.07 cm^2). When the scan rate (υ) was 100 $mV.s^{-1}$, the anodic peak current (I_{pa}) was 8.7×10^{-5}A. The total surface concentration was found to be 1.32×10^{-8} $mol.cm^{-2}$. The heterogeneous electron transfer rate constant (k_s) of the bioelectrode could be obtained by the following equation (3.6) (Laviron 1979):

$$\log(k_s) = \alpha\log(1-\alpha) + (1-\alpha)log\alpha - \log\left(\frac{RT}{nF\vartheta}\right) - \alpha(1-\alpha)\frac{nF\Delta E_p}{2.3RT} \text{.....3.6}$$

The above equation is valid only if the difference of E_{pa} and E_{pc} (ΔE_p) is greater than 200 mV. Taking ΔE_p = 217 mV, at υ = 100 mV/s, n = 1 and α = 0.52, the value of k_s for the bioelectrode was calculated to be 0.67 s^{-1} which signifies efficient electron transfer between ionic species in MWCNT-CB-Nf-OsO_4P4VP-laccase film and the electrode. The Electron transfer characteristics for the bioelectrode are summarized in Table 3.1.

3.3.3. Electrochemical response of laccase bioelectrode to pyrocatechol

Laccase bioelectrode studies were carried out to evaluate the contribution of each modifier materials employed in developing the biosensor. Figure 3.4 shows the voltammograms (DPV) obtained using the a) bare GCE, b) GCE/laccase, (c) GCE/MWCNT-CB/laccase (d) GCE/OsO_4-P4VP/laccase, and e) GCE/MWCNT-CB-Nf-OsO_4–P4VP-laccase in 16 nM pyrocatechol in 0.1 M sodium citrate buffer solution (pH 4.7) in a potential range for cathodic current. The cathodic current of 1, 2-benzoquinone reduction to pyrocatechol was used as the analytical response (cathodic current values are shown in the inset of Figure 3.4). No current was produced with bare GCE (curve a). However, GCE with immobilized laccase had produced current (1.148×10^{-6} A) (curve b), indicating laccase oxidizes pyrocatechol to 1, 2-benzoquinone, which is electrochemically reduced at the electrode

surface. The current was further increased when laccase was immobilized with MWCNT (curve c) or OsO_4–P4VP (curve d) on GCE, while the magnitude of current with the OsO_4–P4VP was higher than the bioelectrode containing MWCNT alone. Interestingly, the level of current was highest when laccase was immobilized on GCE/MWCNT-CB-Nf-OsO_4–P4VP matrix (curve e). Results infer that both MWCNT and osmium polymer provides a better electroactive environment for electron exchange between the electrode and the benzoquinone, and their coexistence in the nanocomposite matrix further facilitates the reduction of 1,2-benzoquinone synergistically on the electrode surface.

3.3.4. Analytical performance of the laccase bioelectrode for pyrocatechol determination

The response characteristics of the GCE/MWCNT-CB-Nf-OsO_4-P4VP-laccase electrode towards pyrocatechol were investigated by DPV in the potential range of -0.05 to +0.3V vs. Ag/AgCl, with a step potential of 50 mVs^{-1}. The GCE/MWCNT-CB-Nf-OsO_4-P4VP-laccase electrode was subjected to the increasing amount of pyrocatechol concentration. It was observed that with the addition of substrate, the current was increasing at +0.14 V, with a negligible shift in peak position (Figure 3.5A). It indicates the electrochemical reduction to pyrocatechol from 1, 2-benzoquinone was obtained at a potential of +0.14 V (vs. Ag/AgCl). Here the cathodic current of 1, 2-benzoquinone reduction to pyrocatechol was used to construct the response curve. The response curve was constructed with current *vs* concentration of pyrocatechol as shown in the Figure 3.5B. As can be observed, the cathodic current increased with pyrocatechol concentration and the response curve was linear from 3.98 nM to 16.71 nM with the regression coefficient $R^2 = 0.97$. The response characteristics of the bioelectrode for pyrocatechol are summarized in Table 3.1. The detection limit (DL) for the constructed biosensor was determined from the expression DL = 3×SD / sensitivity (where SD is the estimated standard deviation for the points used to

construct the calibration curve and sensitivity is its slope). The detection limit obtained with the present fabricated laccase biosensor is lower than aminopyrene reduced graphene oxides-/Chitosan/GCE hybrid film (Zhou et al., 2013), glutaraldehyde functionalized chitosan-MWCNT/GCE (Tan et al., 2009), MB modified MCM-41/ PVA composite film / Au (Xu et al., 2009) and CNT-Chitosan composite film (Liu et al., 2006) matrix based laccase biosensor for determination of pyrocatechol. The high sensitivity of the fabricated bioelectrode over other reported laccase biosensors emphasizes the advantage of MWCNT-CB-Nf-OsO_4-P4VP based electrode for pyrocatechol sensing over other matrices. Based on the CV and DPV studies, the electrocatalytic mechanism of the fabricated bioelectrode in detecting pyrocatechol can be proposed by the following schematic diagram.

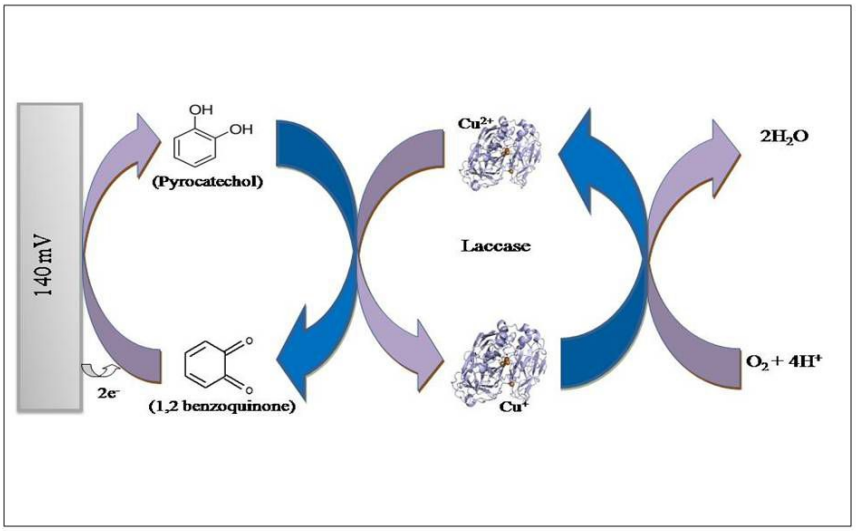

Scheme 3.1. Schematic representation of laccase catalyzed oxidation of pyrocatechol with its subsequent electrochemical reduction on the bioelectrode.

3.3.5. Operational stability, storage stability and reproducibility of the bioelectrode

The operational stability of the bioelectrode was examined by subjecting a freshly prepared bioelectrode at optimal working conditions to a 15 nM pyrocatechol solution and

assessing its response successively for 15 times for a period of 5 h (figure 3.6). After each measurement, the bioelectrode was kept in sodium citrate buffer (0.1 M, pH 4.7). It was observed that the bioelectrode retained ~94 % of its initial activity at the end of the 15 measurements. This high operational stability indicates that there was negligible enzyme leakage from the bioelectrode. This high operational stability may be due to the biocompatible nanocomposite matrix used for immobilization of the enzyme. The storage stability of the bioelectrode was checked by carrying out response measurements at the regular intervals of three days and it was found that it retained about 81% of its initial activity even after three weeks when stored in sodium citrate buffer (pH 4.7) at 4 ^{0}C. The fabrication reproducibility of the bioelectrode was estimated from the response to 15 nM pyrocatechol at three bioelectrodes prepared by the same procedure. The results showed an acceptable reproducibility with a relative standard deviation of 2.8 % for the fabricated bioelectrode.

3.3.6. Interference study

The effect of some potential interferents present in the environment sample such as sodium fluoride (NaF), sodium azide (NaN_3), magnesium sulfate ($MgSO_4$) and zinc sulfate ($ZnSO_4$) on biosensor response was studied (figure 3.7). The response was examined by separately exposing the sensor in 4 nM pyrocatechol solutions with the interferents in 1:1 ratio. Selectivity coefficient (*SC*) of the biosensor for each interferent was estimated with respect to the response of the biosensor obtained when it is subjected to only pyrocatechol using the formula, $SC = I_{c+I} / I_{c,}$ where I_{c+i} and I_c (Saxena et al., 2011a) are biosensor response for pyrocatechol (4 nM) in the presence and absence of each interferent, respectively. In most of the cases, it was found that the contribution of these compounds to the biosensor response is ≤ 5 %, implying negligible significant interference. This high sensitivity towards pyrocatechol and less significant interference from other interfering agents may be due to osmium polymer and Nf present in the matrix. The positively charged

osmium polymer is likely to prevent the positively charged interfering compounds whereas negatively charged Nf is known to prevent negatively charged soluble compounds (Saxena et al., 2011b) to penetrate this polymer based enzyme nano-composite matrix. This study implies that the bioelectrode could be used for pyrocatechol determination without any significant interference from the substances present in the aqueous test sample.

3.4. Conclusions

The study aimed at fabricating an enzymatic biocathode for biofuel cell application. For this purpose, GCE-MWCNT-CB-Nf-OsO_4-P4VP-laccase bioelectrode was fabricated where, GCE was modified by MWCNT and CB, uniformly dispersed in Nf matrix; laccase was immobilized onto this MWCNT-CB-Nf film in which OsO_4-P4VP was used as a mediator. The kinetic parameters at the electrode namely, heterogeneous electron transfer rate constant (k_s), charge transfer coefficient (α) and surface concentration of the ionic species (Γ) were estimated. The response of the electrode for oxygen substrate at the determined formal potential of laccase was established. The results infer the potential application of the constructed bioelectrode as oxygen breathed biocathode for biofuel cell application. The bioelectrode also offers a reliable electrochemical response towards pyrocatechol in a biocatalytic mode. The results of response characteristics, operation stability, minimum detection limit and interference studies also validate the potential application of this stable laccase-based bioelectrode for sensitive, quantitative, and selective detection of pyrocatechol in aqueous samples.

Figures

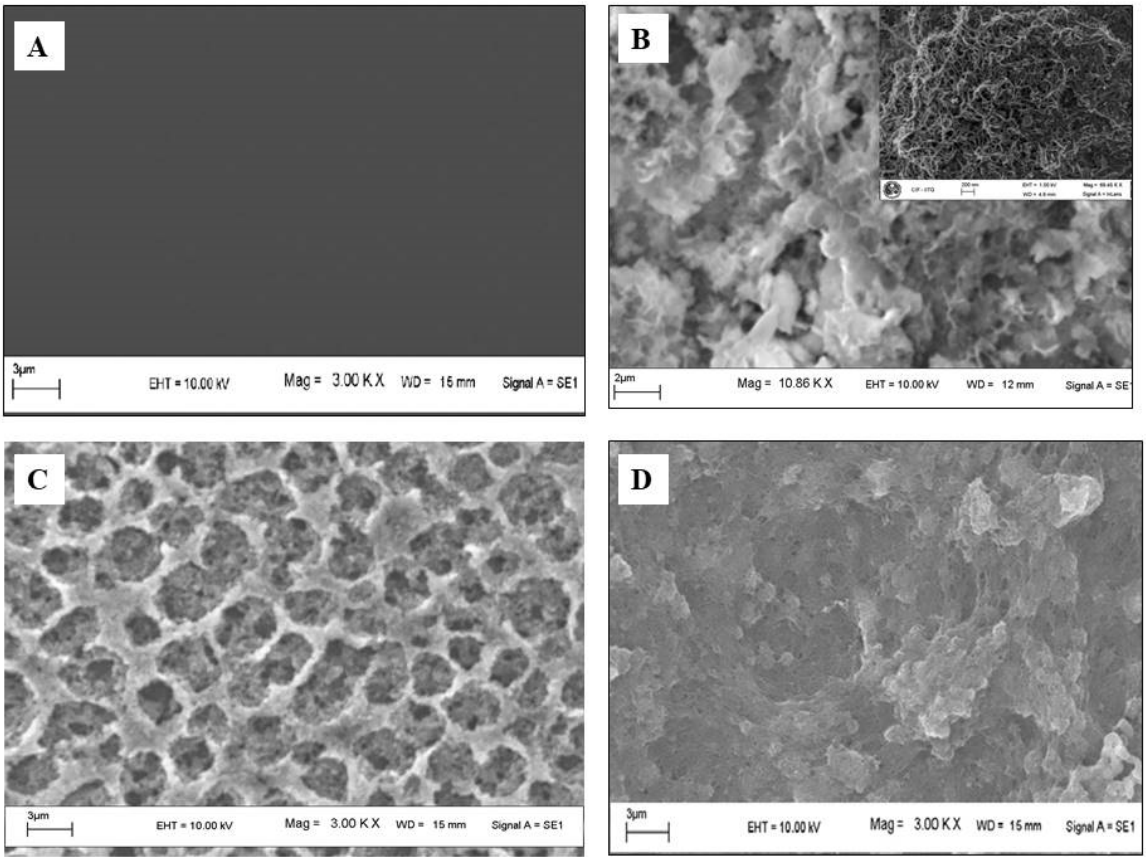

Figure 3.1: SEM images of (A) GCE, (B) GCE/MWCNT–CB–Nf, (C) GCE/MWCNT–CB–Nf–OsO_4–P4VP and (D) GCE/MWCNT–CB–Nf–OsO_4–P4VP–laccase.

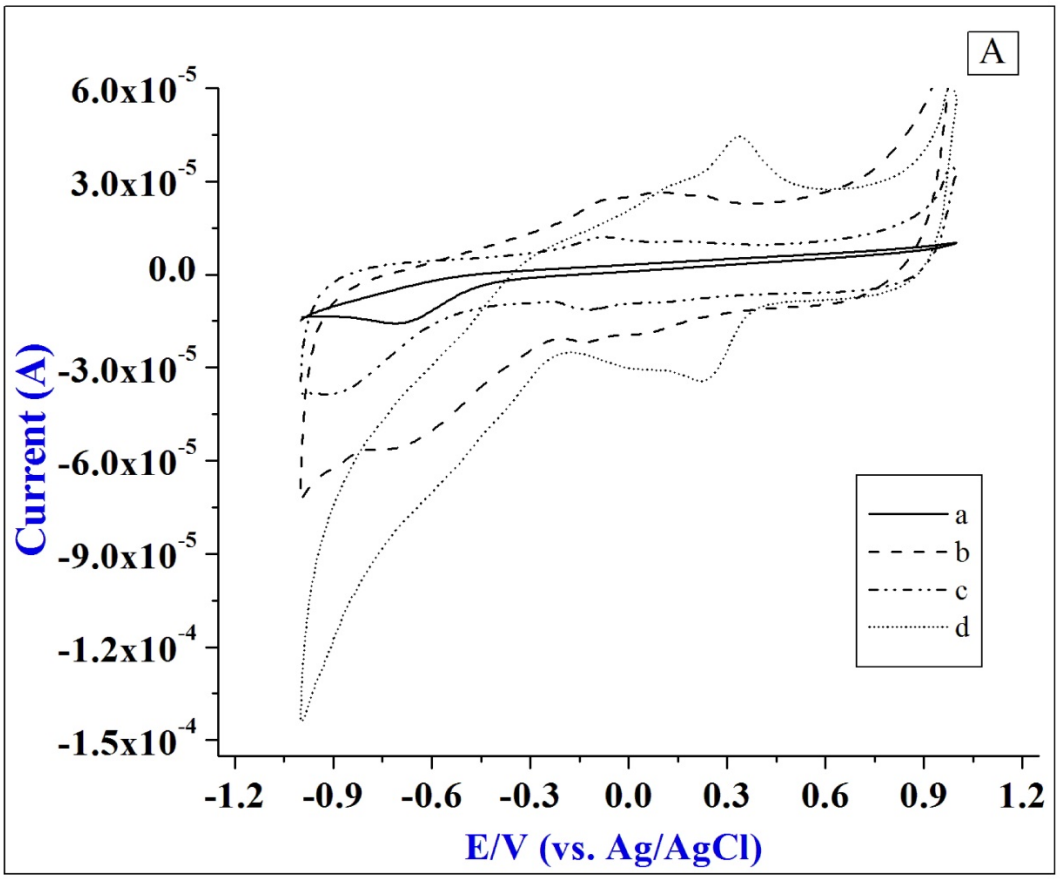

Figure 3.2A: CV of (a) GCE (—), (b) GCE/MWCNT–CB–Nf (- - -), (c) GCE/MWCNT–CB–Nf–OsO4–P4VP (–··–··), (d) GCE/MWCNT–CB–Nf–OsO_4–P4VP–laccase (····), in O_2 gas purged solution of 0.1 M sodium citrate buffer (pH 4.7) at a scan rate of 50 $mV.s^{-1}$.

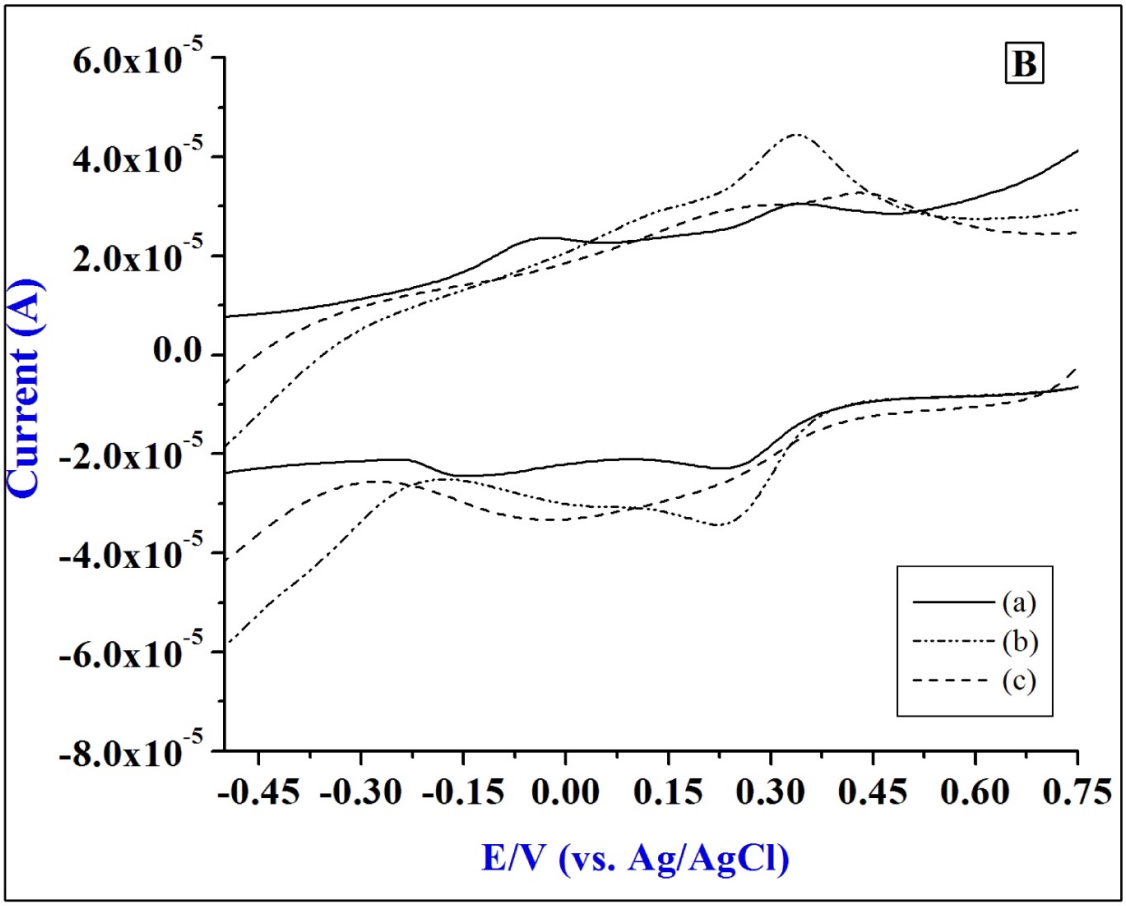

Figure 3.2B: CV of GCE/MWCNT–CB–Nf–OsO_4–P4VP–laccase electrode with (a) argon (—), (b) oxygen (–··–··–), and (c) pyrocatechol (- - -) in 0.1 M sodium citrate buffer (pH 4.7).

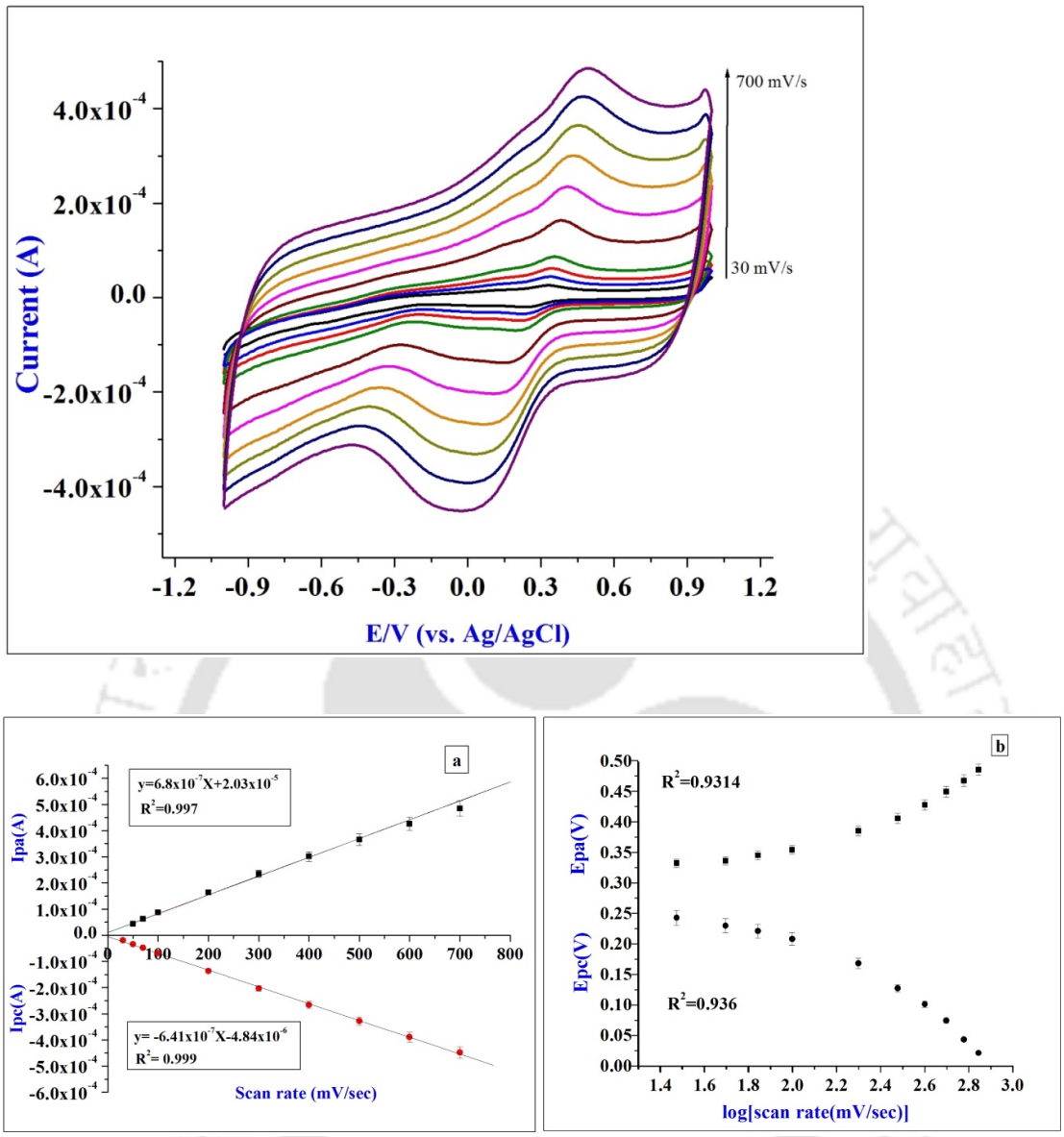

Figure 3.3: CV of laccase electrode with increasing scan rates viz. 30, 50, 70, 100, 200, 300, 400, 500, 600, 700 mV/s in 0.1 M sodium citrate buffer (pH 4.7) purged with O_2 (a) Plot of anodic (I_{pa}) and cathodic (I_{pc}) peak currents vs. scan rate (b) Plot of anodic (E_{pa}) and cathodic (E_{pc}) peak potentials vs. log (scan rate).

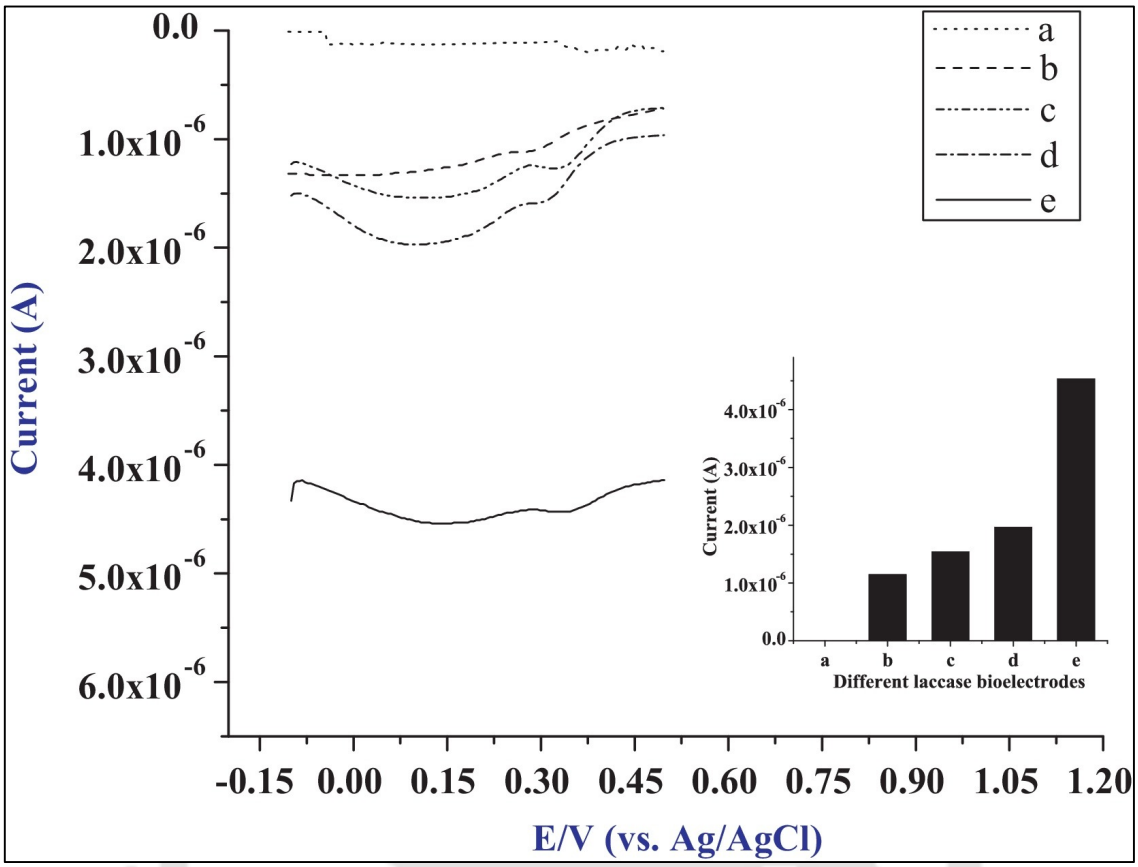

Figure 3.4: DPV of (a) GCE (⋯⋯), (b) GCE–laccase (- - -), (c) GCE/MWCNT–CB–laccase (–··–··–), (d) GCE/OsO4P4VP–laccase (–·–·–) and (e) GCE/MWCNT–CB–Nf–OsO4–P4VP–laccase (—) in 16 nM pyrocatechol in 0.1 M sodium citrate buffer solution (pH 4.7). Inset: cathodic peak current values for bare GCE and different laccase bioelectrodes.

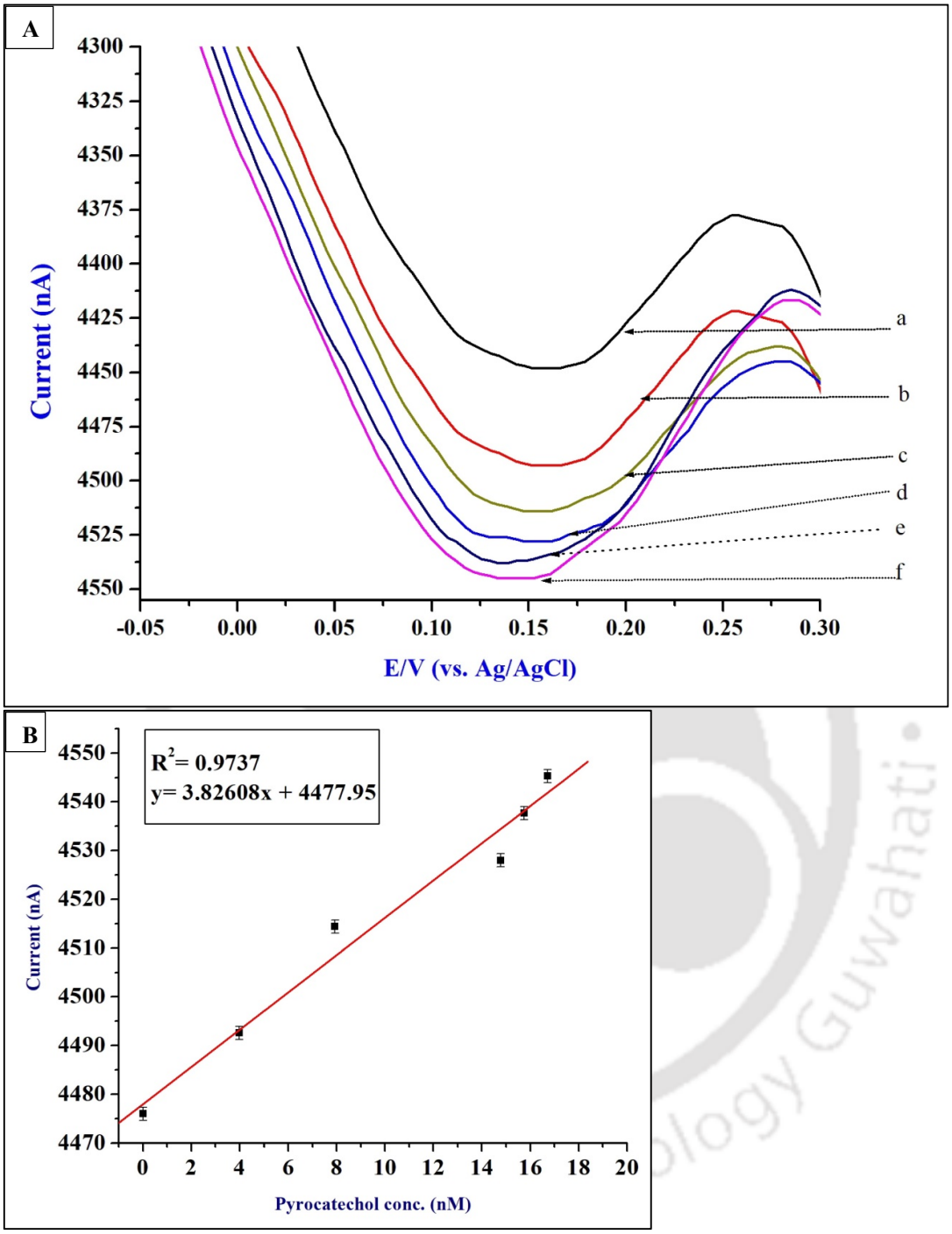

Figure 3.5: (A) DPV of laccase biosensor with increasing substrate concentration (nM): (a) 0, (b) 3.98, (c) 7.93, (d) 14.77, (e) 15.74, (f)16.71. (B) Response curve obtained for laccase biosensor for different concentrations of pyrocatechol in 0.1 M sodium citrate buffer (pH 4.7). Each point is an average of at least three independent experiments, error bars represent the SD.

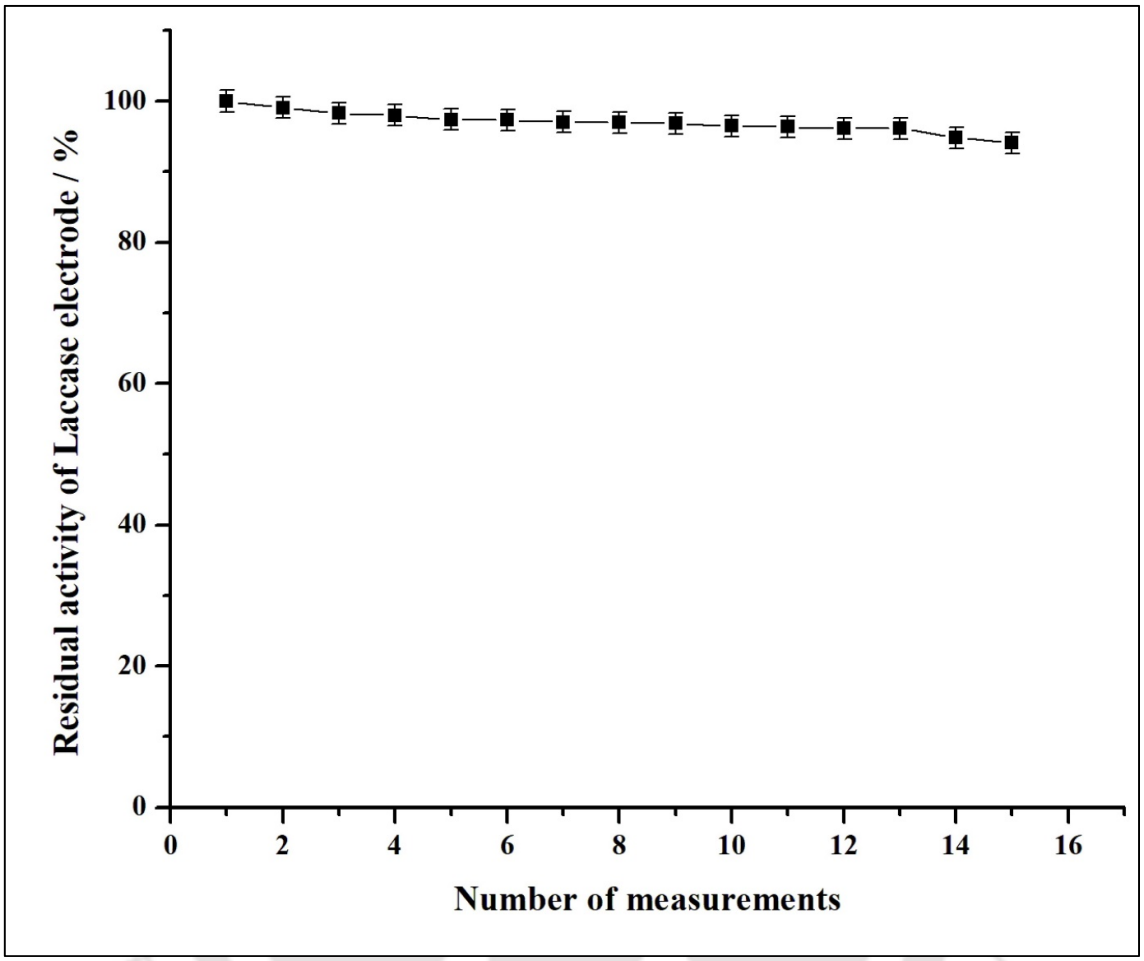

Figure 3.6: Operational stability of the laccase biosensor for substrate pyrocatechol. Each datum point represents the average of the analysis of triplicate values (n=3), error bars represent the SD.

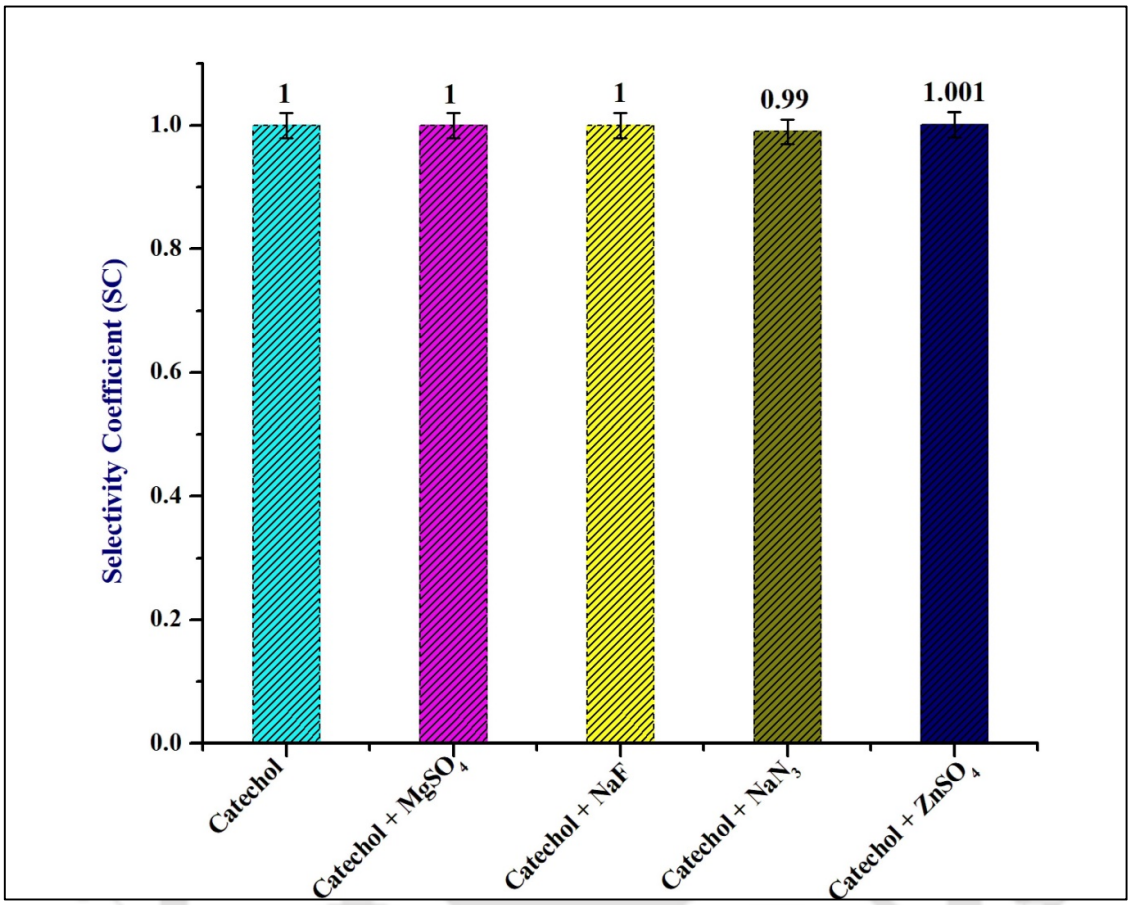

Figure 3.7: Effect of potential interfering agents on the laccase-based biosensor response. In all cases, data points are average of at least three repeat experiments, error bars reflect the SD.

Tables

Parameters	**Characteristic data**
Surface concentration of the ionic species (Γ)	1.32×10^{-8} mol.cm^{-2}
Charge transfer coefficient (α)	0.52
No. of electrons transferred (n)	1
Heterogenous electron transfer rate constant (k_s)	0.67s^{-1}
Linear range	3.98nM - 16.71nM
Detection limit (DL)	2.82 nM
Sensitivity	3.82 ± 0.31 nA nM^{-1}
Standard deviation limit	$3.59 \pm 2.57 \times 10^{-4}$ nA

Table 3.1: Electron transfer kinetics and response characteristics of GCE/MWCNT-CB-Nf-MWCNT-OsO_4P4VP-laccase electrode

CHAPTER IV

Development of a Paper based Enzymatic Biofuel cell for Alcohol Sensing Application

CHAPTER IV

Development of a Paper-based Enzymatic Biofuel cell for Alcohol Sensing Application

4.1. Overview

Enzymatic Biofuel cell (EFC) is emerging as a next generation biosensing platform due to its various advantages such as self-powered facility, high sensitivity, and scope of scaling down its size into a portable device for point of care and point of need applications (Kaushik et al 2021 ; Zhang et al., 2012a). For these biosensing applications, the device should be small, cheap and portable for the convenient of the end-users and to facilitate its penetration to the consumer market. However, the miniaturization of EFCs is a challenge as several critical design factors being associated with its performance and operation need to be carefully addressed. Among the major hurdles, fuel pumping facility and membrane could be reckoned first as these requirements make the devise complex and bulky. There have been few reports on these aspects and a search is on to attain a comprehensive solution on the

subject (Arun et al., 2014; Bich et al., 2019). A recent advancement in this direction is the identification of cellulosic paper as a suitable substrate for the construction of sensing platforms that could facilitate the fuel movement through a passive diffusion mechanism. In general, paper-based materials have received much attention for developing simple, low-cost, and disposable sensor platforms due to its following advantages: (i) portable, cheap, and easily accessible, (ii) compatible with biological samples, (iii) can be effortlessly modified to immobilize different biomolecules (iv) ease of transport, storage and disposal, (v) paper absorbs liquids through capillary action, which eliminates the need for external pumps to drive fluid movement (Kakoti et al., 2015). Hence, paper as a biosensing platform complies well with the 'ASSURED' mandate of the World health organization (WHO) for their application in under-developed and developing nations (Peeling et al., 2006). The word 'ASSURED' implies affordable, selective, sensitive, user-friendly, robust, equipment-free and deliverable.

The detection and quantification of alcohols with high sensitivity and selectivity are required in different areas, such as food, beverage, clinical and forensic analysis, and pulp industries (Thungon et al., 2017). Methanol is the simplest alcohol and is a volatile, colorless, light and flammable liquid. It is of great concern to human health as its even very low concentration (median lethal dose 1–2 $ml.kg^{-1}$ body weight**)** may cause permanent blindness and other serious health problems. Notably, methanol is widely used as solvents, preservatives, and is progressively used as fuel in various industrial sectors. Therefore, there is an urgent need to develop a simple, low-cost, easily operable/accessible, disposable, and self-powered alcohol sensor for point of care (PoC) (including self-diagnosis), and point of need (PoN) applications (Kim et al., 2016). The current alcohol analysis methods are based on long separations steps using gas- (Tiscione et al., 2011), liquid-chromatography (Pellegrino et al., 1999) or electrophoresis (Legros et al., 2002). However, these methods

require expensive equipment and highly trained personnel (Bucur and Lucian, 2008). Such disadvantages could be overcome by using a simple biosensor device containing highly selective enzymes as its bio-recognition elements.

In this chapter, we report a self-powered paper-based EFC for monitoring methanol, which is of low cost, disposable and eco-friendly. For creating hydrophilic anode and cathode chambers and micro-channel for proton movement from anode to cathode, hydrophobic barriers on chromatography paper were created using AKD (alkyl ketene dimer) by using an inkjet printer with a modified cartridge in a suitable solvent. AKD is hydrophobic in nature and acts as a barrier to fluid flow. The as-prepared graphite conductive ink mentioned in the previous chapter was applied over hydrophilic chambers or channels. AOx and BOx enzymes entrapped with chitosan were immobilized over ink coated paper platforms to fabricate anode and cathode respectively. Methanol as an adulterate in other solvents (e.g. ethanol) can also be determined by this method, since enzymes are substrate specific. A single drop of methanol sample could operate this EFC based sensor. The performance of the developed EFC was evaluated for the detection of methanol. A detailed account of the experiment, results and conclusion are described in this chapter.

4.2. Experimental approaches

4.2.1. Reagents

Whatman chromatography paper grade 3 mm Chr (20 cm×20 cm) were procured from GE healthcare, Alcohol oxidase (AOx) from *Pichia pastoris* (21Umg^{-1} protein), bilirubin oxidase (BOx) from *Myrothecium verrucaria* and chitosan were purchased from Sigma-Aldrich. Alkyl ketene dimer (AKD) 1840 was purchased from Flourish Paper and Chemicals Limited (Mumbai, India). Heptane and methanol were purchased from Merck.

Silver conductive epoxy was purchased from MG Chemicals and copper wires were obtained from a local electronics shop. Graphite-PEG-Sericin ink was prepared in the lab using graphite powder, Polyethylene glycol (PEG) and silk sericin (as discussed in chapter III). The stock solutions of AOx (10 U) and BOx (10 U) were freshly prepared in 0.1M potassium phosphate buffer solution (pH 7.5) (KPBS), prior to being used. Again, working solutions of methanol were freshly prepared in MQ water prior to use. The entire experiments were performed using Elix Millipore water (with resistivity of 15 MΩ cm at 25^0 C). All other chemicals were of analytical grade and used without further purification.

4.2.2. Fabrication of paper-based EFC (pEFC) device

The pEFC was developed on Whatman chromatography paper 1. The design pattern of pEFC was created by using Adobe Illustrator CS6. The pattern consists of two circular hydrophilic zones of 1.2 cm (diameter) connected by one hydrophilic channel, which had a dimension of 3 mm width and 4 mm length, where one zone act as anode and the other act as cathode. The electrode areas (6 mm in length), on the left side of the anode and the right side of the cathode are created for the connection of pEFC to the data acquisition system (Agilent 34972A LXI, USA). Figure 4.1 shows the schematic diagram of pEFC configuration. After designing, AKD was printed on paper. AKD is a cellulose hydrophobization agent. The reactive functional group of AKD is the lactone ring. The two hydrocarbon chains of AKD impart hydrophobicity to the paper. Hence, AKD-based chemical modification method was used to make the paper hydrophobic. AKD is added to the –OH groups in cellulose through an esterification reaction and hydrophobicity arises from the resulting addition of hydrocarbon chain moieties (Li et al., 2010) (Figure 4.2).

The AKD printing was done in an HP deskjet-100 printer. The cartridge of the printer was modified by replacing the hydrophobic foam with hydrophilic chromatography

paper and absorbent cotton. The ink cartridge was filled with 5% (v/v) AKD solution in *n*-heptane (Chakma et al., 2016). The printed paper samples were then heated in an oven at 100 ^{0}C for 8 min to cure AKD onto the cellulose fibres (Li et al. 2010). Thus the paper was patterned with distinct boundary between hydrophobic area printed with AKD and hydrophilic area without it. So, the AKD-patterned paper contains two circular hydrophilic zones, corresponding to two electrode areas (to the left of anode, right of cathode) and one hydrophilic channel connecting the anode and cathode. Then, the anode, cathode and electrode areas were painted with graphite conductive ink. The paper electrodes were then allowed to dry overnight for further use. Paper-based bioanode was fabricated by spreading 40 µl of AOx solution entrapped into 1% chitosan (dissolved in 1% acetic acid solution) on a graphite-paper electrode. Again, paper-based biocathode was fabricated by spreading 40µl of BOx solution entrapped into 1% chitosan (dissolved in 1% acetic acid solution) on a graphite-paper electrode. After drying bioanode and biocathode at 4 °C overnight, EFC on paper was obtained. This design allowed the substrate solution to diffuse by capillary force only in the hydrophilic areas, which served as the chambers of the pEFC. Scheme 4.1 depicts the fabrication process for alcohol/air pEFC on a paper platform.

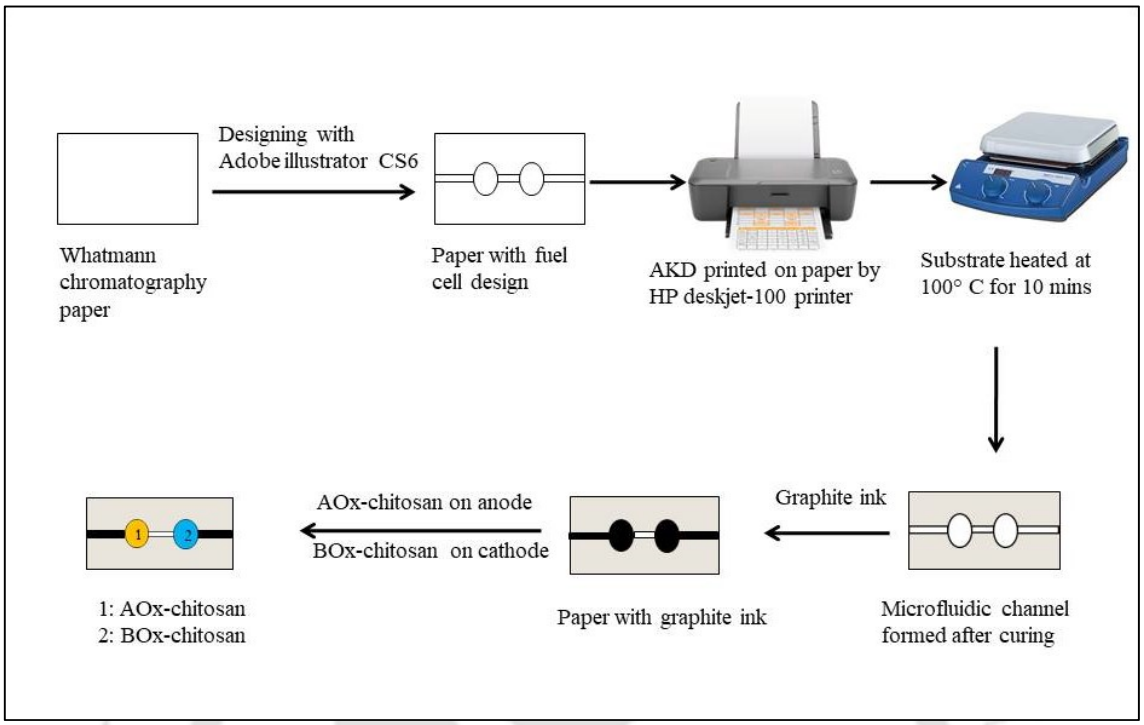

Scheme 4.1: Fabrication process for alcohol/air EFC on paper; 1 is Anode, 2 is cathode, volumetric capacity of anode/cathode is 40 µl.

4.2.3. Apparatus and measurements

The morphological characterization of blank chromatography paper, AKD printed paper, graphite conductive ink coated paper and bioelectrodes was performed by using Field emission scanning electron microscope (FESEM) (Zeiss, Model Sigma, Germany), with EHT 3.00 kV. Apparent contact angles for water on AKD coated chromatography paper samples were measured using Drop Shape Analyzer-DSA25 (Make: Kruss GmbH-Germany). Uniform drops (2 µL) of water (18.2 MΩ.cm) were carefully dropped onto the AKD coated paper by sessile drop method, using a micrometer syringe assembled with the instrument. The potential between the anode and cathode was measured with two electrode Agilent 34972A LXI data acquisition system, USA. An external resistor was used to close the circuit. The current (I) was calculated using Ohm's law ($I = \frac{V}{R_{ex}}$, where V is the voltage, I (A) is the

current and R_{ex} (Ω) is the external load) and were normalized to the projected surface area of the anode; the power output was calculated using the equation, $P = V \times I$, where V is the voltage, I (A) is the current.

4.2.4. Operating principle of the pEFC device in sensing methanol

The operating principle of our paper-based EFC-based alcohol sensor is described in scheme 4.2. When a sample containing methanol is introduced into the anode chamber, methanol oxidization is catalyzed by the AOx (a redox enzyme) immobilized at the anode. The enzyme then transfers its electrons to the anodic surface. These electrons flow to the air-cathode through the external circuit. Protons released by the oxidation reaction travel through the hydrophilic paper channel toward the air-cathode. By using atmospheric oxygen as the electron acceptor, the cathode completes the redox reaction. The open circuit voltage between the electrodes and current/power generation from the EFC is a function of methanol concentration in the sample, creating a self-powered alcohol monitoring system.

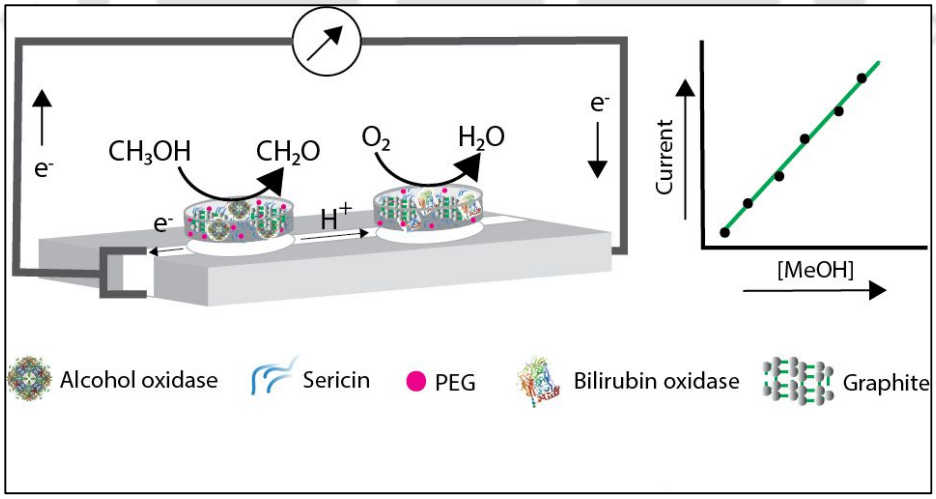

Scheme 4.2: Schematic diagram of operating principle of EFC-based alcohol sensor on paper platform

4.3. Results and discussion

4.3.1. Morphological characterization of pEFC

The surface morphology of the AKD modified surface and the unmodified surface of the device was analyzed through the FESEM technique. Figure 4.3A shows the FESEM image of the blank Whatman chromatography paper, the porous and fibrous structure of the chromatography paper is revealed as expected, whereas porosity of the paper is drastically reduced in AKD printed part (Figure 4.3B) indicating the AKD is penetrated and polymerized deeply into the cellulosic network of the paper. Contact angle measurement confirmed the formation of hydrophobic and hydrophilic zones with corresponding contact angles of 90° and 25°, respectively (Figure 4.4).

The FESEM images of the critical layers prepared for the fabrication of the bioelectrodes were captured (Figure 4.5). The morphology of the blank paper (hydrophilic channel) which possesses porous fibrous like structures (Figure 4.5A) was changed to flake like morphology upon the incorporation of graphite-PEG-sericin ink on it (Figure 4.5B). The morphology further changed to a smooth curvature layer following the addition of AOx (Figure 4.5 C) and BOx (Figure 4.5D) over the ink on chromatography paper indicating deposition of the globular layered structure of enzyme proteins.

4.3.2. Response analysis of the pEFC:

The volumetric capacity of the channel for the substrate methanol was 40µl. The electrical response characteristics of the fabricated EFC against methanol substrate were studied. The OCP with a 0.5 µM methanol sample gradually increased and reached a value of ~397 mV. The power curve for the device with 0.5 µM methanol was generated (Figure 4.6A). The curve was derived and calculated based on the stabilized current value at a given

external resistance (1 MΩ, 560 kΩ, 480 kΩ, 390 kΩ, 150 kΩ, 100 kΩ, 56 kΩ, 22 kΩ, 10 kΩ and 1 kΩ). The maximum power outputs were obtained under a 150 kΩ resistor. So the internal resistance of the system was discerned as 150 kΩ. The high internal resistance observed in our experiments is most likely caused by the poor proton conduction through the less polar electrolyte between the two electrodes caused by the less polar (than water) methanol substrate. However, the magnitude of current generated was sufficient for sensitive detection of methanol. Figure 4.6B shows the calibration curve with a 150 kΩ resistor. The detection limit (*DL*) for the constructed biosensor was determined from the expression,

$DL = \frac{3 \times SD}{Sensitivity}$, where *SD* is the estimated standard deviation for the points used to construct the calibration curve. The biosensor shows a high linearity 0.03125 µM to 0.5 µM (R^2 = 0.9988) with a sensitivity of 0.66245 µAµM^{-1} and 0.022 µM as *DL*.

4.3.3. Interference study:

The effect of some potential interfering agents present in blood sample such as ascorbic acid, uric acid and glucose on biosensor response was studied. The response was examined by separately exposing the sensor to a 0.03125 µM methanol solutions with the interferents in 1:1 ratio. Selectivity coefficient (*SC*) of the biosensor for each interferent was estimated with respect to the response of the biosensor obtained when it is subjected to only methanol using the formula, $SC = \frac{I_{c+i}}{I_c}$, where I_{c+i} and I_c (Saxena et al., 2011a) are biosensor responses for methanol (0.03125 µM) in the presence and absence of each interferent, respectively. In most of the cases, it was found that the contribution of these compounds to the biosensor response is ≤5%, implying negligible significant interference.

4.4. Conclusions

We report here development of a self-powered EFC sensor on the chromatography paper surface for rapid and sensitive detection of methanol in test samples using AOx-based anode and BOx-based air-cathode. The constructed pEFC-based sensor offered several advantages such as the requirement of low sample volume (as small as 40 µL), eco-friendly as it does not involve any hazardous or toxic component or compounds, and it could be disposed of by incineration or through the natural biodegradation process. We expect that the cost of the device will be significantly less than the methanol sensors available in the global market due to the involvement of a very low-cost sensing platform (paper) and design (no external pump) in its fabrication process.

Figures

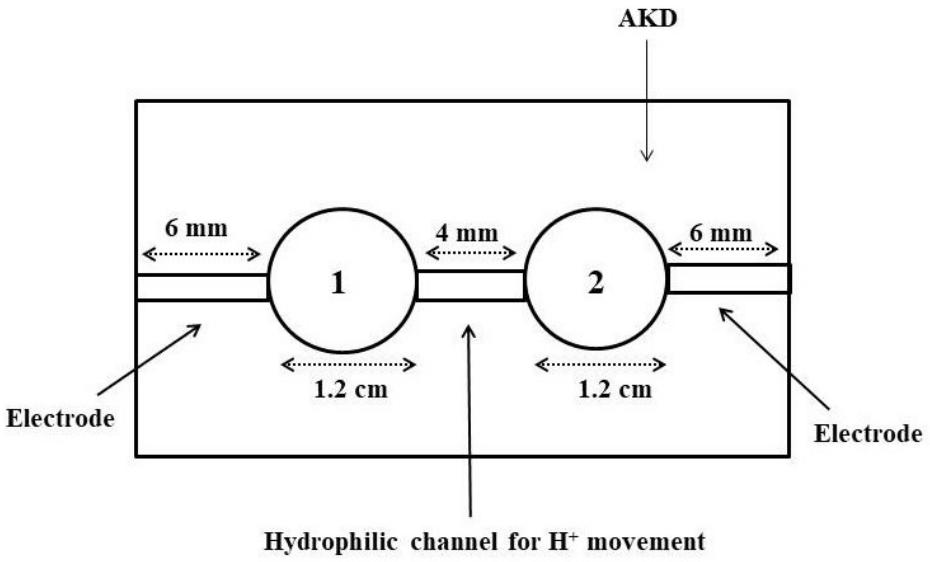

Figure 4.1: Schematic diagram of pEFC configuration, where **1** is **Anode**, **2** is **Cathode;** Surface area of Anode / Cathode: **1.13 cm^2**

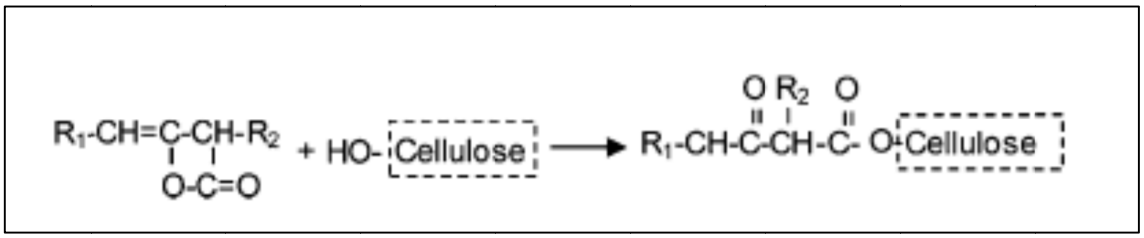

Figure 4.2: The reaction of alkyl and alkenyl ketene dimers with cellulose. Adapted From Li et al., (2009).

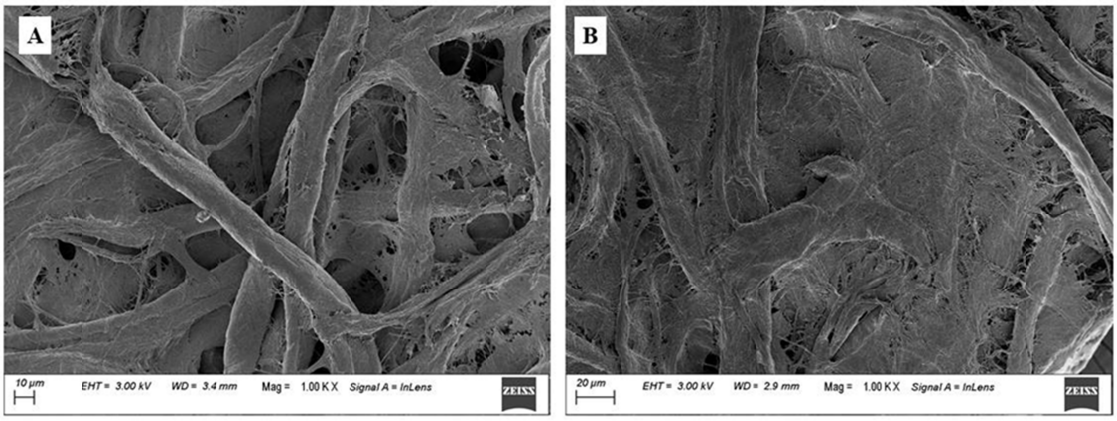

Figure 4.3: FESEM image of (A) blank chromatography paper; (B) AKD printed chromatography paper

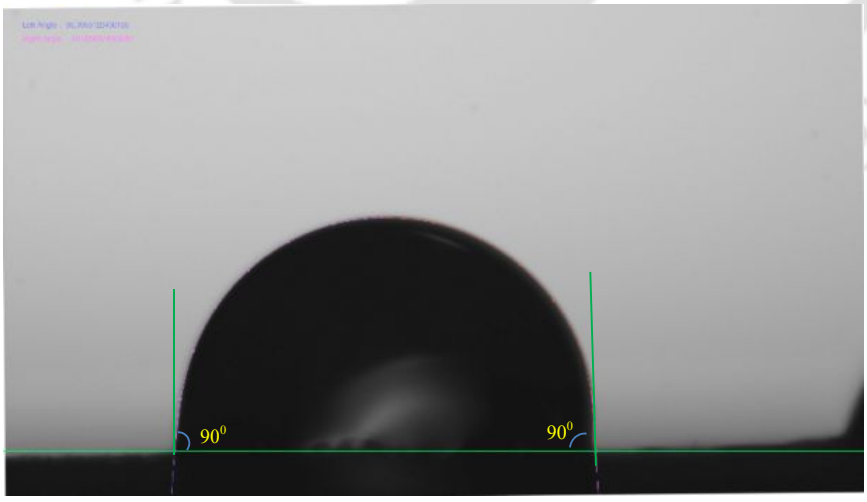

Figure 4.4: A sessile drop of MQ water (2µl) applied to the surface of AKD coated chromatography paper

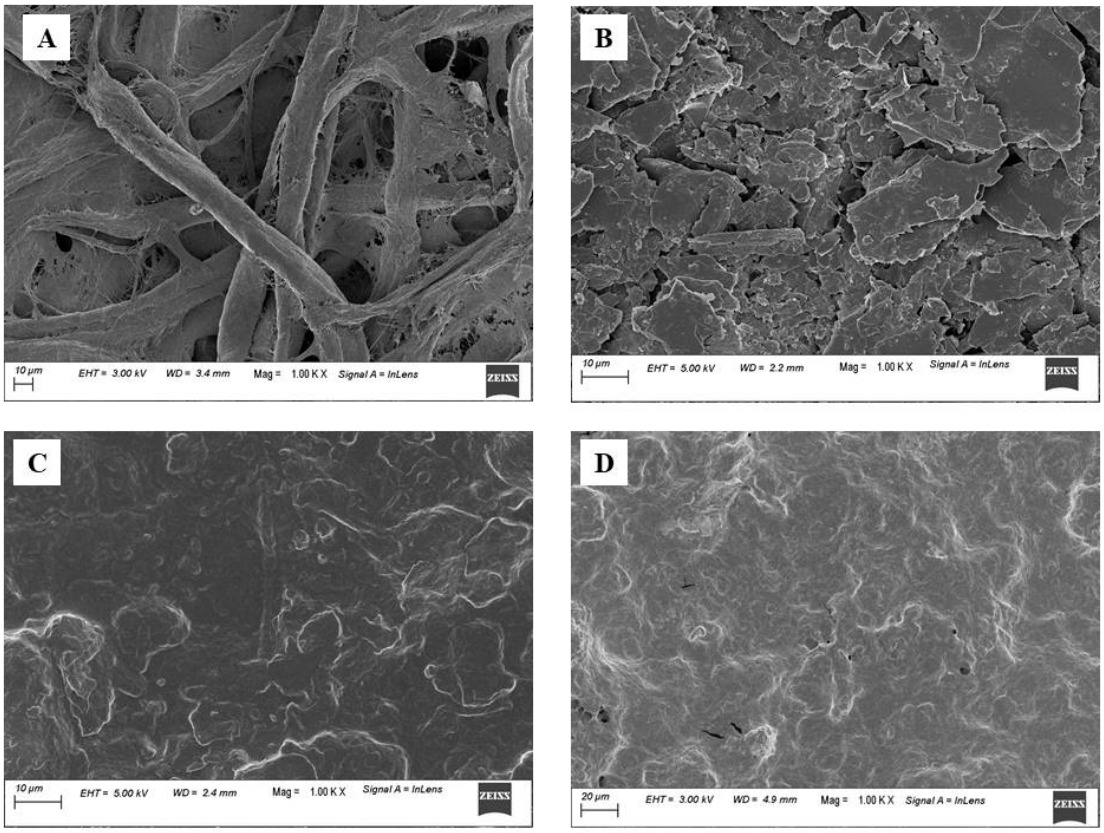

Figure 4.5: FESEM image of (A) blank chromatography paper (hydrophilic zone/channel); (B) Graphite-PEG-Sericin ink over chromatography paper; (C) AOx over Graphite-PEG-Sericin ink on chromatography paper (D) BOx over Graphite-PEG-Sericin ink on chromatography paper.

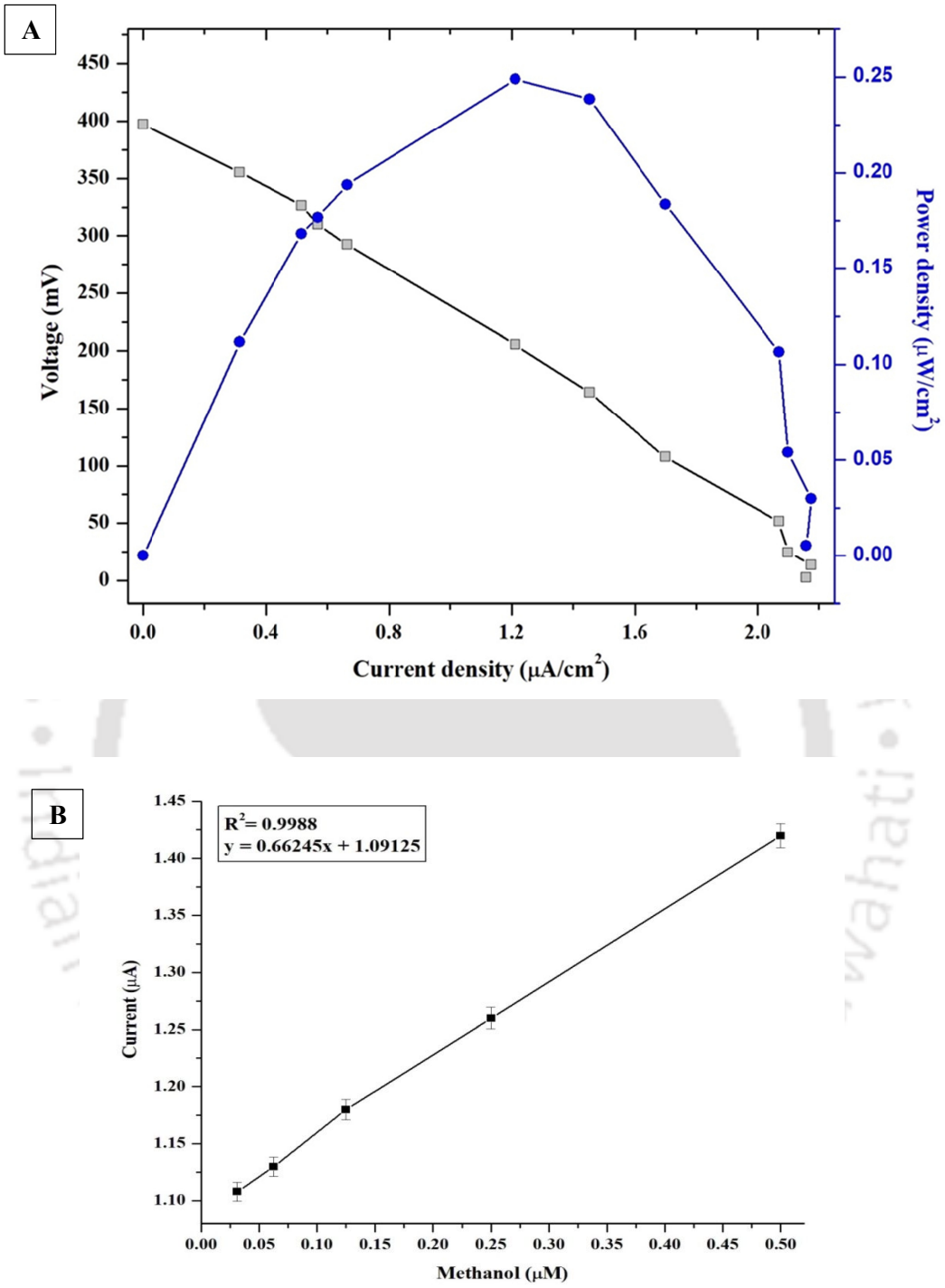

Figure 4.6 (A) Polarization curve with 0.5 μM methanol (B) Calibration curve for methanol detection plotted as output current vs. the concentration of methanol with a 150 kΩ resistor.

CHAPTER V

Development of Methanol Biofuel Cell through Passive Fuel Delivery Facility in the Anode Chamber

CHAPTER V

Development of Methanol Biofuel Cell through Passive Fuel Delivery Facility in the Anode Chamber

5.1. Overview

Efficient energy conversion and stability are the challenging tasks in biological fuel cells that prompted intensive research globally to improve this green energy-harvesting technology for commercial applications. The enzymatic biofuel cells (EFCs), a class of the biological fuel cells, have received considerable research interest as a renewable fuel-based energy generating system for powering small scale devices in various sectors including healthcare, biosensors, and electronics (Cinquin et al., 2010; MacVittie et al., 2013; Garcia et al., 2016; Kaushik et al., 2020). There are many reports of proof-of-concept on EFCs focusing on these as the power generating devices. However, the translation of these concepts to viable products of commercial interest is quite slow due to many technical hurdles, among which, low power density and poor operational stability of the constructs are prominent (Xiao

et al., 2019). In general, the poor operational stability of EFC is mainly caused by the short lifetime of the enzymes being used as electrode catalysts in these devices. Again, for most of the reported EFCs, the voltage at which usable power could be extracted is significantly low for practical applications. This limitation could be viewed from the thermodynamic standpoint. The maximum redox potential gap between two electrodes in most biological fuel cells is significantly low. For example, the gap is ~1.18 V for glucose/O_2 EFCs with two-electron oxidation of glucose, whereas, for lithium-based batteries, it is ~4.2 V. Additionally, the voltage output of EFCs is reduced by the activation and then ohmic losses, which further reduce the overall power output from the system (Xiao et al., 2019).

The performance (potential and power density) of EFCs is often limited by the inefficient electrical communication between the enzymes and the electrodes since the active centers of most of the redox enzymes are usually buried inside the protein matrices. To overcome this obstacle, two approaches are widely used: mediated electron transfer (MET) and direct electron transfer (DET) (Das et al., 2016). The MET approach though offers high redox current, the leaching susceptibility of the mediators from the enzyme–electrode interface and toxic nature of most of the mediating molecules discourage this approach to use for the cases where operational stability and environmental friendly issues are ardent tasks (Seop et al., 2006). Conversely, the DET approach involves the direct transfer of electrons between the enzyme and the electrode (Barton et al., 2004; Prasad et al., 2014). To facilitate the DET, various highly conductive nanostructured materials are widely used. Over the past few years, the magnetic nanoparticles (Fe_3O_4Nps) (MNps) have attracted attention for different applications due to their distinctive properties like good biocompatibility, high surface reactivity, strong super para-magnetism, low toxicity, and strong adsorption ability to immobilize biomolecules (Pakapongpan et al., 2017). Some studies also revealed intrinsic enzyme mimetic activity of MNps (Martins et al., 2010) and their capacity to reduce the

overpotential of some redox enzymes. As a whole, the use of MNps for improving the electrocatalytic performance of enzymes in EFC is limited (Ji et al., 2017; Sarma et al., 2018).

Alcohol as EFC fuel has received increasing attention due to its high energy density, ease of storage and transport, high aqueous solubility, and low cost as these compounds can be readily produced from widely available cheap renewable substrates. Among the alcohols, methanol is the simplest one and superior to many other alternative hydrocarbon substrates as a fuel source (Yue and Lowther, 1986). For developing EFC with ethanol or methanol as fuel, NAD^+ dependent ADH has been widely used (Arrocha et al., 2014) as their low redox potential (Rincón et al., 2011) favors the anode to function at a low potential for generating high cell voltage. However, most of the ADHs being used in EFC are NADH-dependent, with a few exceptions bearing PQQ and heme prosthetic groups (Yakushi and Matsushita, 2010). The ADH based EFC requires to supply NAD^+ externally, which stand as a technical difficulty in developing an efficient EFC system due to the leaching susceptibility of NAD^+ from the electrode, and occurrence of electrode fouling from the polymerization of oxidized products on the electrode surface (Vijayakumar et al., 1996), which rise the overvoltage for the oxidation of NADH. The other prominent alcohol oxidizing enzyme namely, AOx (Alcohol: O_2 Oxidoreductase: EC1.1.3.13) has received increasing interest in fabricating EFC due to their cofactor (FAD) being avidly bound in the reactive center of the enzyme (Goswami et al., 2013). Presently, the reports on EFC with AOx as electrode catalyst are few and their improvement for technological upgradation is not yet adequately known (Arrocha et al., 2014; Das et al., 2014; Ramanavicius et al., 2008; Ulyanova et al., 2014). One of the major challenges of using these FAD-based oxidase enzymes for developing various electrochemical (e.g. EFC and voltammetric biosensors) and other devices is their low stability outside their native environment (Chinnadayyala et al., 2014; Vijayakumar et al.,

1996). Hence, a comprehensive understanding of the stability and its linked technological endeavor is the key issue of research involving the AOx and other oxidoreductase enzymes of its family.

The operation of a typical EFC device usually involves an external pump to facilitate fuel delivery to the electrode that increases the overall cost and complexity and offsetting the output power of the fuel cell. Moreover, the inclusion of an external pump confronts the objective of miniaturization, thus compromising the lightweight and portable applications of these powering devices. To overcome such problems researchers are striving to develop self-driven actuation motion via the capillary effect during the operation of chemical fuel cells, while such studies on the biological fuel cells are yet to be seen (Bich et al., 2019).

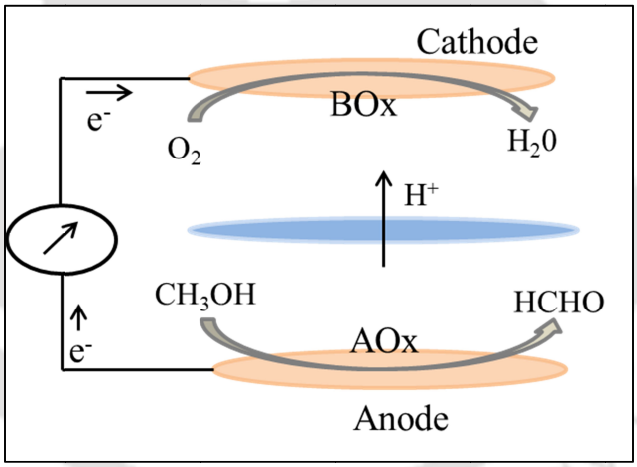

Scheme 5.1: Schematic diagram of central reactions of anode and cathode

Herein, we attempted to address the two major challenges namely coulombic efficiency and operational stability in EFC as discussed above through a new design strategy in a methanol fueled EFC. The EFC was based on the catalysts, AOx (Das et al., 2014) and BOx (EC 1.3.3.5) in anode and cathode, respectively. BOx is a multi-copper redox enzyme that catalyzes the reduction of O_2 to water on a cathodic surface (Murata et al., 2009b). The

fuel was allowed to contact the anode in a controlled manner through capillary action that obviates the need for an external pump to prolong the operation of the cell.

The optimum pH for bilirubin oxidase is 7.4 which is very close to that of alcohol oxidase; on the other hand, laccase has optimum pH of 4.8 which is acidic in nature. In this present investigation of this chapter, the cathode is present above the anode. For better power output, both anode and cathode should possess the same optimum pH range. Hence bilirubin oxidase was chosen instead of laccase, where laccase was used as cathodic enzyme in the previous chapters.

Additionally, the design and composition of the membrane electrode assembly (MEA) adapted here, prevent loss of the volatile fuel through evaporation from the anodic chamber and facilitates bioelectrocatalytic reaction in both the electrodes that drastically improved coulombic efficiency of the cell. Further, the physicochemical environment of the bioelectrodes provides stability to the enzyme catalysts, shielding the AOx from molecular oxygen thus offering exceptional operational stability to the EFC. One of the critical findings of this investigation is that prolonged interaction of AOx with molecular oxygen drastically reduces its activity. To understand this phenomenon, docking studies were also performed and divulged interesting findings on the structural integrity of this enzyme protein upon its interaction with the molecular oxygen. As a part of the design strategy, we also made an effort to improve the current density by connecting unit EFCs through series circuit and substantially improved the power. A detailed account of the characterization and performance of the fabricated EFC has been described in this chapter.

5.2. Experimental approaches

5.2.1. Reagents

Carbon cloth (CC) (MPL-W1S1005) was procured from M/s Graphitestore.com (USA). Hydrophilic conductive paste was prepared in the lab using graphite powder (< 20 µm, synthetic), polyethylene glycol (PEG), and silk sericin, which was extracted in the lab from *Bombyx mori* cocoons following a reported method (Rockwood et al., 2011). AOx from *Pichia pastoris* (21Umg^{-1} protein), BOx from *Myrothecium verrucaria* (25 Umg^{-1} protein), PEG, Nf, and chitosan were bought from Sigma–Aldrich (India). Acrylic glass of 5 mm thickness, absorbent cotton, rubber cork, and glass pipes were purchased from local stores in Guwahati. Methanol was procured from Merck. AOx (1 mg ml^{-1}) and BOx (10 mg ml^{-1}) were freshly prepared in potassium phosphate buffer solution (KPBS) (0.1M, pH 7.5). The entire experiments were performed using Elix Millipore water (with resistivity of 15 MΩ cm at 25 ^{0}C).

5.2.2. Enzyme assay

The AOx activity was measured by HRP-coupled assay method (Kemp et al., 1988). The assay was used to monitor the production of H_2O_2 at λ_{405} nm for ABTS radical at 25 °C (ε_{405}=18,400 µM^{-1} cm^{-1}). One unit of enzyme activity is expressed as the amount of enzyme required to produce 1 µM H_2O_2 min^{-1} at 25 °C. Two sets of AOx enzyme solutions were prepared. One set under aerobic condition while the other set under anaerobic condition were maintained at 4 ^{0}C. An anaerobic environment was created by argon purging and then sealed. Each set was divided into five sets and enzyme activity in each set was measured in a regular interval of seven days.

5.2.3. Spectroscopic measurement

Spectrophotometric measurements were performed on a Cary 300 bio UV–vis spectrophotometer (Varian) using 1cm path length quartz cuvette at 25 ^{0}C. CD spectra were recorded using Jasco J-815 (Japan) spectro polarimeter calibrated with 0.06% (w/v) aqueous solution of (7)-10- camphor sulfonic acid. The spectra were recorded from 290 to 170 nm, in a 0.1 cm path length suprasil quartz cuvette at 20 ^{0}C, at a scan rate of 100 nm min^{-1} and 1 nm bandwidth. The spectra were corrected for baseline. The secondary structure analysis was performed by using DICHROWEB (Whitmore and Wallace, 2008).

5.2.4. Synthesis of Fe_3O_4 (magnetite) nanoparticles (MNps)

MNps were prepared by co-precipitation of ferric and ferrous salts under the presence of N_2 gas (Hariani et al., 2013). A total of 16.25 g of $FeCl_3$ and 6.35 g of $FeCl_2$ were dissolved in 200 mL of deoxygenated distilled water. Chemical precipitation was achieved by vigorous stirring at 30 ^{0}C with 2 M NaOH under Nitrogen atmosphere. Following which a constant pH of 12 and temperature of 70 ^{0}C were maintained for 5h. After the system was cooled to RT, the precipitates were separated by a permanent magnet and washed with deoxygenated distilled water until pH of the washout become neutral. Finally, Fe_3O_4 MNps were washed with acetone and dried in an oven at 60-70 ^{0}C for further use.

5.2.5. Characterization of MNps

The magnetic properties of the MNps were measured by Vibrating Sample Magnetometers (VSM) (Lakeshore, 7410 series, USA) at RT. Thermal stability of the MNps was monitored by thermo-gravimetric analysis (TGA), which was performed in the thermal analyzer (NETZSCH STA-449 F3 Jupiter), India, from RT to 900°C at a rate of 20° C min^{-1} under dry nitrogen. The Brunauer Emmett Teller (BET) specific surface area measurement

was performed by N_2 absorption-desorption at the liquid N_2 temperature using a Quantachrome analyzer (model Autosorb-IQ MP), USA. The sample (0.106 g) was degassed at 120° C for 7 hours before adsorption measurements. The size and morphology of MNps were observed by FETEM (JEOL MODEL: 2100 F, Japan). Image J software was used to deduce the size distribution of the MNps from the FETEM images.

5.2.6. Fabrication of bioelectrodes for EFC

A carbon cloth (CC) of 2.5 cm^2 working area was used as support material for bioelectrode fabrication. A hydrophilic conductive paste consisting of graphite, PEG and sericin was applied over the CC (Scheme. 5.2), and dried overnight at RT. In a separate preparation, a total of 15 mg of MNp was dispersed in 50 µl 5% Nf and sonicated for 30 min. To this MNp solution, 950 µl of 100% ethanol was added and sonicated for 45 min. A total of 200 µl of MNp/Nf/ethanol solution was then dispersed over the hydrophilic conductive paste on CC and dried overnight at RT to prepare a nanocomposite paste (NP). Finally, for preparing the bioanode, 200 µl of 1% AOx solution entrapped in 1% chitosan (CS), was layered over the NP and then dried in a refrigerator at 4 ^{0}C. It resulted in the formation of CC-NP-AOx-chitosan electrode as bioanode. A similar composition and procedure were followed for the fabrication of the biocathode, where BOx was used instead of AO_X that resulted in the formation of CC-NP-BOx-CS biocathode.

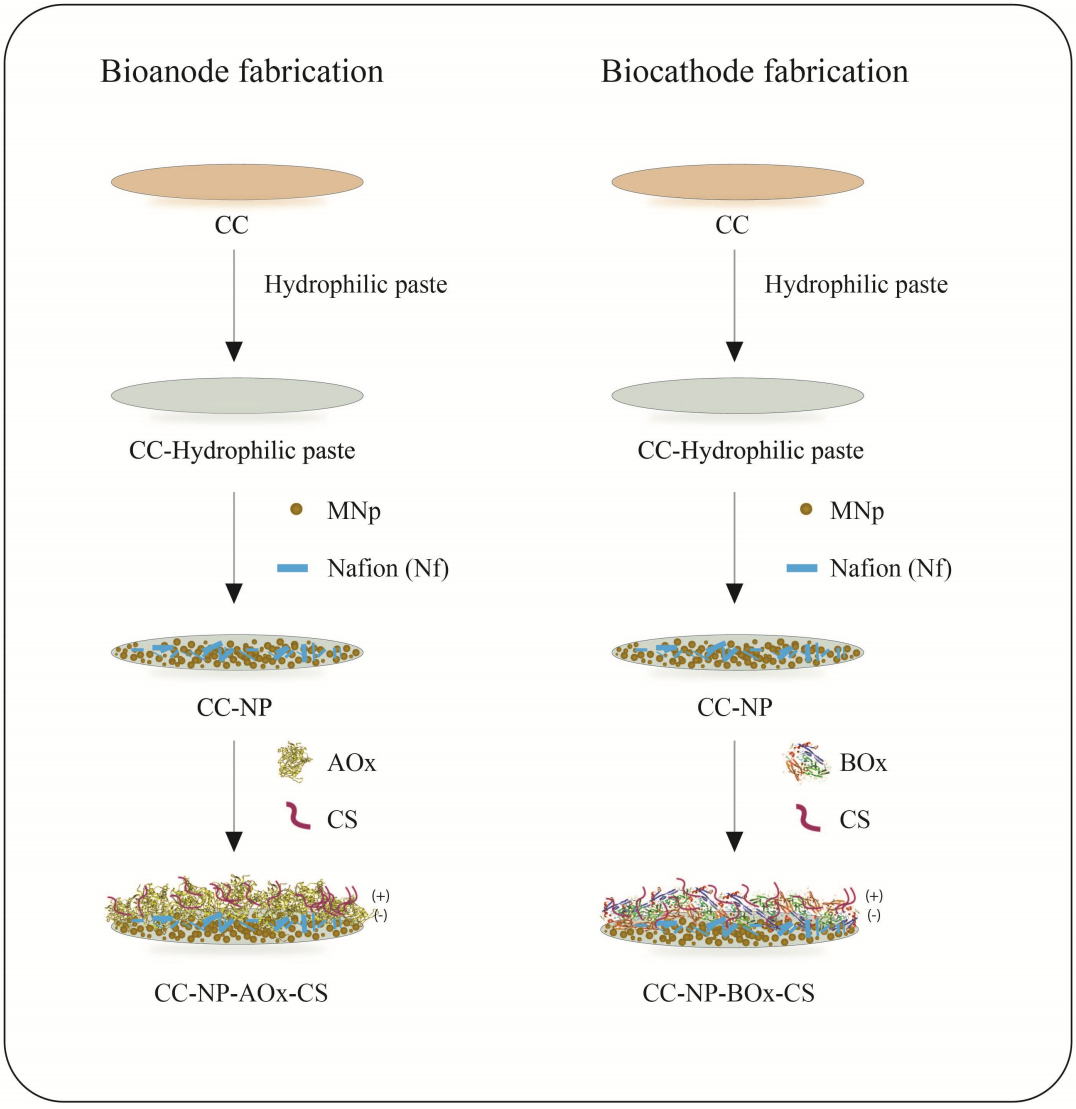

Scheme 5.2. Schematic diagram of fabrication of CC-NP-AOx-CS bioanode and CC-NP-BOx-CS biocathode

5.2.7. Characterization of bioelectrodes

Morphological characterization of bioelectrodes was studied through Field emission scanning electron microscopy (FESEM) (Zeiss, Model Sigma) study at 3 kV to capture the images of the critical layers prepared for the fabrication of the bioelectrodes.

Electrochemical characterization of bioelectrodes was performed by CV. CV was performed in a potentiostat (Autolab PGSTAT 1212, Eco Chemie, Netherland) using a three-electrode system containing Ag/AgCl (saturated KCl) as reference electrode, platinum rod as counter electrode and modified carbon cloth electrode (CC) as the working electrode. All potentials were measured and reported relative to the Ag/AgCl reference electrode. All the CV experiments were done under argon purge condition and at RT.

5.2.8. Fabrication of self-pumping EFC

Biofuel cell setup was fabricated in-house using acrylic glass of 5 mm thickness. The present setup consists of one square plate (11 cm × 11 cm), which acts as the base of the system. One hollow cylinder of height 4.5 cm, outer diameter 9 cm and inner diameter 8 cm was sealed with chloroform over the platform. Chloroform was used to paste the upper portion of the cylinder with acrylic glass containing a hole at the center of 3.3 cm diameter. The lower portion of the total volume capacity of 100 ml serves as the fuel tank of the fuel cell system. A small cylinder of 5.5 cm length, which is made of hard paper and wrapped in aluminium foil, is placed into the large hollow cylinder. Absorbent cotton was stuffed inside the hollow portion of the small cylinder to facilitate uptake of fuel from the fuel tank through capillary action. The membrane electrode assembly (MEA) was fabricated by placing the activated nafion membrane between anode and cathode. The anode side of the MEA was placed over the cotton layer of the cylinder and the system was sealed with a perforated rubber cork placed on top of the cathode side of the MEA. For facilitating sufficient airflow into the cathode side of the MEA, the rubber corks were pierced with glass pipes of 5 mm diameter. The perforated rubber cork was also used for the application of sufficient pressure for maintaining the integrity of the MEA. The fuel tank is provided with a screw cap for introducing fuel when required.

5.2.9. Operation of self-pumping EFC

The biofuel cell was operated in a batch mode at RT. A data acquisition system was used to continuously record the voltage outputs of the EFC. For generating the polarization curve, loads in a range of 1 MΩ to 100 Ω with 20 minutes of stabilization time at each load, was employed. The current (I) and power (P) were calculated using Ohm's law ($I = V/R_{ex}$, where V is the voltage, I (A) is the current, and R_{ex} (Ω) is the external load) and were normalized to the projected surface area of the anode. From the slope of the polarization curve, the internal resistance was calculated (Das et al., 2014). Short circuit current (I_{SC}) of the individual cell was discerned by using the ohm's law, $I_{SC} = \frac{V_{OC}}{r}$, Where, I_{SC} is short circuit current, V_{OC} is open circuit potential, r is resistance. The fill factor (F_f) is a significant factor that depicts the fuel cell performance. The F_f of the EFC was calculated from the following equation,

$$F_f = \frac{P_{cell}}{I_{SC} \times V_{OC}} \quad \text{.....5.1}$$

where V_{oc} is the open circuit potential (OCP) and I_{sc} is the short circuit current, P_{cell} is the maximum power obtained from the polarization curve.

To increase the overall stack voltage, the six individual EFCs (called EFC1 to EFC6) were serially connected. The internal resistance of the series connected EFCs was calculated using Kirchhoff's voltage law, which gives the following formula (equation 5.2) to calculate the internal resistance of the stacked EFC system.

$$r = \left(\frac{V_{OC}}{V_R} - 1\right) R \quad \text{.....5.2}$$

where V_R = Potential across load *'R'*, V_{OC} is Open circuit voltage/potential and R is Resistive load (3kΩ) of the blue LED.

The substrate consumptions in the anodic half-cell of the EFC were analyzed by High Performance Liquid Chromatography (HPLC) using the Hi-plex H column. The concentrations of the substrate were estimated by computing the peak area of the injected samples with the corresponding authentic samples of known concentrations in the chromatograms. The coulombic efficiency (*CE*) of the fuel cell was determined by integration of the area under the current–time curve (Liu et al., 2005) using the following equation:

$$CE = \frac{C_P}{C_{Ti}} \times 100\% \quad \text{.....5.3}$$

Where, C_p, is the total coulombs calculated by integrating the current over time

Again, $C_{Ti} = \frac{Fb_iS_iv}{M_i}$, where, F is Faraday's constant (96,485 C/mol.electrons), b_i is the number of moles of electrons produced per mole of the substrate, S_i is the substrate concentration, v is the volume of substrate used and M_i is the molecular weight of the substrate.

Overall energy recovery or energy efficiency was calculated using the following equation,

$$E_E = \frac{E_P}{E_{Ti}} \times 100\% \quad \text{.....5.4}$$

Where, *Ep* (J), is the total energy calculated by integrating the power over time.

E_{Ti} (J) is the theoretical amount of energy that can be produced from the substrate, calculated as, $E_{Ti} = \frac{\Delta HS_iv}{M_i}$ 5.5

Where, ΔH is the enthalpy change of oxidation of methanol (Liu et al., 2005).

5.2.10. Docking study:

The pdb file of AOx (PDB ID: 5i68) was downloaded from RCSPDB (https://www.rcsb.org/). SDF file of oxygen molecule was collected from Pubchem

(https://pubchem.ncbi.nlm.nih.gov/compound/977). UCSF Chimera was used for Dock preparation of the AOx pdb file. PyRx open-source software for Computer-Aided Drug Design was used for the docking studies. PyRx has an inbuilt AutoDock Vina as the docking software and it also has Open Babel for importing SDF files, removing salts and energy minimization. AOx pdb file is uploaded in the PyRx followed by inserting oxygen molecule in SDF format. Energy minimization of both the molecules is performed and saved in PDBQT file format. AutoDock Vina Plugin of PyRx is finally used and the dimensions for docking are specified and docking was performed. The PLIP online web server (https://projects.biotec.tu-dresden.de/plip-web/plip) was used to further analyze the AOx-Oxygen interaction. Pymol molecular visualization software was used for the visualization of the docking results.

5.2.11 Statistical analysis of data:

All the experiments and assays were carried out in triplicate, mean centered and scaled-up to variance using Origin 6.0 software. Statistical analysis was performed using analysis of variance (ANOVA). Adobe illustrator CS 20.0 was used for the graphic artwork.

5.3. Results and discussion

5.3.1. Development of enzyme bioelectrodes for EFC

CC was used as a support electrode to harvest electrons due to its low-cost, conductive nature, and excellent mechanical flexibility and strength (Wang et al., 2015). The hydrophobic CC was coated with a hydrophilic paste containing graphite powder, PEG and silk sericin for immobilization of the enzymes. PEG is known to offer support for maintaining both the activity and biocompatibility of immobilized enzymes (Melo et al., 2020). Whereas, sericin enhances the crystallinity of the conductive graphene particulates in

the composition (Yun et al., 2013) (Altman et al., 2011), thus promoting conductivity of the hydrophilic paste even in the presence of the non-conductive PEG. The astounding effect of MNps on the function of bioelectrode in biofuel cells is a late entry in the scientific literature (Sarma et al., 2018). The exact mechanism is though not yet known, the unique properties of MNPs including super-paramagnetism, high conductivity, large surface-to-volume ratio, and biocompatibility are often appreciated to justify their applications in bioelectronics fields (Pakapongpan et al., 2017). The prepared MNps were probed for their saturation magnetization (SM) from the hysteresis loop generated by VSM analysis (Figure 5.1). The SM was found to be 69 emu g^{-1}, which is closer to the value (92 emu g^{-1}) for the bulk magnetite (Attallah et al., 2016), (Hariani et al., 2013). TGA analysis of the MNps showed that 89.3% of the residual mass of the sample remains at 896.5 °C; i.e., a reduction in mass of 10.7% was observed (Figure 5.2). This low level of mass reduction could be due to the evaporation of residual water from the sample. The absence of any major changes in the mass of the sample even at such high temperature treatment indicates that the MNps are quite stable within this temperature range. The N_2 adsorption-desorption isotherm of the MNps is shown in Figure 5.3. The specific surface area of the MNps estimated by the BET equation was 91.645 m^2g^{-1}.

FETEM study indicated that MNps are nanocrystalline, though their shape was predominantly spherical with some hexagonal in shape (Figure 5.4A). The average size of the particles is ~13 nm. This size is reproducible when the experiment for synthesis of MNp is conducted exactly similar to the method described in the section 5.2.4. The high-resolution transmission electron microscopy (HRTEM) also clearly showed that the product is crystalline as evident from the lattice pattern despite the particle size was small (Figure 5.4B). The enzymes were immobilized over the MNps following entrapment with chitosan (β-1, 4-poly-D-glucosamine). The favorable properties of chitosan such as good adhesion, high

permeability toward water, biocompatibility and good film formation ability are regarded as a suitable matrix for enzyme immobilization (Zhou et al., 2010). The FESEM images of the critical layers prepared for the fabrication of the bioelectrodes were captured (Figure 5.5). The CC in the magnification of 200X (inset of Figure 5.5A) revealed the network structure of the CC made from carbon fibres with 20 μm diameters. The image of CC with hydrophilic paste appearing as flakes completely covered the CC (Figure 5.5 B). Figure 5.5C is the image of MNp-Nf layer, distributed over the hydrophilic paste and creating small and large pores for facilitating percolation and encapsulation of the enzyme layer to be added next. Figure 5.5D and Figure 5.5E are the evenly layered enzyme images of respective AOx and BOx entrapped with chitosan over the NP on CC. The molecular size of AOx is 600 kDa, whereas the molecular size of BOx is 60 kDa. Due to the large size of AOx, fig 5.5D looks enlarged as compared to that of fig 5.5E.

CV was carried out in KPBS (pH 7.5) purged with argon gas for bare CC and fabricated CC-NP-AOx-CS bioanode at a scan rate of 2 mV s^{-1} (Figure 5.6). No redox peak was observed for bare CC. The bioanode exhibited one anodic peak at -0.24V and one cathodic peak at -0.44V, displaying a pair of clear redox peaks with a formal potential $[(E_{pa}+E_{pc})/2]$ of -0.34V, which is close to the value of redox potential of $FAD/FADH_2$ system (Kano, 2002); (Munteanu et al., 2008). Upon addition of 2 μM methanol to the bioanode, current at the anodic and cathodic peak potential was increased indicating the involvement of DET mechanism in generating current in the anode.

5.3.2. Development of EFC with fuel self-pumping facility

The AOx bioanode, BOx biocathode and the nafion membrane were assembled in a fuel cell MEA as described in Section 5.2.8 (Figure 5.7). The EFC set-up utilized passive diffusion of alcohol fuel through the absorbent cotton material to

the MEA from the fuel tank at a flow rate of 1.63 $\times 10^{-3}$ μls^{-1} thus obviating the need for an external pump for continuous delivering the fuel to the anode.

The power curve was generated for the EFC operated with 1M methanol at RT (Figure 5.8A). The EFC system showed an open circuit potential (OCP) of 0.719 V with a maximum power density of 13.71μWcm^{-2} and a current density of 53μAcm^{-2} at an external load of 1 kΩ. So, the internal resistance of the EFC was discerned as 1 kΩ, which is comparable to a previous report (Katz and Willner, 2003), but lower than some other reports (Amir et al., 2009; Halámková et al., 2012). The low internal resistance implies ease of charge-transfer on the bioelectrodes. Essentially, high internal resistance has been recognized as the major cause of reducing power output in biofuel cells. A close proximity between anode and cathode facilitates charge transfer and reduces the internal resistance (Kaushik et al., 2020). The compact MEA design strategy adopted in this study offers to position the bioelectrodes in close proximity, making internal resistance relatively low. The I_{sc} of the EFC was calculated to be 0.71 mA. The fill factor of the EFC was calculated to be 27.45%, which is at a moderate level on a scale compared to the other reported values (Arrocha et al., 2014), (Katz et al., 1999; Willner et al., 1998). The other reported values of fill factors are tabulated in the table 5.1. The coulombic efficiency of the fuel was 60.05%, which is the highest ever value reported so far for pure EFC with alcohol as a fuel substrate. There are no such other report in literature except Das et al., 2014 (coulombic efficiency of 59.52%) with pure EFC and with alcohol as fuel substrate. The high columbic efficiency of the EFC may be attributed to the airtight anoxic designs adopted for the anodic chamber preventing evaporation of the volatile fuel substrate. Notably, coulombic efficiency is also reduced when the redox enzymes come in contact with molecular oxygen, which is the terminal electron acceptor for the redox reaction under natural conditions (Tasca et al., 2010). The energy efficiency of the system was calculated to be 19.16%. Additionally, the Chitosan entrapped with enzyme of

the constructed enzyme electrodes acted as a barrier for methanol cross over through the Nf membrane. It has been reported that the structurally modified PEM with chitosan drastically reduces methanol crossover (Hasani-Sadrabadi et al., 2011; Hasani-Sadrabadi et al., 2012).

The role of MNps on the performance of the EFC was also examined. The OCP of the EFC with two different electrodes was measured, one with MNp and the other without MNp. The maximum OCP of the EFC obtained with CC-NP-AOx-CS as anode and CC-NP-BOx-CS as cathode was 2.11 times higher than the OCP obtained with the corresponding anode and cathode devoiding of MNps (Figure 5.8B). The results confirmed the positive effect of MNps led enzyme electrode on the performance of the EFC.

A comparative analysis was made on the performance of the EFC with previous reports. Das et al. (2014) developed an EFC using AOx based third-generation bioanode and an air-breathed laccase biocathode for generating power from methanol fuel. The EFC generated an OCP of 0.61(±0.02) V with a maximum power density of 46 (±0.002) $mWcm^{-2}$ at an optimum of 1M methanol concentration. Arrocha et al., (2014) designed an EFC with molecularly orientated AOx and laccase. The EFC achieved OCP of 0.5V with both, ethanol and methanol, while in short circuit the highest current intensity of 250 μA cm^{-2} was obtained with methanol. Ramanavicius et al., (2008) reported AOx as a cathodic enzyme co-immobilized with microperoxidase in ethanol fuelled EFC. The anode of the EFC was fabricated with quino-hemoprotein-alcohol dehydrogenase (QH-ADH). The OCP of the BFC was 240 mV and the stability was also not up to the mark for enduring operation. From the reports, the OCV achieved in the present work for the unit EFC is higher than the previous reports. However, due to a lack of uniformity in expressing the data in different reports, a better comparison could not be made on other parameters.

5.3.3. Power and stability of the stacked EFCs

Biofuel cells are often stacked in series to increase the output voltage of the device (Miyake et al., 2013). Herein, six units of EFCs (called EFC1 to EFC6) were connected in series resulting in an increased OCP to 3.1 V. The series stack produced an I_{SC} of 3.9 mA. The internal resistance of the series connected EFCs was calculated to be 780 Ω, which is marginally lower than the single EFC unit. A blue LED (with 2.7 V operating voltage) when connected as load (3 kΩ) to the stacked EFCs, the voltage of the stacked EFCs dropped from 3.1 V to 2.59V (Figure 5.9 B). The corresponding current and power generated upon loading the LED were 100 µA and 260µWcm^{-2}.

The voltage dropped at the beginning for around 1.5 hours and attained a stable value of 2.46 V, and on the 49th day of the experiment, the voltage was recorded as 2.42 V (Figure 5.9 B). Similarly, after connecting the LED, the initial current recorded was ~100 µA (Figure 5.9C) which decreased for around 1.5 hours and attained a stable current of ~10 µA. Thereafter, the current dropped gradually to about 5-7 µA and maintained a similar pattern until the 49th day. On the 49th day of the experiment, the current recorded was 4.1 µA. Figure 5.9(D) shows the graph of power dissipation by the LED with respect to time from the stacked EFC. The maximum power was recorded to be 260µWcm^{-2}, which steeply decreased for around 1.5 hours and attained an almost stable value of ~ 35µWcm^{-2}. On the 49th day, the power dissipation was ~ 10µWcm^{-2}. Nevertheless, the LED was glowing for the entire period. The most remarkable achievement obtained through this design strategy is the operational stability of the EFC with a half-life ($t_{½}$) of ~372 days (w.r.t the voltage), which is much higher than the available reports (Das et al., 2014; Ramanavicius et al., 2008b).

Efforts made to improve the power generation in pure EFC are vast; however, in most of the cases, the power stability over a time scale with a load is not known to understand the practical applicability of the developed devices (Prasad et al., 2014; Kang et al., 2018;

Miyake et al., 2013). The adoption of stacking the chip based EFC through series connection has been studied with an aim of improving the current signal to a significant level for the sensing applications (Jeerapan et al., 2016). The majority of the studies has utilized glucose or lactate as the fuel substrates with an aim of using these devices as biosensors in the healthcare and sports sectors (Cho et al., 2017; Hickey et al., 2016; Wang et al., 2018). However, the parallel research on using alcohol as fuel for the utility of EFC as a power generating device is limited. High potential stability under a load over an extended period of 49 days with unprecedented coulombic efficiency achieved through this study is a step forward on the technological endeavor of alcohol fuel based EFC.

5.3.4. Role of AOx on the operational stability of the EFC

Poor operational stability of enzyme-based devices is commonly implicated in the low stability of the proteinaceous biological catalysts that are often attributed to their structural change (Xiao et al., 2019). To understand the high operational stability of the EFC developed herein, the kinetic parameters of the AOx enzyme were evaluated under the anoxic operating condition maintained in the EFC and compared the results with the function of the enzyme kept under aerobic condition. Michaelis Menten constant (K_m) and maximum velocity (V_{max}) of the enzyme for the substrate alcohol were discerned from Hanes-Woolf plot for an incubation period of one month with a week interval time (table 5.2). For day one (0 h), the values are same for both aerobic and anoxic enzyme solutions. However, from day 8^{th} onwards only anoxic enzyme solutions show activity. The results confirmed that prolong functional stability of the AOx enzyme is achievable only under anoxic conditions. The effect of saturated dissolved oxygen on the catalytic function (20% inactivation) of AOx has been previously reported (Duff et al., 1991).

To understand the mechanism of oxygen-led inhibition of the enzyme, we analyzed the structural integrity of the AOx proteins incubated under both the aerobic and anoxic conditions separately with the help of CD spectroscopy. Interestingly, there was no significant difference detected in the secondary structural components (helix, beta strand, turn and random coil) of the protein incubated between the aerobic and anoxic conditions (Figure 5.10). Next, we extended the study to understand the effect of oxygen, which is the co-substrate and terminal electron acceptor for the reaction under natural conditions, on the 3D structure of the AOx protein. To this end, docking studies were performed with the assistance of PyRx software. The AutoDock Vina based docking resulted in nine Protein-Ligand interaction models with their respective binding affinities (Figure 5.11). The Best-fit docking structure has a binding affinity of -1.7 kcal mol^{-1}. The docking results indicated that there was no interaction between AOx protein surface and molecular oxygen as the binding affinities obtained were too low. Notably, -1 to -2 kcal mol^{-1} is the lower limit of uncertainty and true convergence of protein-ligand is impossible. The systematic errors of the force field parameters themselves can give values ranging between -1 to -2 kcal mol^{-1} (Limongelli, 2020). The PLIP server also failed to detect any hydrophilic or hydrophobic interactions confirming the lack of any binding of molecular oxygen with the protein surface of AOx.

The results from the enzyme kinetic, CD and docking studies prompted us to conclude that the rapid reduction of enzyme activity of the AOx under aerobic incubation condition was not due to the structural deformation of the enzyme protein. It is likely that a constant interaction of the dioxygen with the chemical moieties in the tunnel or FAD redox center causes a detrimental chemical effect to the functional activity of the enzyme, while the effect is not sufficient to trigger any structural change to the protein. It may be mentioned that AOx belongs to GMC (Glucose-Methanol-Choline) oxidoreductase family with FAD as its cofactor. A widely accepted view is that the molecular oxygen preferentially diffuses through

some specific tunnels of the oxidase protein, converging to the reactive site of the flavin for the redox reaction (Romero et al., 2018).

In a nutshell, we have performed kinetic studies of AOx enzyme along with CD studies in aerobic and anoxic conditions to mimic the fuel cell environment. The results obtained in these experiments contradicted each other. To further understand the reason a simple docking was performed. We already knew from literature and have mentioned in the chapter that oxygen reacts with the FAD cofactor. So docking was performed only to know if oxygen molecule had any reaction with the polypeptides of the protein. Regarding free and immobilized enzyme, we haven't performed any experiment and in future we will look in to the matter.

5.4. Conclusions

A simple EFC design for high operational stability and automatic fuel dispensing facility has been developed for the first time. The device involves an integrated fuel storage tank from which the fuel passively and continuously flows to the MEA for generating power in the EFC. The design makes the fuel cell system compact and allows the fuel flow to the MEA at a rate governed by the enzyme-electrocatalytic reaction kinetic, minimizing its pressure force on the integrity of the enzyme-nanocomposite layer on the electrode surface. Further, the design offers flexibility to use the cells as either bio-battery or biofuel cell with a maximum open circuit potential of 3.1 V for six EFC units connected in series. To improve the power further, the present system offers provision for stacking more number of unit EFCs in series or in parallel or a combination of both. One of the most important advancements offered by the present invention is the rational design of the enzyme electrodes and their mode of assembly in the MEA. These nanocomposite paste-based 3rd generation

enzyme electrodes operating through the DET principle offer biocompatible and conductive supports for the catalysts enzymes in anode and cathodes for their efficient bioelectrocatalytic functions. This new design facilitates adequate airflow to the cathode for enhancing oxygen reduction reactions and maintains uniform pressure to sustain the integrity of the MEA. The unprecedented coulombic efficiency (60.05%) and operational stability (half-life of ~372 days w.r.t voltage) obtained for the EFC has been attributed to the cumulative effect of anoxic design of the anodic chamber, passive fuel dispensing facility to the anode, nanocomposite based MEA for efficient function of the enzyme catalysts, and aerobic design in cathode for facilitating its ORR. A linked critical finding that emerged from this investigation was the detrimental effect of the prolonged interaction of the oxygen on the functional activity of AOx enzymes. Interestingly, it was revealed that the inactivation occurs without any structural distortion of the enzyme protein. The exciting finding has opened up an avenue for further research to understand the exact molecular mechanism on the interaction of dioxygen with the protein matrix and its possible consequence on the functional integrity of the AOx enzyme. With this efficient design construct as a basis, further research to optimize the volumetric power density will greatly facilitate the application potential of the EFC to serve as a stand-alone power supply for small-scale appliances.

Figures

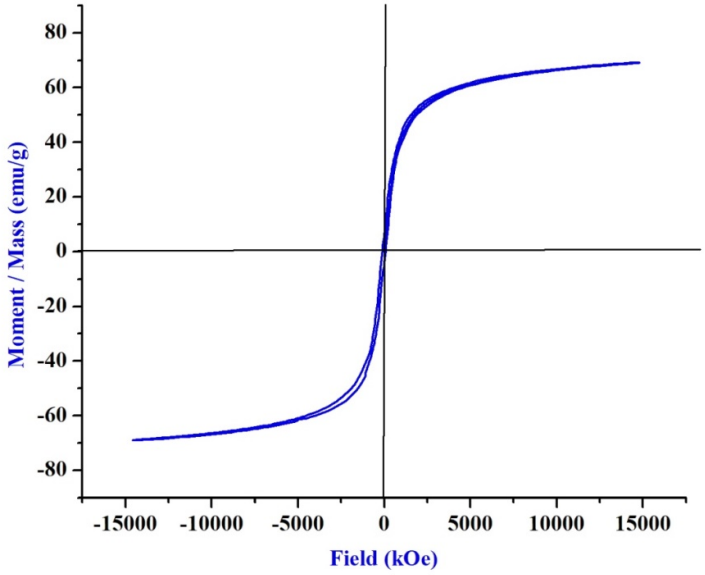

Figure 5.1. Hysteresis loop of MNp by VSM

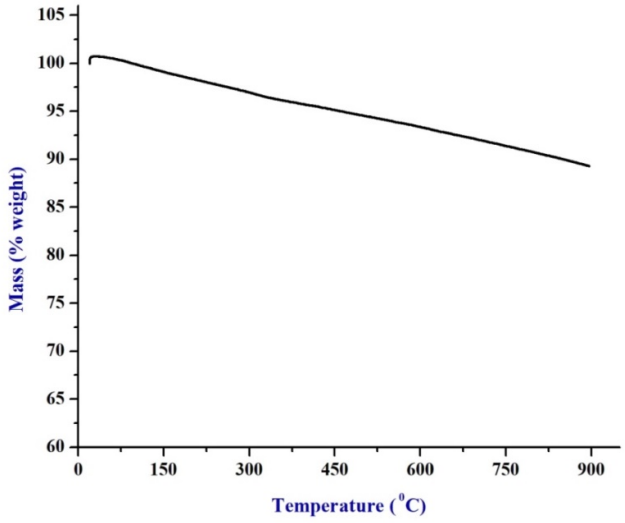

Figure 5.2. TGA curve of MNp

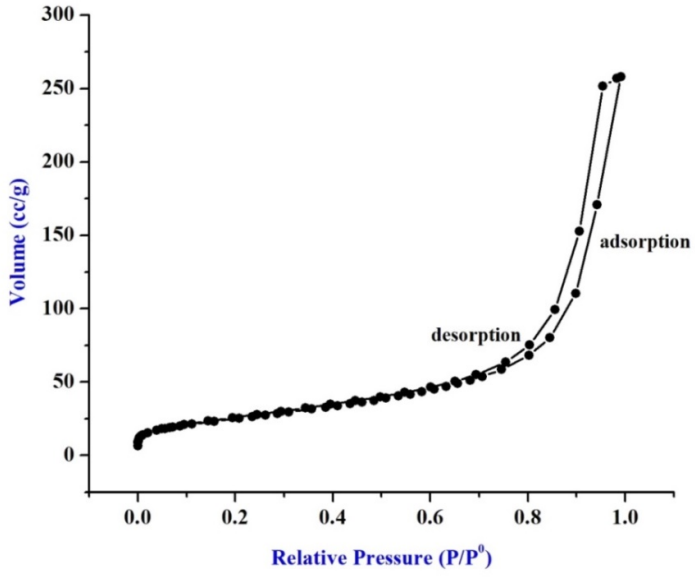

Figure 5.3. Nitrogen adsorption-desorption isotherm for MNp

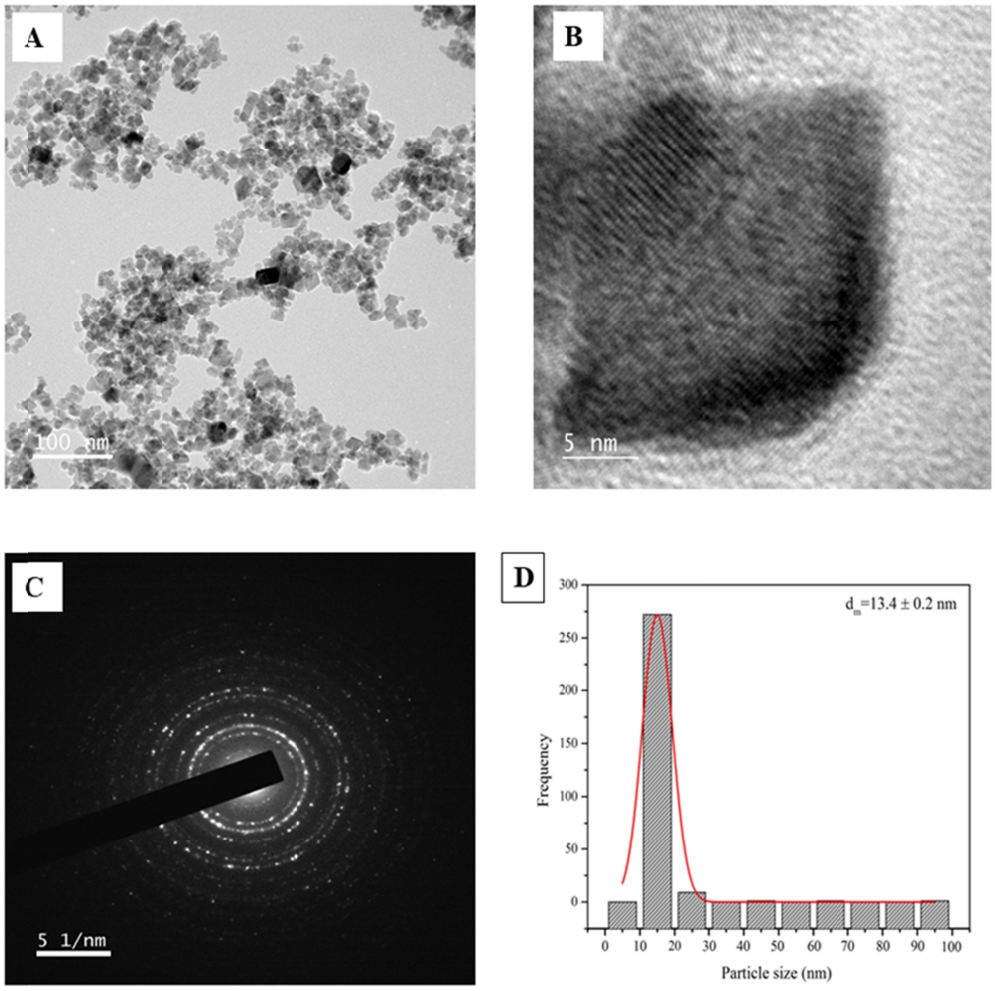

Figure 5.4. (A) TEM images of MNp (B) HRTEM of MNp (C) Selected Area Electron Diffraction (SAED) (D) size distribution of MNp

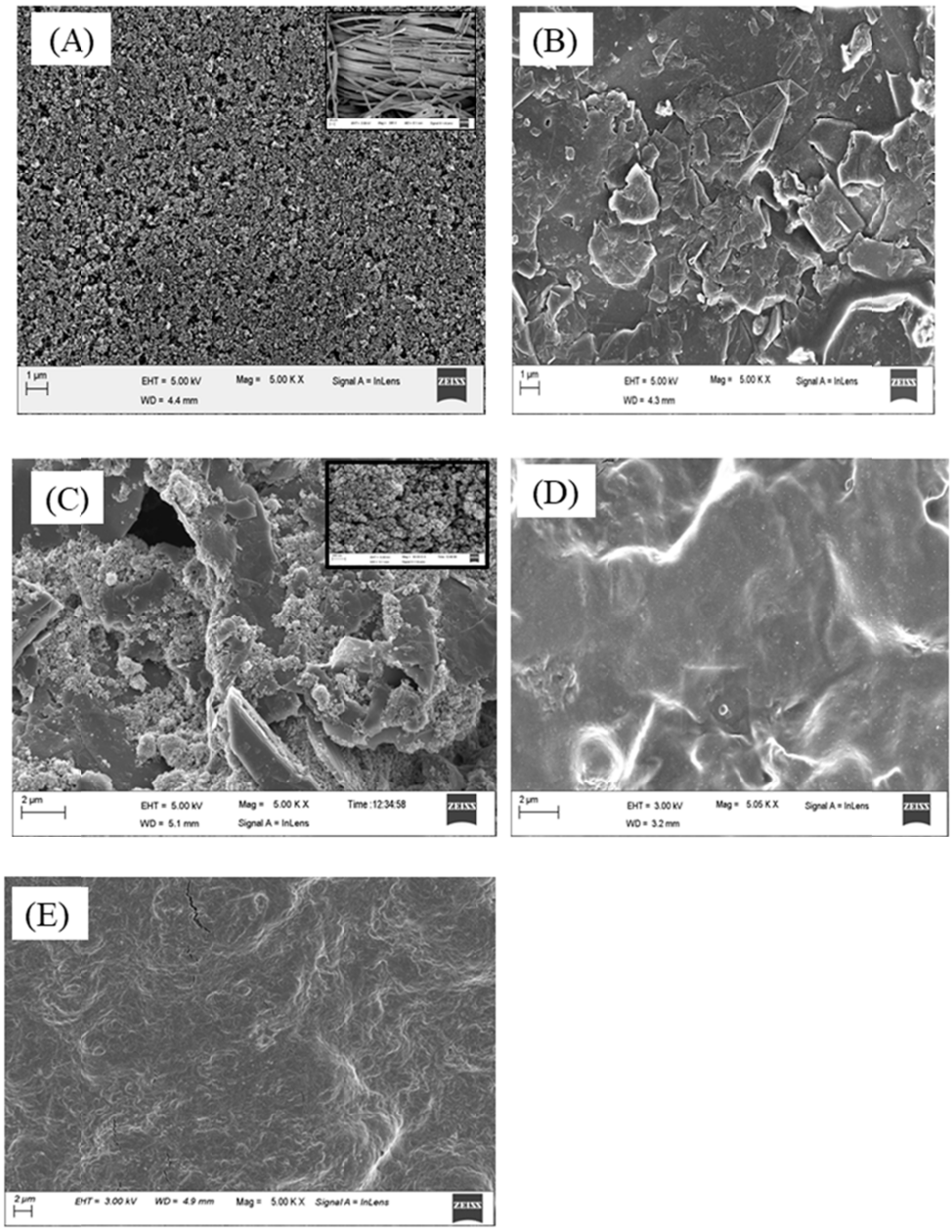

Figure 5.5. FESEM image of (A) blank CC electrode (5 kX) with inset at 200X, (B) CC with hydrophilic paste (5 kX), (C) MNp-Nf layer over the hydrophilic paste on CC (5kX) with inset at 50 kX (D) AOx enzyme entrapped with chitosan over NP on CC (5 kX), (E) BOx enzyme entrapped with chitosan over NP on CC (5kX).

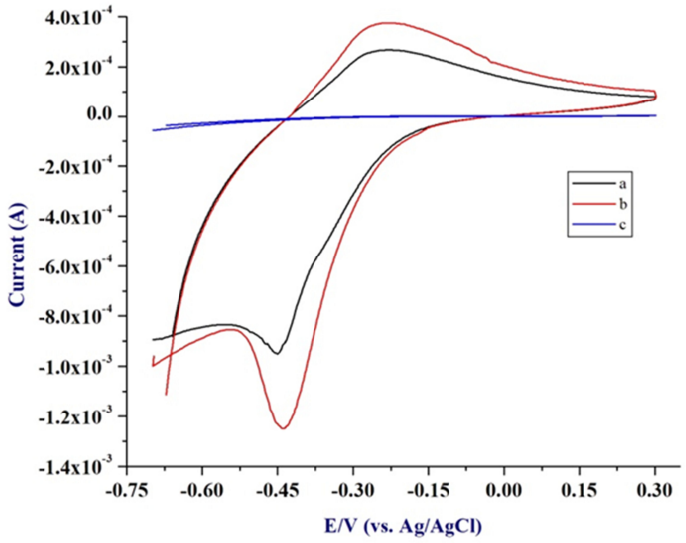

Figure 5.6. CV of (a) CC-NP-AOx-CS bioanode without methanol, (b) CC-NP-AOx-CS bioanode with 2 µM methanol, (c) CC blank electrode in 0.1 M KPBS, pH 7.5.

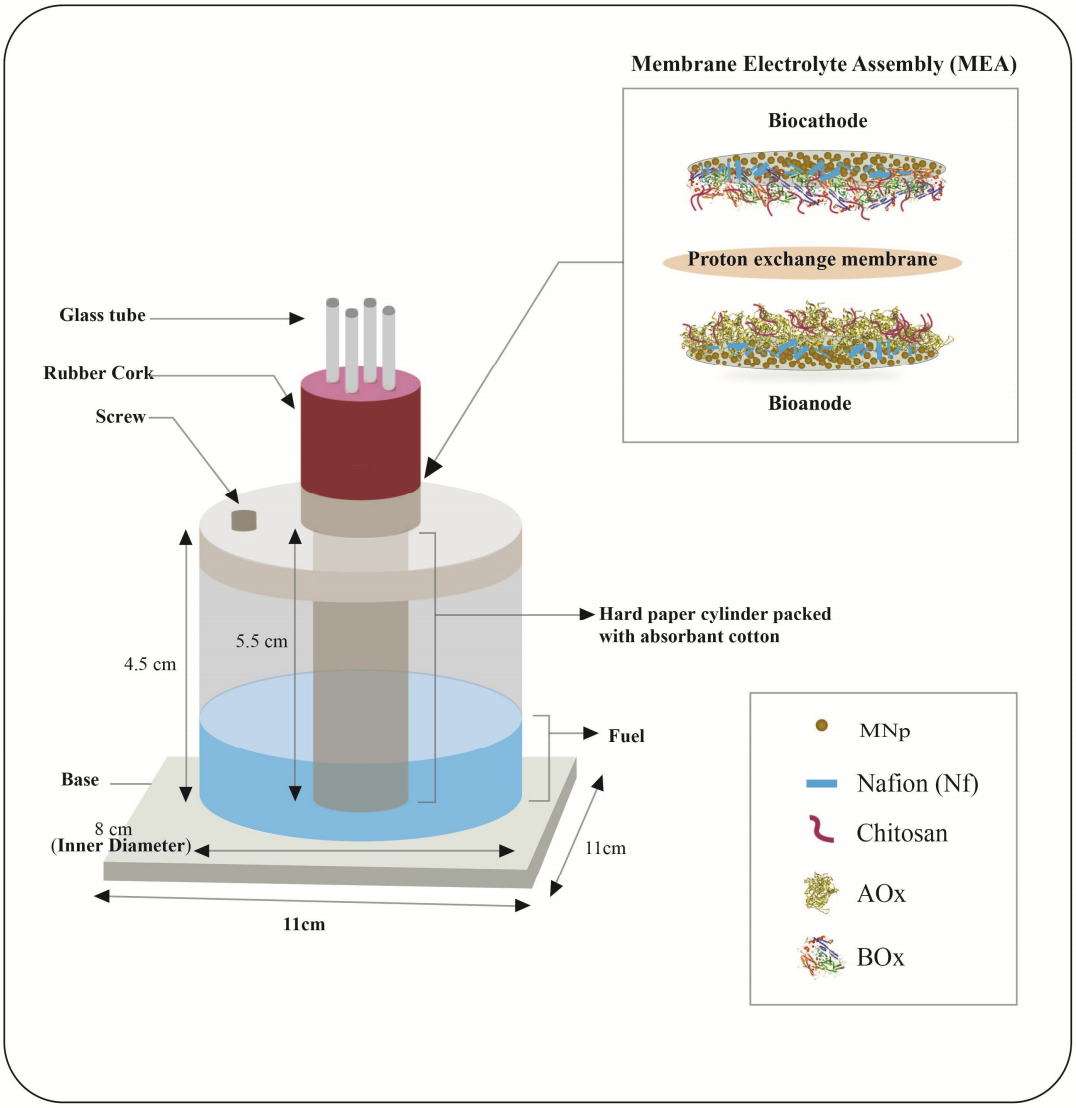

Figure 5.7. Schematic diagram of the EFC set up fabricated with acrylic glass (lateral view).

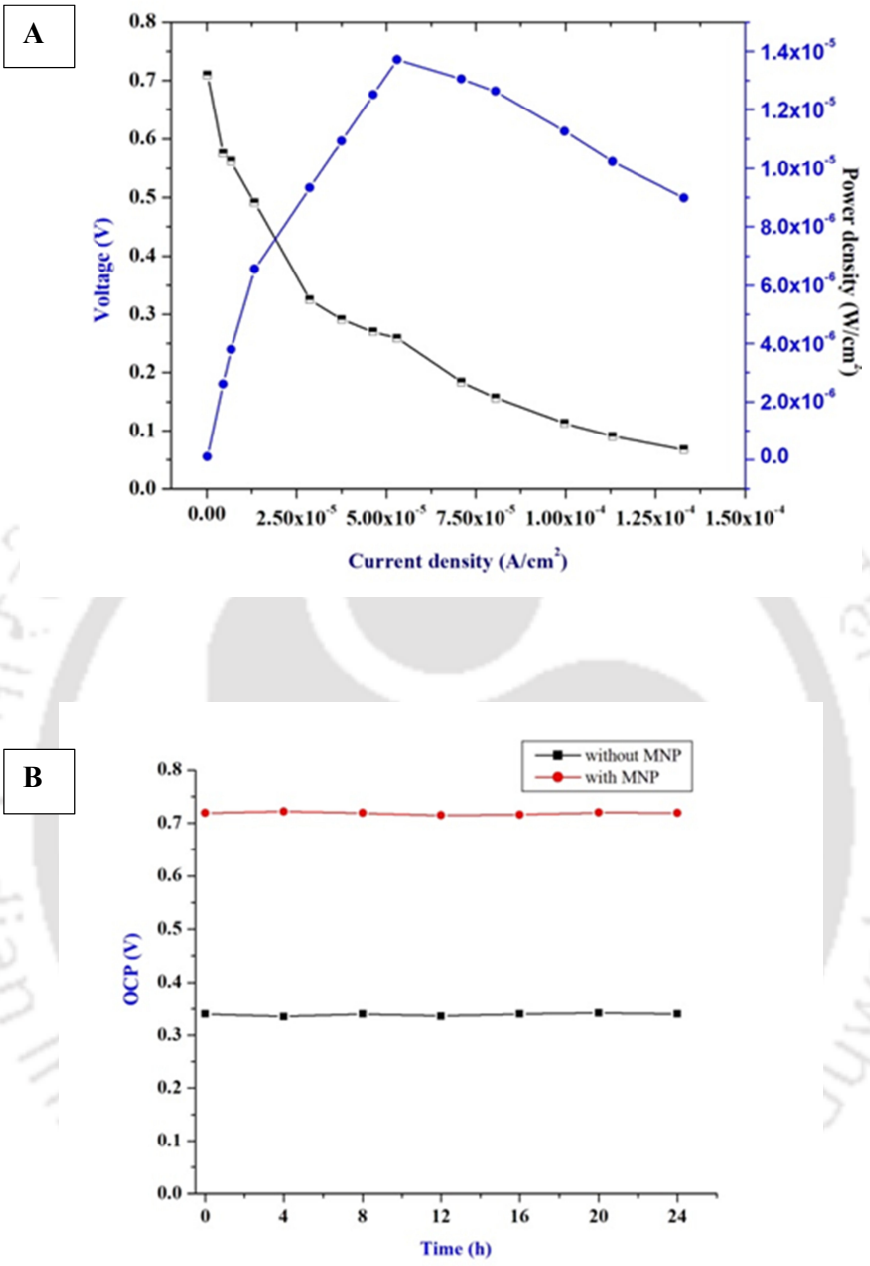

Figure 5.8. (A) Polarization curve of an EFC unit. (B) OCP of EFC with and without MNp

A

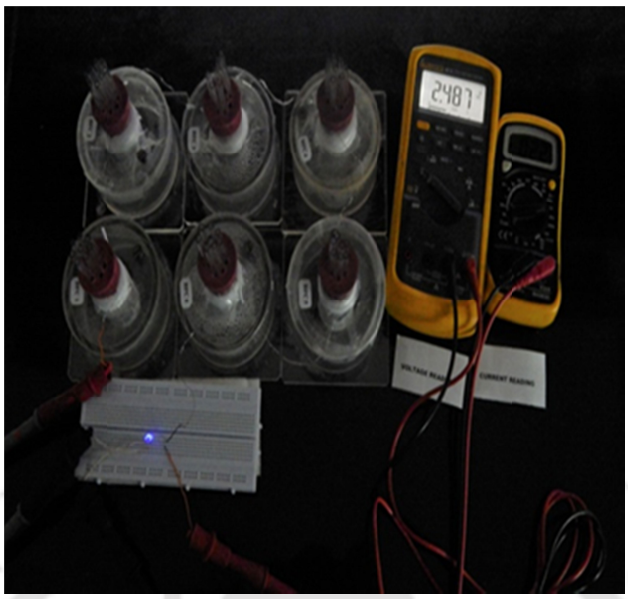

B

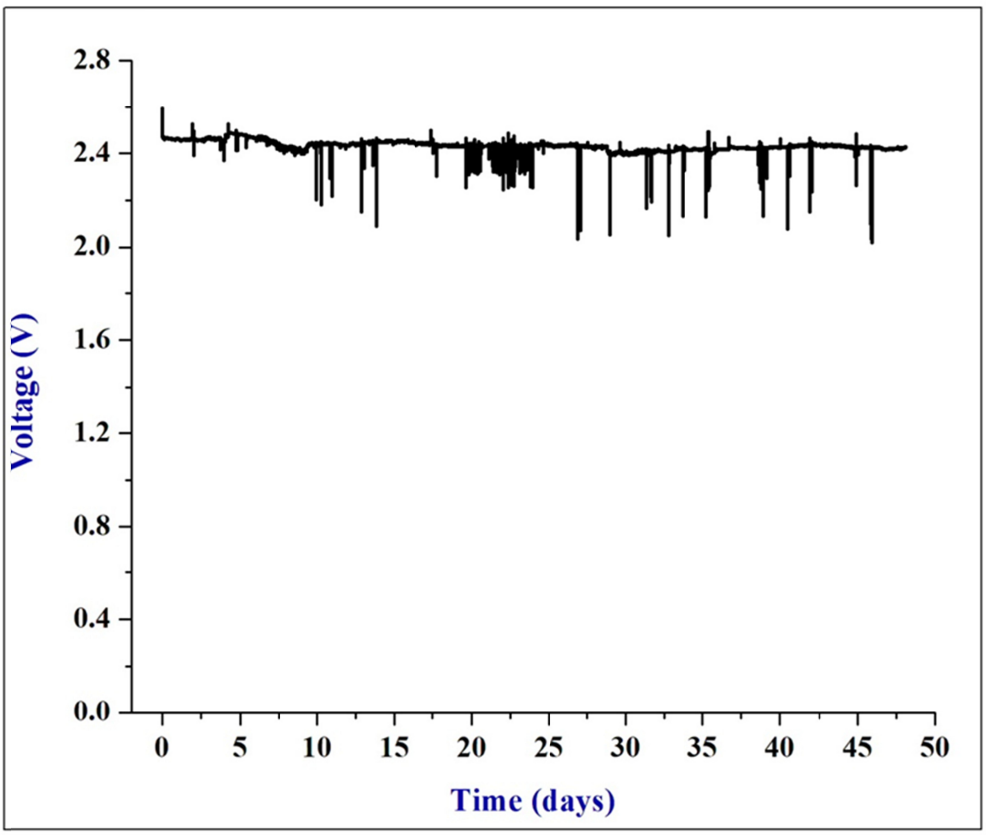

C

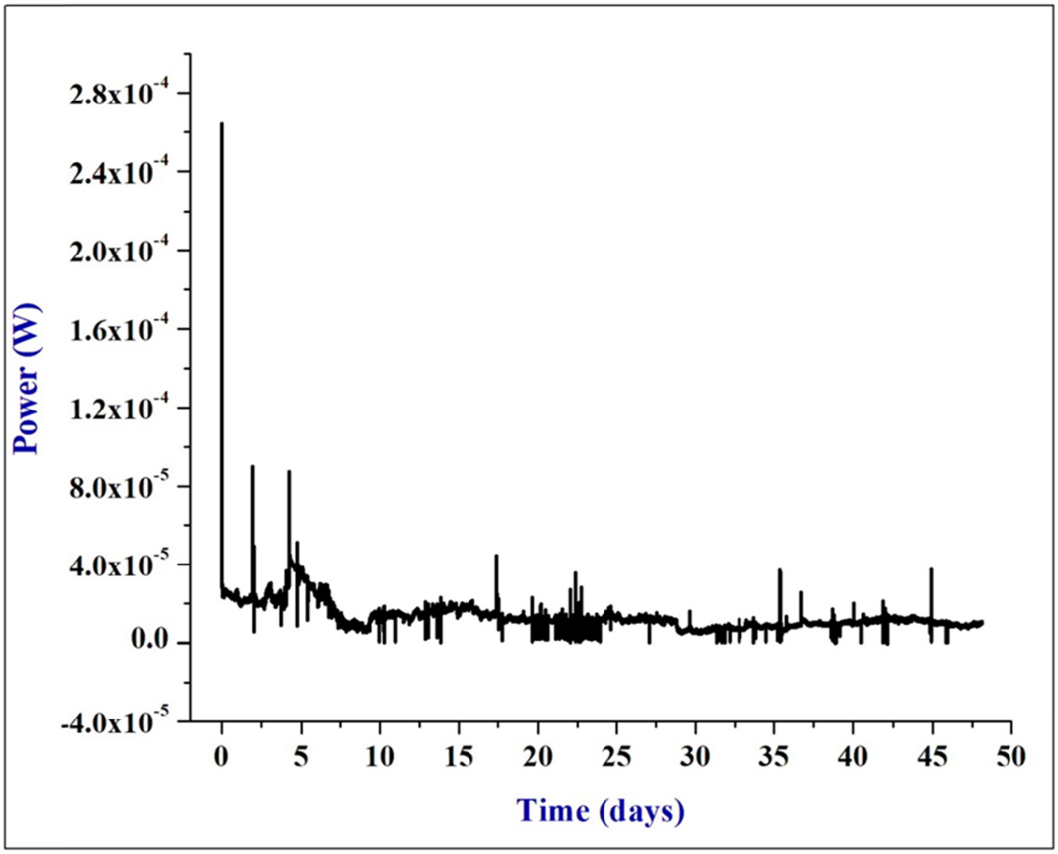

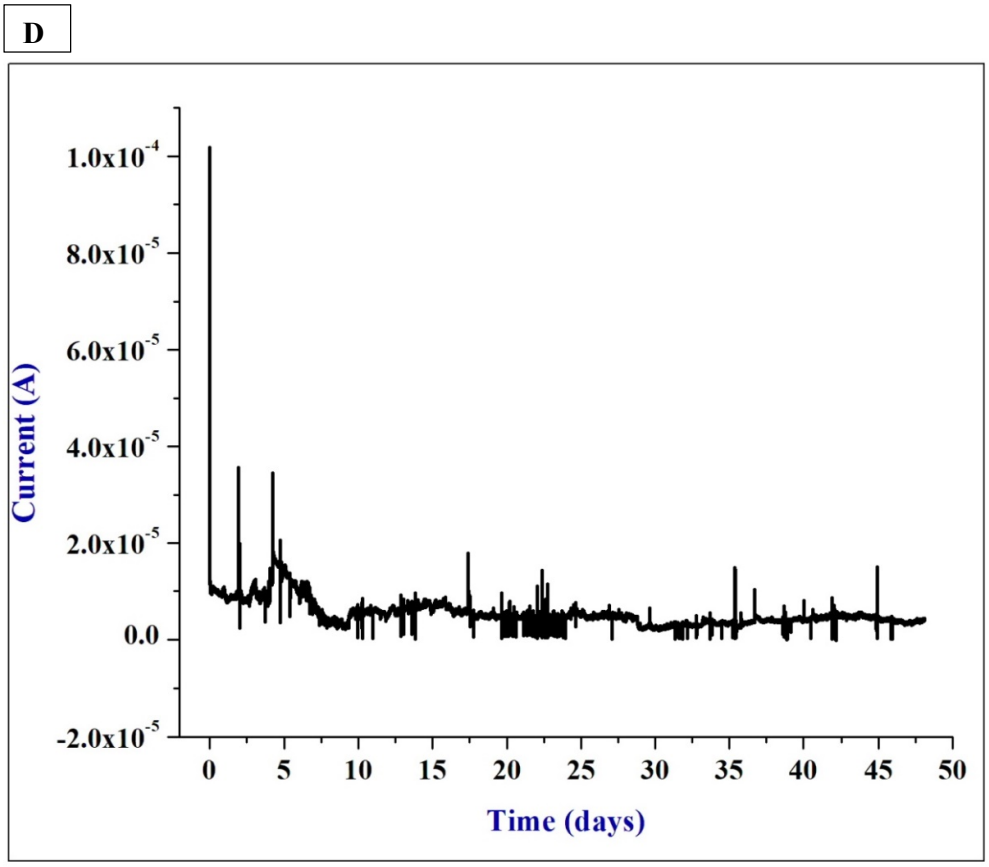

Figure 5.9. (A) Photograph (taken by Nikon Coolpix L830 with 16 megapixel) of the series connected six EFC setup operated by using an LED (B) Voltage with respect to time of the stacked EFC after connecting to LED (C) Current with respect to time of the stacked EFC after connecting to LED (D) Power with respect to time of the stacked EFC after connecting to LED.

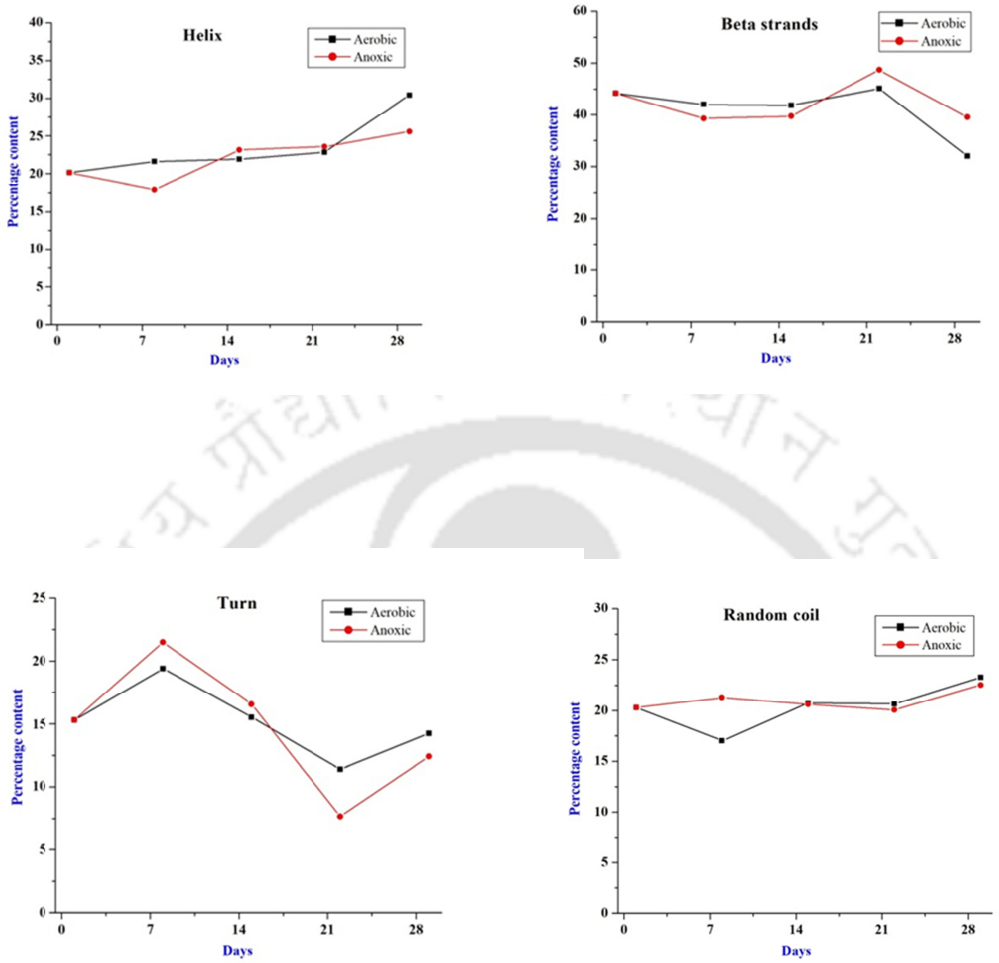

Figure 5.10. CD studies on the secondary structural component (in %) versus incubation time (in days) of AOx protein in aerobic and anoxic conditions.

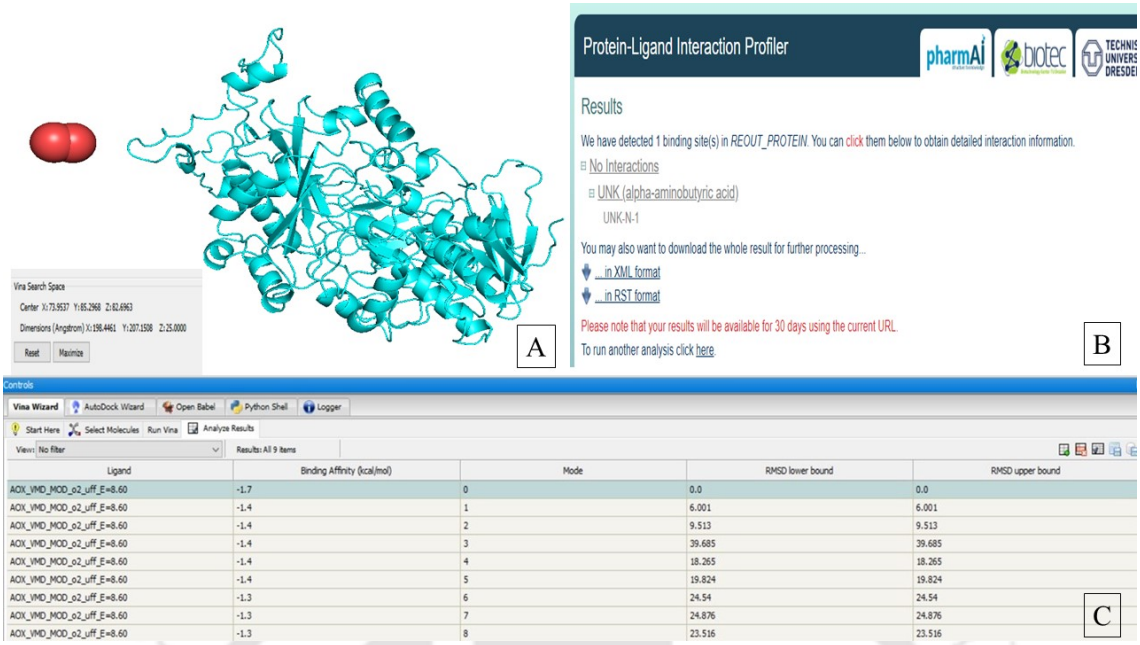

Ligand	Binding Affinity (kcal/mol)	Mode	RMSD lower bound	RMSD upper bound
AOX_VMD_MOD_o2_uff_E=8.60	-1.7	0	0.0	0.0
AOX_VMD_MOD_o2_uff_E=8.60	-1.4	1	6.001	6.001
AOX_VMD_MOD_o2_uff_E=8.60	-1.4	2	9.513	9.513
AOX_VMD_MOD_o2_uff_E=8.60	-1.4	3	39.685	39.685
AOX_VMD_MOD_o2_uff_E=8.60	-1.4	4	18.265	18.265
AOX_VMD_MOD_o2_uff_E=8.60	-1.4	5	19.824	19.824
AOX_VMD_MOD_o2_uff_E=8.60	-1.3	6	24.54	24.54
AOX_VMD_MOD_o2_uff_E=8.60	-1.3	7	24.876	24.876
AOX_VMD_MOD_o2_uff_E=8.60	-1.3	8	23.516	23.516

Figure 5.11 (A) Docked pdb structure obtained from Pymol, AOx with oxygen molecule (inset: Dimensions of the Docking area). (B) PLIP results window screen shot. (C) Tabulation of different binding poses obtained with their respective binding affinities.

Table

Fill factor	**Reference**
40%	Arrocha et al., 2014
25%	Katz et al., 1999
25%	Willner et al., 1998
27.45%	Present work

Table 5.1: Comparative account on the fill factors of some EFCs reported in the literature

	Aerobic condition		Anoxic condition	
Day	K_m (μM)	V_{max} (μM min^{-1})	K_m(μM)	V_{max} (μM min^{-1})
1	3.32	0.016	3.32	0.016
8	–	–	7.41	0.337
15	–	–	10.27	0.110
22	–	–	18.73	0.442
29	–	–	20.18	0.510

Table 5.2: Enzyme activity study of AOx in aerobic and anoxic conditions.

Conclusions and Scope for Future Research

Conclusions and Scope for Future Research

The major objective defined for the present investigation was to develop small scale enzymatic biofuel cell (EFC) for power generation application using alcohol as fuel substrate and for alcohol biosensing application using paper as support material. As the initial step, we conducted a study for the preparation of carbon based conductive ink for making electrodes on paper or other support material for fabricating EFC. For this, we have developed three graphite based conductive paste inks with three biopolymers namely silk sericin, silk fibroin and chitosan as stability and conductive enhancing additives. In all three pastes polyethylene glycol (PEG) acts as a binder or as a dispersant or as a drying-retarder agent. Specifically, graphite pastes containing sericin as an additive showed better conductivity and stability. The increased conductivity of the paste with sericin is due to the increased crystallinity of the graphite upon inclusion of sericin which is validated by powdered XRD study. Again, increased stability of the conductive traces made from the above selected biopolymers might be attributed to the contributions from the lowering of solubility of chitosan at neutral pH, developing highly ordered β structure and glue like properties of silk fibroin and silk sericin, respectively. The incorporation of PEG into the sericin solution is known to induce changes in secondary structure from random coils to β sheets which decrease the solubility of sericin in water resulting in increased stability. The prepared ink may be applied to a rigid or flexible substrate such as paper through direct writing/ brushing technique. Whether the substrate is flexible or rigid in nature, the substrate may or may not have to be pretreated or pre-coated with any other substance before applying the ink. Moreover, direct writing/ brushing technique has an advantage over screen printing or inkjet printing as it requires fewer amounts of ink and is also applicable over a wide range of platforms. Again, since the pastes

are made from biocompatible polymers, this is particularly an important trait while preparing enzyme electrodes for development of biosensor and biofuel cell.

In another work, a laccase-based bioelectrode was successfully developed to act as a biocathode for biofuel cell application. Laccase was immobilized over osmium polymer supported MWCNT based nanocomposite matrix on graphite electrode, which provided an electroactive surface for facile electron transfer between the electrode and the redox center of the enzyme. The kinetic parameters at the electrode namely, heterogeneous electron transfer rate constant (k_s), charge transfer coefficient (α) and surface concentration of the ionic species (Γ) were estimated. The response of the electrode for oxygen substrate at the determined formal potential of laccase was established. The results infer the potential application of the constructed bioelectrode as oxygen breathed biocathode for biofuel cell application. The bioelectrode also offers a reliable electrochemical response towards pyrocatechol in a biocatalytic mode.

In the third phase of our work, we have developed a low-cost, self-powered paper-based biosensor for monitoring methanol utilizing precisely prepared Graphite-PEG-Sericin ink. The platform of EFC was prepared by making hydrophilic chambers and channels surrounded by hydrophobic barriers on chromatography paper through printing alkyl ketene dimer over the paper. The graphite conductive ink was applied over the hydrophilic chambers and channels to act as the electrodes of the EFC. This biofuel cell based biosensor used alcohol oxidase and bilirubin oxidase as anodic and cathodic enzymes, respectively. However, due to pH incompatibility, we couldn't use the laccase enzyme as the cathodic enzyme. The device operating mechanism is based on alcohol/oxygen enzymatic fuel cell using an electrochemical energy conversion as a transducing element for methanol monitoring. The biosensor showed a linear range of output current at 0.03125μM -0.5μM (R^2 = 0.9988) with a sensitivity of 0.66245

$\mu A \mu M^{-1}$ and detection limit of 0.022 μM. Therefore, the prepared device, which is likely to be of low cost, has the potential for sensitive and selective detection of methanol in the clinical and industrial settings of the developing world.

In our final phase of the work, we have developed a simple passively fueled EFC for high operational stability using carbon cloth as supporting electrode material. A nanocomposite paste comprised of precisely prepared Graphite-PEG-Sericin ink with magnetic nanoparticle was applied over carbon cloth for utilizing as immobilizing matrix for AOx and BOx enzyme for fabricating anode and cathode, respectively. The device was fabricated in-house using acrylic glass, which comprised an integrated fuel storage tank from which the fuel passively and continuously flows to the Membrane Electrode Assembly (MEA) for generating power in the EFC. The design makes the fuel cell system compact and permits the fuel flow to the MEA at a rate governed by the enzyme-electrocatalytic reaction kinetic, minimizing its pressure force on the integrity of the enzyme-nanocomposite layer on the electrode surface. Further, the design offers flexibility to use the cells as either bio-battery or biofuel cell with a maximum open circuit potential of 3.1 V for six EFC units connected in series. To improve the power further, the present system offers provision for stacking more unit EFCs in series or in parallel or a combination of both. The unprecedented coulombic efficiency (60.05%) and operational stability (half-life of ~372 days w.r.t voltage) obtained for the EFC has been attributed to the cumulative effect of anoxic design of the anodic chamber, nanocomposite based MEA for efficient function of the enzyme catalysts, passive fuel delivery facility to the anode, and aerobic design in cathode for facilitating its oxygen reduction reaction (ORR). A concomitant critical finding that emerged from this work was the detrimental effect of the prolonged interaction of oxygen on the functional activity of AOx enzymes. Interestingly, it was studied that

the inactivation occurs without any structural distortion of the enzyme protein. The exciting finding has opened up a possibility for further research to understand the exact molecular mechanism on the interaction of dioxygen with the protein matrix and its probable consequence on the functional integrity of the AOx enzyme. With this efficient design construct as a basis, further research to optimize the volumetric power density will greatly facilitate the application potential of the EFC to serve as a stand-alone power supply for small-scale appliances. In regards to the paper-based EFC scheme, the construct needs to be coupled with an electronic read-out system in processor–based integration for quantitative detection of alcohol in the sample. Overall, the proof-of-concepts developed through this investigation for the fabrication of EFCs with alcohol oxidase-bilirubin oxidase based catalytic systems for power generation and sensing applications have great prospects for real-world applications.

Bibliography

Addo, P.K., Arechederra, R.L., Minteer, S.D., 2011. Towards a rechargeable alcohol biobattery. J.Power Sources. 196, 3448-3451.

Aehle, W., 2007. Enzymes in Industry, Production and application. third ed. Weinheim: Wiley-VCH. pp. 74-77.

Agui L., Yanez-Sedeno, P., Pingarron, J., 2008. Role of carbon nanotubes in electroanalytical chemistry A Review. Anal. Chim. Acta 622, 11–47. https://doi.org/10.1016/j.aca.2008.05.070.

Allen, M.J., Tung, V.C., K.R.B., 2010. Honeycomb Carbon: A Review of Graphene. Chem. Rev. 110, 132–145. https://doi.org/10.1016/0090-8258(88)90279-X.

Altman, G.H., Horan, R.L., Adam, L., Chen, J., Beach, V., Vanepps, D., 2011. US 2011/0008406A1. Pat. Appl. Publ. 1.

Amir, L., Tam, T.K., Pita, M., Meijler, M.M., Alfonta, L., Katz, E., 2009. Biofuel cell controlled by enzyme logic systems. J. Am. Chem. Soc. 131, 826–832. https://doi.org/10.1021/ja8076704.

Arechederra, R. L., Minteer, S. D., 2009. Complete Oxidation of Glycerol in an Enzymatic Biofuel Cell. Fuel Cells 9, 63−69.

Arrocha, A.A., Cano-Castillo, U., Aguila, S.A., Vazquez-Duhalt, R., 2014. Enzyme orientation for direct electron transfer in an enzymatic fuel cell with alcohol oxidase and laccase electrodes. Biosens. Bioelectron. 61, 569–574. https://doi.org/10.1016/j.bios.2014.06.009.

Arun, R.K., Halder, S., Chanda, N., Chakraborty, S., 2014. A paper based self-pumping and self-breathing fuel cell using pencil stroked graphite electrodes. Lab Chip 14, 1661–1664. https://doi.org/10.1039/c4lc00029c.

Asefa, T., Duncan, C.T., Sharma, K.K., 2009. Recent advances in nanostructured chemosensors and biosensors. Analyst., 134, 1980-1990.

Attallah, O.A., Girgis, E., Abdel-Mottaleb, M.M.S.A., 2016. Synthesis of non-aggregated nicotinic acid coated magnetite nanorods via hydrothermal technique. J. Magn. Magn. Mater. 399, 58–63. https://doi.org/10.1016/j.jmmm.2015.09.059.

Bandodkar, A.J., Jia, W., Ramirez, J., Wang, J., 2015. Biocompatible Enzymatic Roller Pens for Direct Writing of Biocatalytic Materials: "Do-it-Yourself" Electrochemical Biosensors. Adv. Healthcare Mater. 4, 1215–1224.

Barriere, F., Kavanagh, P., Leech, D., 2006, A laccase-glucose oxidase biofuel cell prototype operating in a physiological buffer, Electrochim Acta, 51, 5187-5192.

Barron, M.K., Young, T.J., Johnston, K.P., Williams, R.O., 2003. Investigation of processing parameters of spray freezing into liquid to prepare polyethylene glycol polymeric particles for drug delivery. AAPS PharmSciTech 4, 1–13. https://doi.org/10.1208/pt040212.

Bartlett, P.N., Simon, E., Toh, C.S., 2002. Modified electrodes for NADH oxidation and dehydrogenase based biosensors. Bioelectrochem. 56, 117-122.

Barton, S.C., Gallaway, J., Atanassov, P., 2004. Enzymatic biofuel cells for implantable and microscale devices. Chem. Rev. 104, 4867–4886. https://doi.org/10.1021/cr020719k.

Barton, S.C., Kim, H.H., Binyamin, G., Zhang, Y., Heller, A., 2001, Electroreduction of O_2 to water on the "wired" laccase cathode, J.Phys. Chem B 105, 11917-11921.

Behera, S., Raj, C.R., 2007. Mercaptoethylpyrazine promoted electrochemistry of redox protein and amperometric biosensing of uric acid. Biosens. Bioelectron. 23, 556–561. https://doi.org/10.1016/j.bios.2007.06.012.

Bich, N., Wang, C., Zhen, L., Ting, W., Yang, H., 2019. Development of a facile and low-cost chitosan-modified carbon cloth for efficient self-pumping enzymatic biofuel cells. J. Power Sources 429, 111–119. https://doi.org/10.1016/j.jpowsour.2019.05.001.

Bucur, B., Lucian, Æ.G., 2008. Analysis of methanol – ethanol mixtures from falsified beverages using a dual biosensors amperometric system based on alcohol dehydrogenase and alcohol oxidase. Eur Food Res Technol 226, 1335–1342. https://doi.org/10.1007/s00217-007-0662-4.

Bullen, R.A., Arnot, T.C., Lakeman, J.B., Walsh, F.C., 2006. Biofuel cells and their development. Biosens. Bioelectron. 21, 2015–2045. https://doi.org/10.1016/j.bios.2006.01.030.

Campbell, A.S., Jeong, Y.J., Geier, S.M., Koepsel, R.R., Russell, A.J., Islam, M.F., 2015. Membrane/mediator-free rechargeable enzymatic biofuel cell utilizing graphene/single-wall carbon nanotube cogel electrodes. ACS Appl. Mater. Interfaces 7, 4056–4065. https://doi.org/10.1021/am507801x.

Chaki, N.K., Vijayamohanan, K., 2002. Self-assembled monolayers as a tunable platform for biosensor applications. Biosens. Bioelectron. 17, 1–12.

Chakma, B., Jain, P., Singh, N.K., Goswami, P., 2016. Development of an Indicator Displacement Based Detection of Malaria Targeting HRP-II as Biomarker for Application in Point-of-Care Settings. Anal. Chem. 88, 10316–10321. https://doi.org/10.1021/acs.analchem.6b03315.

Chakraborty, M., Hashmi, M.S.J., 2017. An overview of Biosensors and Devices, Reference module in Material Science and Materials Engineering.

Chen, H., Zhang, Y., Ma, Y., Chen, S., Wu, Y., Lu, Y., Ren, H., Xin, S., Bai, Y., 2021. Sand-Milling Exfoliation of Structure Controllable Graphene for Formulation of Highly Conductive and Multifunctional Graphene Inks. Adv. Mater. Interfaces. 8, 2000888.

Chen, T., Barton, S.C., Binyamin, G., Gao, Z., Zhang, Y., Kim, H., Heller, A., 2001. A miniature biofuel cell. J. Am. Chem. Soc, 123, 8630-8631.

Cheong, G.L.M., Lim, K.S., Jakubowicz, A., Martens, P.J., Poole-warren, L.A., Green, R.A., 2014. Conductive hydrogels with tailored bioactivity for implantable electrode coatings. Acta Biomater. 10, 1216–1226. https://doi.org/10.1016/j.actbio.2013.12.032.

Chinnadayyala, S.R., Kakoti, A., Santhosh, M., Goswami, P., 2014. A novel amperometric alcohol biosensor developed in a 3rd generation bioelectrode platform using peroxidase coupled ferrocene activated alcohol oxidase as biorecognition system. Biosens. Bioelectron. 55, 120–126. https://doi.org/10.1016/j.bios.2013.12.005.

Cho, E., Mohammadifar, M., Choi, S., 2017. A single-use, self-powered, paper-based sensor patch for detection of exercise-induced hypoglycemia. Micromachines 8, 265–276. https://doi.org/10.3390/mi8090265.

Cho, K.Y., Moon, J.Y., Lee, Y.W., Lee, K.G., Yeo, J.H., Kweon, H.Y., Kim, K.H., Cho, C.S., 2003. Preparation of self-assembled silk sericin nanoparticles. Int. J. Biol. Macromol. 32, 36–42. https://doi.org/10.1016/S0141-8130 (03)00023-0.

Chouler, J., Cruz-Izquierdo, Á., Rengaraj, S., Scott, J.L., Di Lorenzo, M., 2018. A screen-printed paper microbial fuel cell biosensor for detection of toxic compounds in water. Biosens Bioelectron. 102, 49–56.

Christwardana, M., Kim, D.H., Chung, Y., Kwon, Y., 2018. A hybrid biocatalyst consisting of silver nanoparticle and naphthalenethiol self-assembled monolayer prepared for anchoring glucose oxidase and its use for an enzymatic biofuel cell. Appl. Surf. Sci. 429, 180–186. https://doi.org/10.1016/j.apsusc.2017.07.023.

Ciniciato, G.P.M.K., Lau, C., Cochrane, A., Sibbett, S.S., Gonzalez, E.R., Atanassov, P., 2012. Development of paper based electrodes : From air-breathing to paintable enzymatic cathodes. Electrochim. Acta 82, 208–213. https://doi.org/10.1016/j.electacta.2012.06.094

Cinquin, P., Gondran, C., Giroud, F., Mazabrard, S., Pellissier, A., Boucher, F., Alcaraz, J.P., Gorgy, K., Lenouvel, F., Mathé, S., Porcu, P., Cosnier, S., 2010. A glucose Biofuel cell implanted in Rats. PLoS One 5, 1–7. https://doi.org/10.1371/journal.pone.0010476.

Clauwaert, P., Aelterman, P., Pham, T.H., De Schamphelaire, L., Carballa, M., Rabaey, K., Verstraete, W., 2008. Minimizing losses in bio-electrochemical systems: The road to applications. Appl. Microbiol. Biotechnol. 79, 901–913. https://doi.org/10.1007/s00253-008-1522-2.

Cooney, M.J., Svoboda, V., Lau, C., Martin, G., Minteer, S.D., 2008. Enzyme catalysed biofuel cells. Energy Environ. Sci. 1, 320–337. https://doi.org/10.1039/b809009b.

Costa, S.A., Azevedo, H.S., Reis, R.L., 2005. Enzyme immobilization in biodegradable polymers for biomedical applications. in: Reis, R.L., Roman, J.S., (Eds.), Biodegradable

Systems in Tissue Engineering and Regenerative Medicine. London: CRC Press LLC. pp. 301–323.

Coyle, E., Simmons, R., 2014. Understanding the Global Energy Crisis. Purdue University Press West Lafayette, Indiana.

Das, M., Barbora, L., Das, P., Goswami, P., 2014. Biofuel cell for generating power from methanol substrate using alcohol oxidase bioanode and air-breathed laccase biocathode. Biosens. Bioelectron. 59, 184–191. https://doi.org/10.1016/j.bios.2014.03.016.

Das, P., Das, M., Chinnadayyala, S.R., Singha, I.M., Goswami, P., 2016. Recent advances on developing 3rd generation enzyme electrode for biosensor applications. Biosens. Bioelectron. 79, 386–397. https://doi.org/10.1016/j.bios.2015.12.055.

Davis, F., Higson, S.P.J., 2005. Structured thin films as functional components within biosensors. Biosens. Bioelectron. 21, 1–20. https://doi.org/10.1016/j.bios.2004.10.001.

Davis, G., Hill, HAO, Aston, W.J., Higgins, I.J., Turner, A.P.F., 1983, Bioelectrochemical fuel cell and sensor based on a quinoprotein, alcohol dehydrogenase, Enzym Microbial Technol., 5, 383-388.

De Poulpiquet, A., Ciaccafava, A., Lojou, E., 2014. New trends in enzyme immobilization at nanostructured interfaces for efficient electrocatalysis in biofuel cells. Electrochim. Acta 126, 104–114. https://doi.org/10.1016/j.electacta.2013.07.133.

Desmet, C., Marquette, C.A., Blum, L.J., Doumèche, B., 2016, Paper electrodes for bioelectrochemistry : Biosensors and biofuel cells. Biosens. Bioelectron. 76, 145–163. https://doi.org/10.1016/j.bios.2015.06.052.

Diaconu, M., Litescu, S.C., Radu, G.L., 2010. Laccase-MWCNT-chitosan biosensor-A new tool for total polyphenolic content evaluation from in vitro cultivated plants. Sensors Actuators, B Chem. 145, 800–806. https://doi.org/10.1016/j.snb.2010.01.064.

Duff, S.J.B., Murray, W.D., Overend, R.P., 1991. Oxygen and temperature effects on acetaldehyde-induced catabolite inactivation in Pichia pastoris. Appl. Microbiol. Biotechnol. 36, 82–86. https://doi.org/10.1007/BF00164703.

El-Molla, M.M., 2007. Synthesis of polyurethane acrylate oligomers as aqueous UV-curable binder for inks of ink jet in textile printing and pigment dyeing. Dye. Pigment. 74, 371–379. https://doi.org/10.1016/j.dyepig.2006.02.021.

Erickson, K., Erni, R., Lee, Z., Alem, N., Gannett, W., Zettl, A., 2010. Determination of the local chemical structure of graphene oxide and reduced graphene oxide. Adv. Mater. 22, 4467–4472. https://doi.org/10.1002/adma.201000732.

Fischer, C., Fraiwan, A., Choi, S., 2016. A 3D paper-based enzymatic fuel cell for self-powered, low-cost glucose monitoring. Biosens. Bioelectron. 79, 193–197. https://doi.org/10.1016/j.bios.2015.12.020.

Freire, R.S., Pessoa, C.A., Mello, L.D., Kubota, L.T., 2003. Direct electron transfer: An approach for electrochemical biosensors with higher selectivity and sensitivity. J. Braz. Chem. Soc. 14, 230–243. https://doi.org/10.1590/S0103-50532003000200008.

Gai, P., Gu, C., Hou, T., Li, F., 2017. Ultrasensitive Self-Powered Aptasensor Based on Enzyme Biofuel Cell and DNA Bioconjugate: A Facile and Powerful Tool for Antibiotic Residue Detection. Anal. Chem. 89, 2163–2169. https://doi.org/10.1021/acs.analchem.6b05109.

Gantayat, S., Prusty, G., Rout, D.R., Swain, S.K., 2015. Expanded graphite as a filler for epoxy matrix composites to improve their thermal , mechanical and electrical properties. New Carbon Mater. 30, 432–437. https://doi.org/10.1016/S1872-5805 (15)60200-1.

Gao, F., Viry, L., Maugey, M., Poulin, P., Mano, N., 2010. Engineering hybrid nanotube wires for high-power biofuel cells. Nat. Commun. 1, 1–7. https://doi.org/10.1038/ncomms1000.

Garcia, S.O., Ulyanova, Y. V, Figueroa-Teran, R., Bhatt, K.H., Singhal, S., Atanassov, P., 2016. Wearable Sensor system powered by a biofuel cell for detection of Lactate Levels in Sweat. ECS J Solid State Sci Technol. 5, M3075-M3081. https://doi.org/10.1149/2.0131608jss.

Gellett, W., Kesmez, M., Schumacher, J. Akers,N. Minteer, S.D., 2010. Biofuel cells for portable power. Electroanalysis, 22, 727-731.

Germain, M.N., Arechederra, R.L., Minteer, S.D., 2008. Nitroaromatic actuation of mitochondrial bioelectrocatalysis for self-powered explosive sensors. J. Am. Chem. Soc. 130, 15272–15273. https://doi.org/10.1021/ja807250b.

Gomez, C., Shipovskov, S., Ferapontova, E.E., 2010, Peroxidase biocathodes for a biofuel cell development, Renewable Sustainable energy Reviews, 2, 013103-013103-12.

Gooding, J.J., 2005. Nanostructuring electrodes with carbon nanotubes : A review on electrochemistry and applications for sensing. Electrochim. Acta 50, 3049–3060. https://doi.org/10.1016/j.electacta.2004.08.052.

Gorecka, E., Jastrzebska, M., 2011. Immobilization techniques and biopolymer carriers. Biotechnol Food Sci. 75, 65–86.

Gorton, L., Lindgren, A., Larsson, T., Munteanu, F.D., Ruzgas, T., Gazaryan, I., 1999. Direct electron transfer between heme-containing enzymes and electrodes as basis for third generation biosensors. Anal. Chim. Acta 400, 91–108.

Goswami, P., Chinnadayyala, S. S. R, Chakraborty, M. Kumar, A.K., Kakoty, A., 2013. An overview on alcohol oxidases and their potential applications. Appl Microbiol Biotechnol 97, 4259–4275. https://doi.org/10.1007/s00253-013-4842-9.

Halámková, L., Halámek, J., Bocharova, V., Szczupak, A., Alfonta, L., Katz, E., 2012. Implanted biofuel cell operating in a living snail. J. Am. Chem. Soc. 134, 5040–5043. https://doi.org/10.1021/ja211714w.

Han, J. -W., Kim, B., Li, J., Meyyappan, M., 2014. Carbon nanotube ink for writing on cellulose paper. Mater. Res. Bull. 50, 249-253.

Hariani, P.L., Faizal, M., Ridwan, R., Marsi, M., Setiabudidaya, D., 2013. Synthesis and Properties of Fe_3O_4 Nanoparticles by Co-precipitation Method to Removal Procion Dye. Int. J. Environ. Sci. Dev. 4, 336–340. https://doi.org/10.7763/ijesd.2013.v4.366.

Hasani-Sadrabadi, M.M., Dashtimoghadam, E., Majedi, F.S., Hojjati Emami, S., Moaddel, H., 2011. A high-performance chitosan-based double layer proton exchange membrane with reduced methanol crossover. Int. J. Hydrogen Energy 36, 6105–6111. https://doi.org/10.1016/j.ijhydene.2011.01.010.

Hasani-Sadrabadi, M.M., Dashtimoghadam, E., Mokarram, N., Majedi, F.S., Jacob, K.I., 2012. Triple-layer proton exchange membranes based on chitosan biopolymer with reduced methanol crossover for high-performance direct methanol fuel cells application. Polymer (Guildf). 53, 2643–2651. https://doi.org/10.1016/j.polymer.2012.03.052.

Heller, A., 1992. Electrical Connection of Enzyme Redox Centers to Electrodes. J. Phys. Chem. 96, 3579–3587. https://doi.org/10.1021/j100188a007.

Heller, A., 2004. Miniature biofuel cells. Phys. Chem. Chem. Phys. 6, 209–216. https://doi.org/10.1039/b313149a.

Hickey, D.P., Reid, R.C., Milton, R.D., Minteer, S.D., 2016. A self-powered amperometric lactate biosensor based on lactate oxidase immobilized in dimethylferrocene-modified LPEI. Biosens. Bioelectron. 77, 26–31. https://doi.org/10.1016/j.bios.2015.09.013.

Ivnitski, D., Artyushkova, K., Khripin, C., Luckarift, H., Ramasamy, R., Johnson, G., Brinker, C.J., Atanassov, P., 2009. Surface Characterization and Direct Electrochemistry of Multi-Copper Oxidases. 216th ECS Meet. Abstr. https://doi.org/10.1149/ma2009-02/39/2969.

Ivnitski, D., Atanassov, P., 2007, Electrochemical studies of intramolecular electron transfer in laccase from Trametes versicolor. Electroanal. 19, 2307-2313.

Ivnitski, D., Branch, B., Atanassov, P., Apblett, C., 2006, Glucose oxidase anode for biofuel cell based on direct electron transfer, Electrochem Commun. 8, 1204-1210.

Ivnitski, D.M., Khripin, C., Luckarift, H.R., Johnson, G.R., Atanassov, P., 2010. Surface characterization and direct bioelectrocatalysis of multicopper oxidases. Electrochim. Acta 55, 7385–7393. https://doi.org/10.1016/j.electacta.2010.07.026.

Jeerapan, I., Sempionatto, J.R., Pavinatto, A., You, J.M., Wang, J., 2016. Stretchable biofuel cells as wearable textile-based self-powered sensors. J. Mater. Chem. A 4, 18342–18353. https://doi.org/10.1039/C6TA08358G.

Jenkins, P., Tuurala, S., Vaari, A., Valkiainen, M., Smolander, M., Leech, D., 2012. A mediated glucose / oxygen enzymatic fuel cell based on printed carbon inks containing aldose dehydrogenase and laccase as anode and cathode. Enzyme Microb. Technol. 50, 181–187. https://doi.org/10.1016/j.enzmictec.2011.12.002.

Ji, Y., Gai, P., Feng, J., Wang, L., Zhang, J., Zhu, J., 2017. A Fe_3O_4–carbon nanofiber/gold nanoparticle hybrid for enzymatic biofuel cells with larger power output. J. Mater. Chem. A Mater. energy Sustain. 5, 11026–11031. https://doi.org/10.1039/C7TA01931A.

Jia, W., Wang, X., Imani, S., Bandodkar, A.J., Ramírez, J., Mercier, P.P., Wang, J., 2014. Wearable textile biofuel cells for powering electronics. J. Mater. Chem. A 2, 18184–18189. https://doi.org/10.1039/c4ta04796f.

Kakoti, A., Siddiqui, M.F., Goswami, P., 2015. A low cost design and fabrication method for developing a leak proof paper based microfluidic device with customized test zone. Biomicrofluidics 026502. https://doi.org/10.1063/1.4918641.

Kamyshny, A., Magdassi, S., 2014. Conductive nanomaterials for printed electronics. Small 10, 3515–3535. https://doi.org/10.1002/smll.201303000.

Kang, Z., Jiao, K., Cheng, J., Peng, R., Jiao, S., Hu, Z., 2018. A novel three-dimensional carbonized PANI 1600 @ CNTs network for enhanced enzymatic biofuel cell. Biosens. Bioelectron. 101, 60–65. https://doi.org/10.1016/j.bios.2017.10.008.

Kano, K., 2002. Redox Potentials of Proteins and Other Compounds of Bioelectrochemical Interest in Aqueous Solutions. Rev. Polarogr. 48, 29–46. https://doi.org/10.5189/revpolarography.48.29.

Katz, E., Bu, A.F., Weg, M., 2001. Self-Powered Enzyme-Based Biosensors. J. Am. Chem. Soc. 123, 10752–10753.

Katz, E., Filanovsky, B., Willner, I., 1999. A biofuel cell based on two immiscible solvents and glucose oxidase and microperoxidase-11 monolayer-functionalized electrodes. New J. Chem. 23, 481–487. https://doi.org/10.1039/a808561g.

Katz, E., Willner, I., 2003. A biofuel cell with electrochemically switchable and tunable power output. J. Am. Chem. Soc. 125, 6803–6813. https://doi.org/10.1021/ja034008v.

Kaushik, S., Jacob, C.A., Goswami, P., 2021. Biofuel cells as an Emerging Biosensing Device, in: Goswami, P. (Eds.), Advanced Materials and Techniques for Biosensors and

Bioanalytical Applications. CRC Press, Taylor & Francis Group., Boca Raton London New York pp. 211-232.

Kaushik, S., Thungon, P.D., Goswami, P., 2020. Silk Fibroin: An Emerging Biocompatible Material for Application of Enzymes and Whole Cells in Bioelectronics and Bioanalytical Sciences. ACS Biomater. Sci. Eng. 6, 4337–4355. https://doi.org/10.1021/acsbiomaterials.9b01971.

Kemp, G.D., Dickinson, F.M., Ratledge, C., 1988. Inducible long chain alcohol oxidase from alkane-grown Candida tropicalis. Appl. Microbiol. Biotechnol. 29, 370–374. https://doi.org/10.1007/BF00265821.

Kim, D., Jeong, S., Moon, J., 2006. Synthesis of silver nanoparticles using the polyol process and the influence of precursor injection. Nanotechnology 17, 4019–4024. https://doi.org/10.1088/0957-4484/17/16/004.

Kim, J., Grate, J.W., Wang, P., 2008, Nanobiocatalysis and its potential applications, Trends Biotechnol, 26, 639-646.

Kim, J., Jeerapan, I., Imani, S., Cho, T.N., Bandodkar, A., Cinti, S., Mercier, P.P., Wang, J., 2016. Noninvasive Alcohol Monitoring Using a Wearable Tattoo-Based Iontophoretic-Biosensing System. ACS Sensors 1, 1011–1019. https://doi.org/10.1021/acssensors.6b00356.

Kim, J., Jia, H., Wang, P., 2006. Challenges in biocatalysis for enzyme-based biofuel cells. Biotechnol. Adv. 24, 296–308. https://doi.org/10.1016/j.biotechadv.2005.11.006.

Kim, Y.H., Campbell, E., Yu, J., Minteer, S.D., Banta, S., 2013. Complete oxidation of methanol in biobattery devices using a hydrogel created from three modified dehydrogenases. Angewandte Chemie International Edition. 52, 1437-1440.

Kjeang, E., Djilali, N., Sinton, D., 2009. Microfluidic fuel cells: A review. J. Power Sources 186, 353–369. https://doi.org/10.1016/j.jpowsour.2008.10.011.

Kjeang, E., Proctor, B.T., Brolo, A.G., Harrington, D.A., Djilali, N., Sinton, D., 2007. High-performance microfluidic vanadium redox fuel cell. Electrochim. Acta, 52, 4942–4946.

Komoda, N., Nogi, M., Suganuma, K., Otsuka, K., 2012. Highly sensitive antenna using inkjet overprinting with particle-free conductive inks. ACS Appl. Mater. Interfaces 4, 5732–5736. https://doi.org/10.1021/am301747p.

Kong, X., Gai, P., Ge, L., Li, F., 2020. Laser-Scribed N-Doped Graphene for Integrated Flexible Enzymatic Biofuel Cells. ACS Sustain. Chem. Eng. 8, 12437–12442. https://doi.org/10.1021/acssuschemeng.0c03051.

Kulys, J., Vidziunaite, R., 2003. Amperometric biosensors based on recombinant laccases for phenols determination. Biosens. Bioelectron. 18, 319–325. https://doi.org/10.1016/S0956-5663(02)00172-0.

Kuri, P.R., Das, P., Goswami, P., 2021. Fundamentals of Biosensors, in: Goswami, P. (Eds.), Advanced Materials and Techniques for Biosensors and Bioanalytical Applications. CRC Press, Taylor & Francis Group., Boca Raton London New york pp. 2-28.

Lau, C., Moehlenbrock, M.J., Arechederra, R.L., Falase, A., Garcia, K., Rincon, R., Minteer, S.D., Banta, S., Gupta, G., Babanova, S., Atanassov, P., 2015. Paper based biofuel cells: Incorporating enzymatic cascades for ethanol and methanol oxidation. Int. J. Hydrogen Energy 1–6. https://doi.org/10.1016/j.ijhydene.2015.06.108.

Laviron, E., 1974. Adsorption, autoinhibition and autocatalysis in polarography and in linear potential sweep voltammetry. Electroanal. Chem. Interfacial Electrochem. 52, 355–393. https://doi.org/10.1016/S0022-0728(74)80448-1.

Laviron, E., 1979. General expression of the linear potential sweep voltammogram in the case of diffusionless electrochemical systems. J Electroanal Chem. 101, 19-28.

Legros, F.J., Nuyens, V., Minet, E., Emonts, P., Boudjeltia, K.Z., Courbe, A., Ruelle, J.L., Colicis, J., De L'Escaille, F., Henry, J.P., 2002. Carbohydrate-deficient transferrin isoforms measured by capillary zone electrophoresis for detection of alcohol abuse. Clin. Chem. 48, 2177–2186. https://doi.org/10.1093/clinchem/48.12.2177.

Li, L., Liang, B., Li, F., Shi, J., Mascini, M., Lang, Q., Liu, A., 2013. Co-Immobilization of Glucose Oxidase and Xylose Dehydrogenase Displayed Whole Cell on Multiwalled Carbon Nanotube Nano- composite Films Modified Electrode for Simultaneous Voltammetric Detection of D-Glucose and D-Xylose. Biosens. Bioelectron. 42, 156−162.

Li, X., Tian, J., Garnier, G., Shen, W., 2010. Fabrication of paper-based microfluidic sensors by printing. Colloids Surfaces B Biointerfaces 76, 564–570. https://doi.org/10.1016/j.colsurfb.2009.12.023.

Li, Y., and Trush, M.A., 1994. Reactive oxygen-dependent DNA damage resulting from the oxidation of phenolic compounds by a copper-redox cycle mechanism. Cancer Res 54, 1895-1898.

Limongelli, V., 2020. Ligand binding free energy and kinetics calculation in 2020. Wiley Interdiscip. Rev. Comput. Mol. Sci. 10, 1–32. https://doi.org/10.1002/wcms.1455.

Liu, H., Cheng, Shaoan, Logan, B., 2005. Production of Electricity from Acetate or Butyrate Using a Single-Chamber Microbial Fuel Cell. Environ. Sci. Technol. 39, 658–662.

Liu, Y., Qu, X., Guo, H., Chen, H., Liu, B., Dong, S., 2006. Facile preparation of amperometric laccase biosensor with multifunction based on the matrix of carbon nanotubes chitosan composite. Biosens. Bioelectron. 21, 2195–2201. https://doi.org/10.1016/j.bios.2005.11.014.

Logan, B.E., Hamelers, B., Rozendal, R., Schröder, U., Keller, J., Freguia, S., Aelterman, P., Verstraete, W., Rabaey, K., 2006. Microbial fuel cells: Methodology and technology. Environ. Sci. Technol. 40, 5181–5192. https://doi.org/10.1021/es0605016.

MacVittie, K., Halámek, J., Halámková, L., Southcott, M., Jemison, W.D., Lobel, R., Katz, E., 2013. From "cyborg" lobsters to a pacemaker powered by implantable biofuel cells. Energy Environ. Sci. 6, 81–86. https://doi.org/10.1039/c2ee23209j.

Mano, N., 2008, A 280 μWcm^{-2} biofuel cell operating at low glucose concentration, Chemical Commun, 19, 2221-2223.

Mano, N., Mao, F., Heller, A., 2002. A miniature biofuel cell operating in a physiological buffer. J. Am. Chem. Soc. 124, 12962–12963. https://doi.org/10.1021/ja028514g

Mano, N., Mao, F., Heller, A., 2003. Characteristics of a miniature compartment-less glucose-O2 biofuel cell and its operation in a living plant. J. Am. Chem. Soc. 125, 6588–6594. https://doi.org/10.1021/ja0346328.

Mao, F., Mano, N., Heller, A., 2003. Long tethers binding redox centers to polymer backbones enhance electron transport in enzyme "wiring" hydrogels. J. Am. Chem. Soc. 125, 4951–4957. https://doi.org/10.1021/ja029510e.

Marcus, R. a., Sutin, N., 1985. Electron transfers in chemistry and biology. Biochim. Biophys. Acta - Rev. Bioenerg. 811, 265–322. https://doi.org/10.1016/0304-4173(85)90014-X.

Martinez, A.W., Phillips, S.T., Butte, M.J., Whitesides, G.M., 2007. Patterned paper as a platform for inexpensive, low-volume, portable bioassays. Angew. Chemie - Int. Ed. 46, 1318–1320. https://doi.org/10.1002/anie.200603817.

Martinez, A.W., Phillips, S.T., Whitesides, G.M., Carrilho, E., 2010. Diagnostics for the developing world: Microfluidic paper-based analytical devices. Anal. Chem. 82, 3–10. https://doi.org/10.1021/ac9013989.

Martins, M.V.A., Bonfim, C., Da Silva, W.C., Crespilho, F.N., 2010. Iron (III) nanocomposites for enzyme-less biomimetic cathode: A promising material for use in biofuel cells. Electrochem. commun. 12, 1509–1512. https://doi.org/10.1016/j.elecom.2010.08.020.

Matsumoto, N., Oshima, A., Yumura, M., Hata, K., Futaba, D.N., 2020. Crystalline and Electrical Property Improvement of Filtrated, Exfoliated Graphite Sheets by an In-Plane Current and Heating Treatment. Nanoscale Res Lett. 15, 195.

Mayer, A.M., Staples, R.C., 2002. Laccase: New functions for an old enzyme. Phytochemistry 60, 551–565. https://doi.org/10.1016/S0031-9422 (02)00171-1.

Mazurenko, I., Wang, X., de Poulpiquet, A., Lojou, E., 2017. H2/O2 Enzymatic Fuel Cells: From Proof-of-Concept to Powerful Devices. Sustainable Energy Fuels 1, 1475−1501.

Melo, M.N., Pereira, F.M., Rocha, M.A., Ribeiro, J.G., Diz, F.M., Monteiro, W.F., Ligabue, R.A., Severino, P., Fricks, A.T., 2020. Immobilization and characterization of horseradish peroxidase into chitosan and chitosan/PEG nanoparticles: A comparative study. Process Biochem. 98, 160–171. https://doi.org/10.1016/j.procbio.2020.08.007.

Mersal Gaber, A.M., 2009. Electrochemical sensor for Voltammetric determination of catechol based on screen printed graphite electrode. Int. J. Electrochem. Sci 4:1167-1177.

Minteer, S.D., Liaw, B.Y., Cooney, M.J., 2007. Enzyme-based biofuel cells. Curr. Opin. Biotechnol. 18, 1–7. https://doi.org/10.1016/j.copbio.2007.03.007.

Miyake, T., Haneda, K., Yoshino, S., Nishizawa, M., 2013. Flexible, layered biofuel cells. Biosens. Bioelectron. 40, 45–49. https://doi.org/10.1016/j.bios.2012.05.041.

Mohamad, N.R., Marzuki, N.H.C., Buang, N.A., Huyop, F., Abdul, Wahab R., 2015, Review; agriculture and environmental biotechnology, An overview of technologies for immobilization of enzymes and surface analysis techniques for immobilized enzymes. Taylor and Francis Biotechnology & Biotechnological Equipment, 29, 205–220.

Mohtasham, J., 2015. Review Article-Renewable Energies. Energy Procedia 74, 1289–1297. https://doi.org/10.1016/j.egypro.2015.07.774.

Morozova, O. V, Shumakovich, G.P., Gorbacheva, M.A., Shleev, S. V, Yaropolov, A.I., 2007. " Blue " Laccases. Biochem. 72, 1136–1150.

Munteanu, F.D., Ferreira, P., Ruiz-Dueñas, F.J., Martínez, A.T., Cavaco-Paulo, A., 2008. Bioelectrochemical investigations of aryl-alcohol oxidase from Pleurotus eryngii. J. Electroanal. Chem. 618, 83–86. https://doi.org/10.1016/j.jelechem.2008.02.023.

Murata, K., Kajiya, K., Nakamura, N., Ohno, H., 2009b. Direct electrochemistry of bilirubin oxidase on three-dimensional gold nanoparticle electrodes and its application in a biofuel cell. Energy & Environ Sci. 1280–1285. https://doi.org/10.1039/b912915d.

Murata, K., Suzuki, M., Kajiya, K., Nakamura, N., Ohno, H., 2009a, High performance bioanode based on direct electron transfer of fructose dehydrogenase at gold nanoparticle modified electrodes, Electrochemistry Communication, 11, 668-671.

Narváez, C.W., Lau, C., Ciniciato, G.P.M.K., Garcia, S.O., Sibbett, S.S., Petsev, D.N., Gupta, G., Atanassov, P., 2014. Practical electricity generation from a paper based biofuel cell powered by glucose in ubiquitous liquids. Electrochem. commun. 45, 44–47. https://doi.org/10.1016/j.elecom.2014.05.010.

Neto, S.A., Suda, E.L., Xu, S., Meredith, M.T., De Andrade, A.R., Minteer, S.D., 2013, Direct electron transfer based bioanodes for ethanol biofuel cells using PQQ-dependent alcohol and aldehyde dehydrogenase, Electrochim Acta, 87, 323-329.

Oh, S.E., Logan, B.E., 2007. Voltage reversal during microbial fuel cell stack operation. J. Power Sources 167, 11–17. https://doi.org/10.1016/j.jpowsour.2007.02.016.

Osman, M.H., Shah, a. a., Walsh, F.C., 2011. Recent progress and continuing challenges in bio-fuel cells. Part I: Enzymatic cells. Biosens. Bioelectron. 26, 3087–3102. https://doi.org/10.1016/j.bios.2011.01.004.

Ozimek, P., Veenhuis, M., van der Klei I.J., 2005, Alcohol oxidase: a complex peroxisomal, oligomeric flavoprotein, FEMS Yeast Research, 5, 975-983.

P. L. Yue and K. Lowther, 1986. Enzymatic Oxidation of C1 Compounds in a Biochemical fuel cell. Chem. Eng. J. 33, 69–77.

Pakapongpan, S., Tuantranont, A., Poo-Arporn, R.P., 2017. Magnetic Nanoparticle-Reduced Graphene Oxide Nanocomposite as a Novel Bioelectrode for Mediatorless-Membraneless Glucose Enzymatic Biofuel Cells. Sci. Rep. 7, 1–12. https://doi.org/10.1038/s41598-017-12417-0.

Pal, R.K., Farghaly, A.A., Collinson, M.M., Kundu, S.C., Yadavalli, V.K., 2016. Photolithographic Micropatterning of Conducting Polymers on Flexible Silk Matrices. Adv. Mater. 28, 1406–1412. https://doi.org/10.1002/adma.201504736.

Palmore, G. T. R., Bertschy, H., Bergens, S. H., Whitesides, G. M. A., 1998. Methanol/Dioxygen Biofuel Cell that Uses NAD(+)-Dependent Dehydrogenases as Catalysts: Application of an Electro-Enzymatic Method to Regenerate Nicotinamide Adenine Dinucleotide at Low Overpotentials. J. Electroanal. Chem. 443, 155−161.

Park, B.K., Kim, D., Jeong, S., Moon, J., Kim, J.S., 2007. Direct writing of copper conductive patterns by ink-jet printing. Thin Solid Films 515, 7706–7711. https://doi.org/10.1016/j.tsf.2006.11.142.

Park, B.W., Yoon, D.Y., Kim, D.S., 2010. Recent progress in bio-sensing techniques with encapsulated enzymes. Biosens. Bioelectron. 26, 1–10. https://doi.org/10.1016/j.bios.2010.04.033.

Peeling, R.W., Holmes, K.K., Mabey, D., Ronald, 2006. Rapid tests for sexually transmitted infections (STIs): the way forward. Sex. Transm. Infect. 82 Suppl 5, v1–v6. https://doi.org/10.1136/sti.2006.024265.

Pellegrino, S., Bruno, F.S., Petrarulo, M., 1999. Liquid chromatographic determination of ethyl alcohol in body fluids. J. Chromatogr. B Biomed. Sci. Appl. 729, 103–110. https://doi.org/10.1016/S0378-4347 (99)00131-0.

Perelaer, J., Smith, P.J., Mager, D., Soltman, D., Volkman, S.K., Subramanian, V., Korvink, J.G., Schubert, U.S., 2010. Printed electronics: The challenges involved in printing devices, interconnects, and contacts based on inorganic materials. J. Mater. Chem.20, 8446–8453. https://doi.org/10.1039/c0jm00264j.

Pielichowski, K., Flejtuch, K., 2002. Differential scanning calorimetry studies on poly (ethylene glycol) with different molecular weights for thermal energy storage materials. Polym. Adv. Technol. 13, 690–696.

Pingarron, J.M., Yanez-Sedeno, P., Gonzalez-Cortes, A., 2008, Gold nanoparticle based electrochemical biosensors, Electrochem Acta., 53, 5848-5866.

Prasad, K.P., Chen, Y., Chen, P., 2014. Three-Dimensional Graphene-Carbon Nanotube Hybrid for High- Performance Enzymatic Biofuel Cells. ACS Appl. Mater. Interfaces 6, 3387–3393. https://doi.org/10.1021/am405432b.

Quiocho, F.A., Richards, F.M., 1964. Intermolecular cross-linking of a protein in the crystalline state: carboxypeptidase A. Proc Natl Acad Sci. 52, 833-839.

Ramanavicius, A., Kausaite, A., Ramanaviciene, A., 2008 Enzymatic biofuel cell based on anode and cathode powered by ethanol. Biosens. Bioelectron. 24, 761–766. https://doi.org/10.1016/j.bios.2008.06.048.

Ramanavicius, A., Ramanaviciene, A., 2009, Hemoproteins in design of biofuel cells, Fuel Cells, 9, 25-36.

Ramesan, M.T., Athira, V.K., Jayakrishnan, P., Gopinathan, C., 2016. Preparation, characterization, electrical and antibacterial properties of sericin/poly (vinyl

alcohol)/poly(vinyl pyrrolidone) composites. J. Appl. Polym. Sci. 133, 1–10. https://doi.org/10.1002/app.43535.

Rincón, R.A., Lau, C., Luckarift, H.R., Garcia, K.E., Adkins, E., Johnson, G.R., Atanassov, P., 2011. Enzymatic fuel cells: Integrating flow-through anode and air-breathing cathode into a membrane-less biofuel cell design. Biosens. Bioelectron. 27, 132–136. https://doi.org/10.1016/j.bios.2011.06.029.

Rockwood, D.N., Preda, R.C., Yucel, T., Wang, X., Lovett, M.L., Kaplan, D.L., 2011. Materials fabrication from Bombyx mori silk fibroin. Nat Protoc 6, 1612–1631. https://doi.org/10.1038/nprot.2011.379.

Romero, E., Gómez Castellanos, J.R., Gadda, G., Fraaije, M.W., Mattevi, A., 2018. Same Substrate, Many Reactions: Oxygen Activation in Flavoenzymes. Chem. Rev. 118, 1742–1769. https://doi.org/10.1021/acs.chemrev.7b00650.

Roy, J.J., Abraham, T.E., Abhijith, K.S., Kumar, P.V.S., Thakur, M.S., 2005. Biosensor for the determination of phenols based on Cross-Linked Enzyme Crystals (CLEC) of laccase. Biosens. Bioelectron. 21, 206–211. https://doi.org/10.1016/j.bios.2004.08.024.

Ruff, A., Pinyou, P., Nolten, M., Conzuelo, F., Schuhmann, W., 2017. A Self-Powered Ethanol Biosensor. Chem Electro Chem 4, 890–897. https://doi.org/10.1002/celc.201600864.

Safarıkova, M., Safarik, I., 1999. Use of magnetic techniques for the isolation of cells. J Chromatogr B 722, 33–53.

Sakai, H., Nakagawa, T., Tokita, Y., Hatazawa, T., Ikeda, T., Tsujimura, S., Kano, K., 2009. A high-power glucose/oxygen biofuel cell operating under quiescent conditions. Energy Environ. Sci. 2, 133–138. https://doi.org/10.1039/b809841g.

Sarma, A.K., Vatsyayan, P., Goswami, P., Minteer, S.D., 2009. Recent advances in material science for developing enzyme electrodes. Biosens. Bioelectron. 24, 2313–2322. https://doi.org/10.1016/j.bios.2008.09.026.

Sarma, M.K., Quadir, M.G.A., Bhaduri, R., Kaushik, S., 2018. Composite polymer coated magnetic nanoparticles based anode enhances dye degradation and power production in

microbial fuel cells. Biosens. Bioelectron. 119, 94–102. https://doi.org/10.1016/j.bios.2018.07.065.

Saxena, U., Chakraborty, M., Goswami, P., 2011a. Covalent immobilization of cholesterol oxidase on self-assembled gold nanoparticles for highly sensitive amperometric detection of cholesterol in real samples. Biosens. Bioelectron. 26, 3037–3043. https://doi.org/10.1016/j.bios.2010.12.009.

Saxena, U., Das, M., Ahmad, S., Barbora, L., Borthakur, M., Verma, A., Bora, U., Goswami, P., 2011b. Multiwalled carbon nanotube-based bi- enzyme electrode for total cholesterol estimation in human serum. J. Exp. Nanosci. 6, 84–95. https://doi.org/10.1080/17458080.2010.487230.

Schaetzle, O., Barriere, F., Schroder, U., 2009, An improved microbial fuel cell with laccase as the oxygen reduction catalyst, Energy Env Sc., 2, 96-99.

Schmidt, H.L., Schuhmann, W., 1996. Reagentless oxidoreductase sensors. Biosens. Bioelectron. 11, 127–135. https://doi.org/10.1016/0956-5663 (96)83720-1.

Schweigert, N., Zehnder, A. J. B., Eggen, R. I. L., 2001. Chemical properties of catechols and their molecular modes of toxic action in cells, from microorganisms to mammals. Environmental Microbiology 3, 81-91.

Scott, R.A., Lukehart, C.M., 2007. Applications of physical methods to inorganic and bioinorganic chemistry, 10 edn. Hoboken, NJ: Wiley. 594 pp.

Sekretaryova A.N., Beni, V., Eriksson M., Karyakin A.A., Turner P.F., Vagin, M.Y., 2014. Cholesterol Self-Powered Biosensor. Anal. Chem. 86, 9540–9547.

Sheldon, R.A., Schoevaart, R., Langen, L.M.V., 2005. Cross-linked enzyme aggregates (CLEAs): A novel and versatile method for enzyme immobilization (a review). Biocatalysts Biotransformation 23, 141-147.

Shitanda I., Kato S., Hoshi Y., Itagaki M., T.S., 2013. Flexible and high-performance paper-based biofuel cells using printed porous carbon electrodes †. Chem. Commun. 49, 11110–11112. https://doi.org/10.1039/c3cc46644b.

Shitanda, I., Nohara, S., Hoshi, Y., Itagaki, M., Tsujimura, S., 2017. Short communication. A screen-printed circular-type paper-based glucose/O_2 biofuel cell. J. Power Sources 360, 516–519. https://doi.org/10.1016/j.jpowsour.2017.06.043.

Shleev, S., Pita, M., Yaropolov, A.I., Ruzgas, T., Gorton, L., 2006. Direct heterogeneous electron transfer reactions of *Trametes hirsuta* laccase at bare and thiol-modified gold electrodes. Electroanalysis 18, 1901–1908. https://doi.org/10.1002/elan.200603600.

Singh, N.K., Sanjay, M., Goswami, P., 2021. Carbon based Nanomaterials for Sensing Applications, in: Goswami, P. (Eds.), Advanced Materials and Techniques for Biosensors and Bioanalytical Applications. CRC Press, Taylor & Francis Group., Boca Raton London New York pp.164-182.

Sokic-Lazic, D., Minteer, S. D., 2009. Pyruvate/Air Enzymatic Biofuel Cell Capable of Complete Oxidation. Electrochem. Solid-State Lett. 12, F26−F28.

Solomon, E.I., Sundaram, U.M., Machonkin, T.E., 1996. Multicopper oxidases and oxygenases. Chem. Rev. 96, 2563–2605. https://doi.org/10.1021/cr950046o.

Southcott M., MavVittie K., Jemison, W.D., Lobel, R., Katz, E., 2013. Operating under conditions mimicking the human. Phys. Chem. Chem. Phys. 15, 6278–6283. https://doi.org/10.1039/c3cp50929j

Stock, R., Rice, C.B.F., 1974. Chromatographic Methods, 3rd ed., John Wiley & Sons, New York, 106.

Sun, Y., He, K., Zhang, Z., Zhou, A., Duan, H., 2015. Real-time electrochemical detection of hydrogen peroxide secretion in live cells by Pt nanoparticles decorated graphene-carbon nanotube hybrid paper electrode. Biosens. Bioelectron. 68, 358–364. https://doi.org/10.1016/j.bios.2015.01.017.

Tan, Y., Deng, W., Ge, B., Xie, Q., Huang, J., Yao, S., 2009. Biofuel cell and phenolic biosensor based on acid-resistant laccase-glutaraldehyde functionalized chitosan-multiwalled carbon nanotubes nanocomposite film. Biosens. Bioelectron. 24, 2225–2231. https://doi.org/10.1016/j.bios.2008.11.026.

Tasca, F., Gorton, L., Kujawa, M., Patel, I., Harreither, W., Peterbauer, C.K., Ludwig, R., Nöll, G., 2010. Increasing the coulombic efficiency of glucose biofuel cell anodes by combination of redox enzymes. Biosens. Bioelectron. 25, 1710–1716. https://doi.org/10.1016/j.bios.2009.12.017.

Teramoto, H., Miyazawa, M., 2003. Analysis of structural properties and formation of Sericin fiber by infrared spectroscopy. J. Insect Biotechnol. Sericology. https://doi.org/10.11416/jibs.72.157

Thungon, P.D., Kakoti, A., Ngashangva, L., Goswami, P., 2017. Advances in developing rapid , reliable and portable detection systems for alcohol. Biosens. Bioelectron. 97, 83–99. https://doi.org/10.1016/j.bios.2017.05.041.

Thurston. Christopher F., 1994. The structure and function of fungal laccases. Microbiology 140, 19–26.

Tiscione, N.B., Alford, I., Yeatman, D.T., Shan, X., 2011. Ethanol analysis by headspace gas chromatography with simultaneous flame-ionization and mass spectrometry detection. J. Anal. Toxicol. 35, 501–511. https://doi.org/10.1093/anatox/35.7.501.

Togo, M., Takamura, A., Asai, T., Kaji, H., Nishizawa, M., 2007, An enzyme based microfluidic biofuel cell using vitamin K_3-mediated glucose oxidation, Electrochinm Acta., 52, 4669-4674.

Topcagic, S., Minteer, S.D., 2006, Development of a membraneless ethanol/oxygen biofuel cell, Electrochem Acta., 51, 2168-2172.

Ulyanova, Y., Arugula, M.A., Rasmussen, M., Pinchon, E., Lindstrom, U., Singhal, S., Minteer, S.D., 2014. Bioelectrocatalytic Oxidation of Alkanes in a JP - 8 Enzymatic Biofuel Cell. ACS Catal. 4, 4289–4294. https://doi.org/10.1021/cs500802d.

Vatsyayan, P., Bordoloi, S., Goswami, P., 2010. Large catalase based bioelectrode for biosensor application. Biophys. Chem. 153, 36–42. https://doi.org/10.1016/j.bpc.2010.10.002

Venkata Mohan, S., Velvizhi, G., Annie Modestra, J., Srikanth, S., 2014. Microbial fuel cell: Critical factors regulating bio-catalyzed electrochemical process and recent

advancements. Renew. Sustain. Energy Rev. 40, 779–797. https://doi.org/10.1016/j.rser.2014.07.109.

Vijayakumar, A.R., Csöregi, E., Heller, A., Gorton, L., 1996. Alcohol biosensors based on coupled oxidase-peroxidase systems. Anal. Chim. Acta 327, 223–234. https://doi.org/10.1016/0003-2670(96)00093-1.

Wang, J., Musameh, M., Lin, Y., 2003. Solubilization of carbon nanotubes by Nafion toward the preparation of amperometric biosensors. J. Am. Chem. Soc. 125, 2408–2409. https://doi.org/10.1021/ja028951v.

Wang, L., Shao, H., Lu, X., Wang, W., Zhang, J.R., Song, R. Bin, Zhu, J.J., 2018. A glucose/O_2 fuel cell-based self-powered biosensor for probing a drug delivery model with self-diagnosis and self-evaluation. Chem. Sci. 9, 8482–8491. https://doi.org/10.1039/c8sc04019b.

Wang, W., Liu, W., Zeng, Y., Han, Y., Yu, M., Lu, X., Tong, Y., 2015. A novel exfoliation strategy to significantly boost the energy storage capability of commercial carbon cloth. Adv. Mater. 27, 3572–3578. https://doi.org/10.1002/adma.201500707.

Wang, X., Hagen, J.A., Papautsky, I., 2013. Paper pump for passive and programmable transport. Biomicrofluidics, 7, 014107-1–014107-10.

Wang, Y., Ge, L., Wang, P., Yan, M., Yu, J., Ge, S., 2014. A three-dimensional origami-based immuno-biofuel cell for self-powered, low-cost, and sensitive point-of-care testing. Chem. Commun. 50, 1947–1949. https://doi.org/10.1039/c3cc47731b.

Warren, H., Gately, R.D., Moffat, H. N., Panhuis, M. in het., 2013. Conducting carbon nanofibre networks: dispersion optimisation, evaporative casting and direct writing. RSC Adv. 3, 21936-21942.

Whitmore, L., Wallace, B.A., 2008. Protein secondary structure analyses from circular dichroism spectroscopy: Methods and reference databases. Biopolymers 89, 392–400. https://doi.org/10.1002/bip.20853.

Willner, I., Arad, G., Katz, E., 1998. A biofuel cell based on pyrroloquinoline quinone and microperoxidase-11 monolayer-functionalized electrodes. Bioelectrochemistry Bioenerg. 44, 209–214.

Wojtoniszak, M., Chen, X., Kalenczuk, R.J., Wajda, A., Łapczuk, J., Kurzewski, M., Drozdzik, M., Chu, P.K., Borowiak-palen, E., 2012. Synthesis, dispersion, and cytocompatibility of graphene oxide and reduced graphene oxide. Colloids Surfaces B Biointerfaces 89, 79–85. https://doi.org/10.1016/j.colsurfb.2011.08.026.

Wollenberger, U., Lisdat, F., Rose, A., Streffer, K., 2008. Phenolic biosensors. In, Bioelectrochemistry: Fundamentals, Experimental Techniques and Applications, John Wiley & Sons, Ltd. Ed. Bartlet P pp 219-247.

Xia, H.-q., So, K., Kitazumi, Y., Shirai, O., Nishikawa, K., Higuchi, Y., Kano, K., 2016. Dual Gas-Diffusion Membrane- and Mediatorless Dihydrogen/Air-Breathing Biofuel Cell Operating at Room Temperature. J. Power Sources. 335, 105−112.

Xiao, X., Xia, H., Wu, R., Bai, L., Yan, L., Magner, E., Cosnier, S., Lojou, E., Zhu, Z., Liu, A., 2019. Tackling the Challenges of Enzymatic (Bio) Fuel Cells. Chem. Rev. 119, 9509–9558. https://doi.org/10.1021/acs.chemrev.9b00115.

Xu, L., Armstrong, F.A., 2015. Pushing the limits for enzyme-based membrane-less hydrogen fuel cells-achieving useful power and stability. RSC Adv. 5, 3649–3656. https://doi.org/10.1039/c4ra13565b.

Xu, X., Lu, P., Zhou, Y., Zhao, Z., Guo, M., 2009. Laccase immobilized on methylene blue modified mesoporous silica MCM-41 / PVA. Mater. Sci. Eng. C 29, 2160–2164. https://doi.org/10.1016/j.msec.2009.04.019.

Yahiro, A.T., Lee, S.M., Kimble, D.O., 1964. Bioelectrochemistry. I. Enzyme utilizing bio-fuel cell studies. BBA - Spec. Sect. Biophys. Subj. 88, 375–383. https://doi.org/10.1016/0926-6577(64)90192-5.

Yakushi, T., Matsushita, K., 2010. Alcohol dehydrogenase of acetic acid bacteria: Structure, mode of action, and applications in biotechnology. Appl. Microbiol. Biotechnol. 86, 1257–1265. https://doi.org/10.1007/s00253-010-2529-z.

Yang, J.T., Wu, C.S.C., Martinez, H.M., 1986. Calculation of Protein Conformation from Circular Dichroism. Methods Enzymol. 130, 208–269. https://doi.org/10.1016/0076-6879(86)30013-2

Yue, H., Khoshtariya, D., Waldeck, D.H., Grochol, J., Hildebrandt, P., Murgida, D.H., 2006. On the Electron Transfer Mechanism between Cytochrome c and Metal Electrodes. Evidence for Dynamic Control at Short Distances, J. Physical Chemistry B. 110, 19906-19913.

Yun, H., Kim, M.K., Kwak, H.W., Lee, J.Y., Kim, M.H., Kim, E.H., Lee, K.H., 2013. Preparation and characterization of silk sericin/glycerol/graphene oxide nanocomposite film. Fibers Polym. 14, 2111–2116. https://doi.org/10.1007/s12221-013-2111-2.

Zhang 2002, US Patent application No US20090269825A1.

Zhang, H., Zhang, L., Han, Y., Yu, Y., Xu, M., Zhang, X., Huang, L., Dong, S., 2017. RGO/Au NPs/N-doped CNTs supported on nickel foam as an anode for enzymatic biofuel cells. Biosens. Bioelectron. 97, 34–40. https://doi.org/10.1016/j.bios.2017.05.030.

Zhang, H.; Deng, L.; Yang, M;, Min, S.' Yang, L., Zhu, L., 2011. Enhancing effect of glycerol on the tensile properties of bombyx mori cocoon sericin filmsInt. J. Mol. Sci. 12, 3170–3181.

Zhang, J.L., Wang, Y.H., Huang, K., Huang, K.J., Jiang, H., Wang, X.., 2021. Enzyme-based biofuel cells for biosensors and in vivo power supply. Nano Energy 84, 105853. https://doi.org/10.1016/j.nanoen.2021.105853

Zhang, L., Zhou, M., Dong, S., 2012a. A Self-Powered Acetaldehyde Sensor Based on Biofuel Cell. Anal. Chem. 84, 10345–10349.

Zhang, L., Zhou, M., Wen, D., Bai, L., Lou, B., Dong, S., 2012b. Small-size biofuel cell on paper. Biosens. Bioelectron. 35, 155–159. https://doi.org/10.1016/j.bios.2012.02.035.

Zhang, Y.Q., 2002. Applications of natural silk protein sericin in biomaterials. Biotechnol. Adv. 20, 91–100. https://doi.org/10.1016/S0734-9750(02)00003-4.

Zhao, F., Slade, R.C.T., Varcoe, J.R., 2009. Techniques for the study and development of microbial fuel cells: An electrochemical perspective. Chem. Soc. Rev. 38, 1926–1939. https://doi.org/10.1039/b819866g.

Zhao, Xiao Mei, Xia, Y., Whitesides, G.M., 1997. Soft lithographic methods for nano-fabrication. J. Mater. Chem. 7, 1069–1074. https://doi.org/10.1039/a700145b.

Zhou, K., Zhu, Y., Yang, X., Luo, J., Li, C., Luan, S., 2010. A novel hydrogen peroxide biosensor based on Au-graphene-HRP-chitosan biocomposites. Electrochim. Acta 55, 3055–3060. https://doi.org/10.1016/j.electacta.2010.01.035.

Zhou, X.H., Liu, L.H., Bai, X., Shi, H.C., 2013. A reduced graphene oxide based biosensor for high-sensitive detection of phenols in water samples. Sensors Actuators, B Chem. 181, 661–667. https://doi.org/10.1016/j.snb.2013.02.021.

Zhu, Z., Kin Tam, T., Sun, F., You, C., Zhang, Y.-H. P., 2014. A High- Energy-Density Sugar Biobattery Based on a Synthetic Enzymatic Pathway. Nat. Commun. 5, 3026.

Zhu, Z., Wang, Y., Minteer, S. D., Zhang, Y.-H. P., 2011. Maltodextrin-Powered Enzymatic Fuel Cell through a Non-Natural Enzymatic Pathway. J. Power Sources 196, 7505−7509.

Zlateva T, Boteva R, Filippi B, Veenhuis M, van der Klei IJ .,2001, Deflavination of flavor- oxidases by nucleophilic reagents. Biochim Biophys Acta 1548, 213-219.

Zloczewska, A., Celebanska, A., Szot, K., Tomaszewska, D., Opallo, M., Jönsson-Niedziolka, M., 2014. Self-powered biosensor for ascorbic acid with a Prussian blue electrochromic display. Biosens. Bioelectron. 54, 455–461. https://doi.org/10.1016/j.bios.2013.11.033.

List of Publications and Award

Patents filed:

1. Pranab Goswami, **Priyanki Das,** Mallesh Santhosh, Phurpa Dema Thungon (**2016**). Title of the invention: Graphite paste ink with silk sericin for enhancing the conductivity and stability. Patent No. 348844 / Application No. 201631022633 / Patentee: Prof. Pranab Goswami (**Granted and published**).

2. Pranab Goswami, **Priyanki Das,** Lepakshi Barbora, Arup Dutta, Mrinal Kumar Sarma (2019) Title of the invention: Enzymatic Biofuel Cell. Application No. 201931046354.

Published International Journal Articles:

1. **Priyanki Das**, Lepakshi Barbora, Madhuri Das, Pranab Goswami*, Highly sensitive and stable laccase based amperometric biosensor developed on nano-composite matrix for detecting pyrocatechol in environmental samples. ***Sensors & Actuators B. Chemical*** 192,737-744 (2014).

2. **Priyanki Das**, Madhuri Das, Somasekhar R. Chinnadayyala, Irom Manoj Singha, Pranab Goswami***,*** Recent advances on developing 3rd generation enzyme electrode for biosensor applications, ***Biosensors and Bioelectronics*** 79, 386-397 (2016).

3. **Priyanki Das**, Vinay Bachu, Lepakshi Barbora, Arup Dutta, Mrinal Kumar Sarma and Pranab Goswami*, Passive fuel delivery and efficient anoxic condition in anode improve performance of methanol biofuel cell, ***Applied Energy*** 305, 117824-117834 (2022).

4. **Priyanki Das**, Mallesh Santhosh and Pranab Goswami, Enzyme electrodes prepared by sericin induced-crystalline graphite based conductive ink for sensing methanol through Microfluidic biofuelcell (communicated).

5. Madhuri Das, Lepakshi Barbora, **Priyanki Das**, Pranab Goswami***,*** Biofuel cell for generating power from methanol substrate using alcohol oxidase bioanode and air-breathed laccase biocathode, ***Biosensors and Bioelectronics*** 59,184–191 (2014).

6. Arup Dutta, Caraline Ann Jacob, **Priyanki Das**, Eduardo Corton, Devard Stom, Lepakshi Barbora, Pranab Goswami, A review on power management systems: An electronic tool to enable Microbial Fuel Cells for powering range of electronic appliances, ***Journal of Power Sources*** (accepted).

Book Chapter:

1. Pooja Rani Kuri*, **Priyanki Das*** and Pranab Goswami, Fundamentals of Biosensors; in Advanced Materials and Techniques for Biosensors and Bioanalytical Applications; Edited by Pranab Goswami, CRC Press, Taylor & Francis Group, 2021 (***equal first author contribution**).

Award:

1. **Fourth prize** in Guwahati Biotech Park's **Talent Search Contest 2021** for research proposal entitled "Alcohol biofuel cell, a simple enzymatic biofuel cell device using alcohol as fuel for powering small scale electronic appliances" on 6th March 2021 organized jointly by Assam Science Society and Guwahati Biotech Park.

2. **Best Poster award** during National Conference on "**Technologies shaping the future of Energy scenario and its impact in North East**" organized by SECONE at NEDFI Convention Centre, Guwahati, Assam, India, on 1st February, 2020.

Conference/workshop Proceedings:

1. Madhuri Das, Lepakshi Barbora, **Priyanki Das**, Pranab Goswami*, Development of laccase based biocathode for biofuel cell application, The 18th International Conference (POST ISCBC-2012) IASST Guwahati, Assam, India, January 28-30, 2012, Abstract page no. 246.

2. **Priyanki Das**, Madhuri Das, Lepakshi Barbora Pranab Goswami*, Power generation from alcohol biofuel cell utilizing alcohol oxidase and laccase as biocatalysts, Frontier Energy

Research with Industry Academia partnership (FERIAP 2015) organized by Centre for Energy, Indian Institute of Technology Guwahati, March 20th – 21th 2015.

3. **Priyanki Das**, Pranab Goswami*, Fuel cell based methanol biosensor using biocompatible graphite conductive ink on paper surface, IUMRS-International Conference of Young Researchers on Advanced Materials (IUMRS-ICYRAM 2016) organized by Materials Research Society of India (MRSI) and Indian Institute of Science Bangalore, held at Indian Institute of Science Bangalore, India, during 11th -15th December 2016. Conference proceeding page No. 128.

4. **Priyanki Das**, Pranab Goswami, Silk Sericin for enhancing the conductivity and stability of graphite paste ink, "International conference on Sophisticated Instruments in Modern Research" (ICSIMR) organized by Central Instruments Facility, Indian Institute of Technology Guwahati, held at IIT Guwahati, during 30th June-1st July 2017.

5. **Priyanki Das**, Pranab Goswami, Development of membrane less biofuel cell on paper substrate for rapid, reliable and low cost detection of alcohol, 5th Bioprocessing India Conference held at IIT Guwahati, India during 9th December to 11th December, 2017.

6. **Priyanki Das** and Pranab Goswami, A Paper based small sized alcohol biofuel cell for powering micro-scale electronic devices, National conference on waste to Energy conversion (NCWEC-2018) organized by NIT Mizoram, Aizawl, Mizoram, India, December 28th-29th, 2018.

7. **Priyanki Das**, Lepakshi Barbora, Arup Dutta, Pranab Goswami* Enzymatic alcohol biofuel cell for powering small scale electronic appliances, conference on "Technologies shaping the future of Energy scenario and its impact in North East" organized by SECONE, Synergy for Energy held at NEDFI Convention Centre, Guwahati, on 1st February, 2020.

Front Page of the Papers and Book chapter Published in International Journals and Book

Applied Energy 305 (2022) 117824

Contents lists available at ScienceDirect

Applied Energy

journal homepage: www.elsevier.com/locate/apenergy

Passive fuel delivery and efficient anoxic condition in anode improve performance of methanol biofuel cell

Priyanki Das [a], Vinay Bachu [b], Lepakshi Barbora [a], Arup Dutta [a], Mrinal Kumar Sarma [a], Pranab Goswami [b,*]

[a] School of Energy Science and Technology, Indian Institute of Technology Guwahati, Guwahati 781039, Assam, India
[b] Department of Biosciences and Bioengineering, Indian Institute of Technology Guwahati, Guwahati 781039, Assam, India

HIGHLIGHTS

- An enzymatic biofuel cell with passive delivery system for methanol fuel developed.
- The control fuel delivery with sealing O_2 contact to anode improved the performance.
- A record operational stability and coulombic efficiency gained with the stacked cells.
- The high stability and efficiency greatly contributed to its scope of applications.

GRAPHICAL ABSTRACT

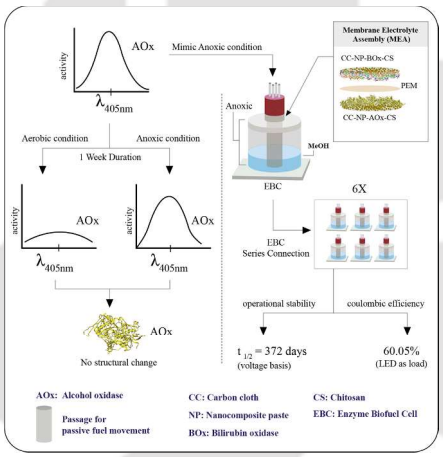

ARTICLE INFO

Keywords:
Alcohol oxidase
Bilirubin oxidase
Enzymatic biofuel cell
Magnetic nanoparticle
Methanol
Self –pumping

ABSTRACT

The operational stability, power efficiency, and technical simplicity of enzymatic biofuel cells are the focus area of research for practical applications of this green energy-generating device. Here, we report some critical findings on these issues on a methanol-fuelled pure biofuel cell fabricated by using alcohol oxidase and bilirubin oxidase as anodic and cathodic catalysts, respectively. The cell was fabricated with a new design strategy comprising efficient anoxic condition in the anodic chamber, adequate airflow to the cathode for enhancing oxygen reduction reactions, and a passive fuel pumping facility to the anode. A magnetic nanoparticle-based bio-nanocomposite matrix on the carbon-cloth electrode offered as a biocompatible enzyme immobilization matrix for harvesting electrons in the cell through the direct electron transfer mechanism as validated by cyclic voltammetry. Six units of the cells, when connected in a series, the device's potential increased to 4.3-fold (3.1 V) and rested at a stable state under a load with a half-life of ~ 372 days and a coulombic efficiency of 60%. This high operational stability has been attributed to the efficient anoxic setup in the anodic chamber that supported the stability of alcohol oxidase, the activity of which was intact even after 49 days of the operation. This work

* Corresponding author.
E-mail address: pgoswami@iitg.ac.in (P. Goswami).

https://doi.org/10.1016/j.apenergy.2021.117824
Received 25 February 2021; Received in revised form 4 September 2021; Accepted 6 September 2021
Available online 14 September 2021

Biosensors and Bioelectronics 79 (2016) 386–397

Contents lists available at ScienceDirect

Biosensors and Bioelectronics

journal homepage: www.elsevier.com/locate/bios

Recent advances on developing 3rd generation enzyme electrode for biosensor applications

Priyanki Das [a], Madhuri Das [a], Somasekhar R. Chinnadayyala [b], Irom Manoj Singha [a], Pranab Goswami [b,*]

[a] Centre For Energy, Indian Institute of Technology Guwahati, Guwahati 781039, Assam, India
[b] Department of Biosciences and Bioengineering, Indian Institute of Technology Guwahati, Guwahati 781039, Assam, India

ARTICLE INFO

Article history:
Received 16 September 2015
Received in revised form
17 December 2015
Accepted 18 December 2015
Available online 19 December 2015

Keywords:
Direct electrochemistry
Enzyme electrode
3rd generation biosensors
Protein film voltammetry
Cyclic voltammetry
Electron transfer rate constant

ABSTRACT

The electrochemical biosensor with enzyme as biorecognition element is traditionally pursued as an attractive research topic owing to their high commercial perspective in healthcare and environmental sectors. The research interest on the subject is sharply increased since the beginning of 21st century primarily, due to the concomitant increase in knowledge in the field of material science. The remarkable effects of many advance materials such as, conductive polymers and nanomaterials, were acknowledged in the developing efficient 3rd generation enzyme bioelectrodes which offer superior selectivity, sensitivity, reagent less detection, and label free fabrication of biosensors. The present review article compiles the major knowledge surfaced on the subject since its inception incorporating the key review and experimental papers published during the last decade which extensively cover the development on the redox enzyme based 3rd generation electrochemical biosensors. The tenet involved in the function of these direct electrochemistry based enzyme electrodes, their characterizations and various strategies reported so far for their development such as, nanofabrication, polymer based and reconstitution approaches are elucidated. In addition, the possible challenges and the future prospects in the development of efficient biosensors following this direct electrochemistry based principle are discussed. A comparative account on the design strategies and critical performance factors involved in the 3rd generation biosensors among some selected prominent works published on the subject during last decade have also been included in a tabular form for ready reference to the readers.

Contents

1. Introduction . . . 387
2. Principles on 3rd generation biosensor . . . 387
3. Characterization of the 3rd generation biosensor . . . 388
4. Fabrication strategies and applications of the 3rd generation biosensor . . . 389
   4.1. Nanofabrication of electrode . . . 389
   4.2. Polymer based approach . . . 391
   4.3. Self-assembled approach . . . 391
   4.4. Reconstitution based approach . . . 392
5. Problems and challenges for developing 3rd generation biosensors . . . 393
6. Conclusion and future perspectives for developing 3rd generation biosensors . . . 396
Acknowledgments . . . 396
References . . . 396

* Corresponding author. Tel.: +91 361 2582202; fax: +91 361 2582249.
E-mail address: pgoswami@iitg.ernet.in (P. Goswami).

http://dx.doi.org/10.1016/j.bios.2015.12.055
0956-5663/

Sensors and Actuators B 192 (2014) 737–744

Contents lists available at ScienceDirect

Sensors and Actuators B: Chemical

journal homepage: www.elsevier.com/locate/snb

Highly sensitive and stable laccase based amperometric biosensor developed on nano-composite matrix for detecting pyrocatechol in environmental samples

Priyanki Das [a], Lepakshi Barbora [a], Madhuri Das [a], Pranab Goswami [b,*]

[a] Centre for Energy, Indian Institute of Technology Guwahati, Guwahati 781039, Assam, India
[b] Department of Biotechnology, Indian Institute of Technology Guwahati, Guwahati 781039, Assam, India

ARTICLE INFO

Article history:
Received 4 July 2013
Received in revised form
19 September 2013
Accepted 7 November 2013
Available online 22 November 2013

Keywords:
Biosensor
Pyrocatechol
Laccase
Nanocomposite matrix
Multiwalled carbon nanotube
Osmium tetroxide

ABSTRACT

The present study aims at fabricating a laccase based amperometric biosensor for detection of pyrocatechol in environmental samples. *Trametes versicolor* laccase was co-immobilized in a nanocomposite matrix comprising of osmium tetroxide on poly 4-vinylpyridine, multiwalled carbon nanotubes, Nafion and carbon black on glassy carbon electrode. The nanocomposite matrix provides a porous structure for easy immobilization of the enzyme as evident from the SEM images and a highly electroactive surface for facile diffusion free electron transfer kinetics as discerned from the cyclic voltametric studies. The heterogeneous electron transfer rate constant (K_s) and surface concentration of the ionic species (Γ) of the bioelectrode were 0.67 s^{-1} and 1.32×10^{-8} mol cm^{-2}, respectively. The response of the constructed biosensor was generated at a potential of 0.14 V from the electrocatalyzed reduction of 1,2-benzoquinone formed from the biocatalyzed oxidation of pyrocatechol. The bioelectrode when subjected to differential pulse voltammetry exhibited a linear faradaic current response against pyrocatechol in the concentration range of 3.98 nM–16.71 nM with a minimum detection limit of 2.82 nM and a sensitivity of 3.82 ± 0.31 nA nM^{-1}. The bioelectrode also shows high operational stability and optimum storage stability up to 3 weeks. The nanocomposite based fabrication method of the laccase bioelectrode thus shows a great promise for developing a highly sensitive, selective and stable biosensor for detection of pyrocatechol in environmental samples.

1. Introduction

Phenolic compounds are widely used in large scale manufacturing of resins, plastics, pesticides, explosives, detergents and pharmaceutical products. These compounds are frequently leached out during their production, transportation and utilization, which pollute the environment. Besides, certain phenols have been reported to be genotoxic, mutagenic, and hepatotoxic [1,2]. Amongst these, pyrocatechol or catechol (1,2-dihydroxybenzene) is a potential phenolic compound of concern, as it reacts with different biomolecules, like DNA, protein, membranes and leads to their non repairable damage [3]. Additionally, pyrocatechol in combination with heavy metals (e.g. Cu^{2+}, Fe^{3+}) and in presence of molecular oxygen can cause breakage of DNA strands [4]. Again, many of these compounds are highly resistant to biotic and abiotic degradation and therefore, remain in the environment at toxic levels. Thus, there is a continuously increasing demand for selective and sensitive detection of these phenolic compounds for evaluating their toxicity in environmental samples. Apart from the classical method of Folin–Ciocalteau, many analytical methods based on spectrophotometry [5], chemical, and gas chromatographic principles [6] have been developed for the detection of pyrocatechol. Although some of these methods are highly sensitive and reliable, they are relatively difficult and often need derivatization and pre-concentration steps. Such disadvantages could be overcome by using biosensor devices for fast, specific, accurate and highly sensitive detection of pyrocatechol in real samples [7–9].

Over the past decade, many biosensors have been developed using redox enzymes, such as tyrosinase, peroxidase, laccase as biorecognition elements for the detection of phenolic compounds [10]. Laccase biosensors have unique merits over tyrosinase biosensors in having high sensitivity and high stability [11]. It also has more advantage over peroxidases as biorecognition element, since the background current from hydrogen peroxide limits the sensitivity of peroxidase biosensor [12]. Laccase (EC 1.10.3.2) a multicopper redox enzyme, widely occurring in fungi and less frequently in higher plants and bacteria [13], have been identified as a potential catalyst for the determination of phenolic compounds [14].

* Corresponding author. Tel.: +91 361 2582202; fax: +91 361 2582249.
E-mail address: pgoswami@iitg.ernet.in (P. Goswami).

0925-4005/$ – see front matter © 2013 Elsevier B.V. All rights reserved.
http://dx.doi.org/10.1016/j.snb.2013.11.021

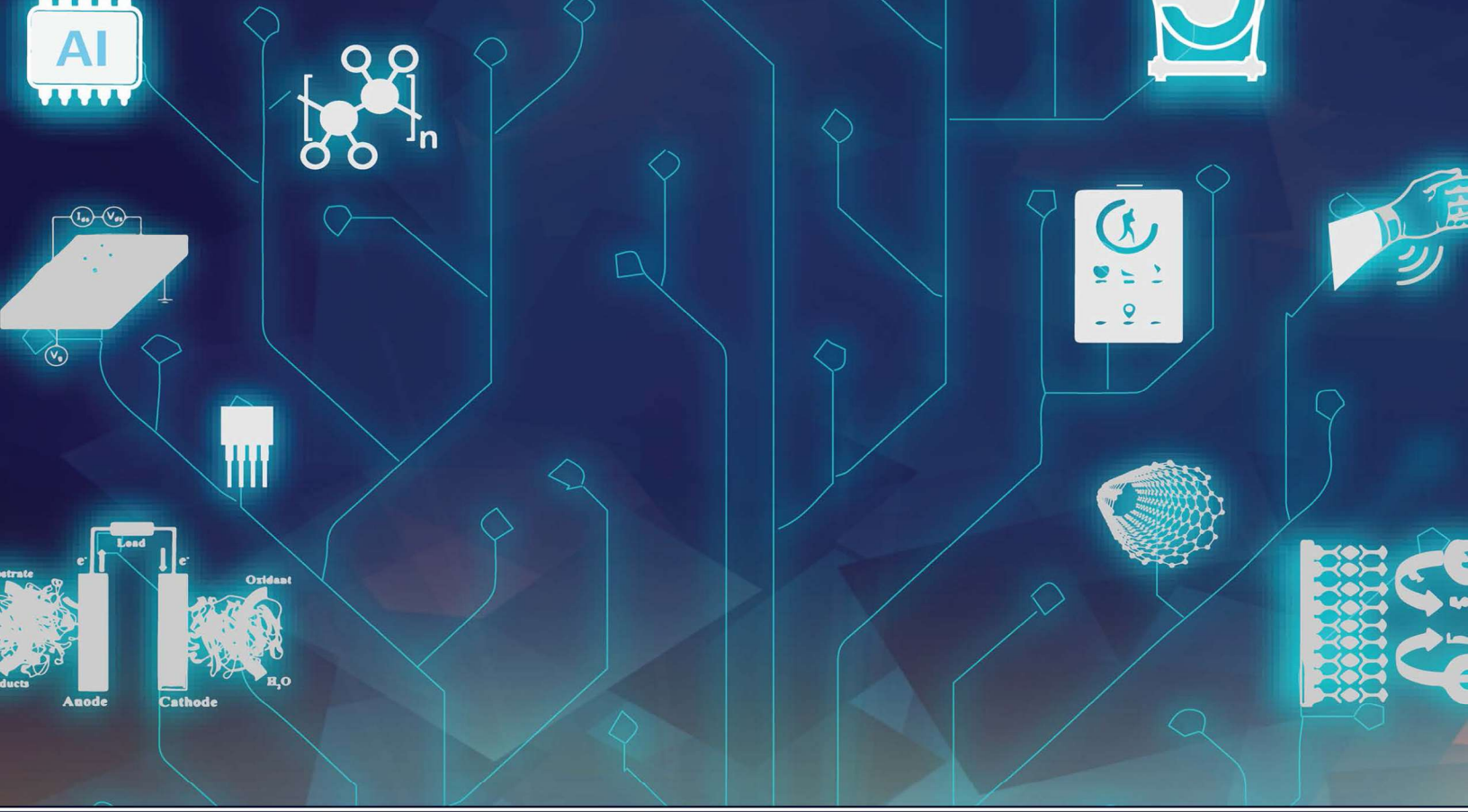

ADVANCED MATERIALS AND TECHNIQUES FOR BIOSENSORS AND BIOANALYTICAL APPLICATIONS

EDITED BY
PRANAB GOSWAMI

CRC Press
Taylor & Francis Group

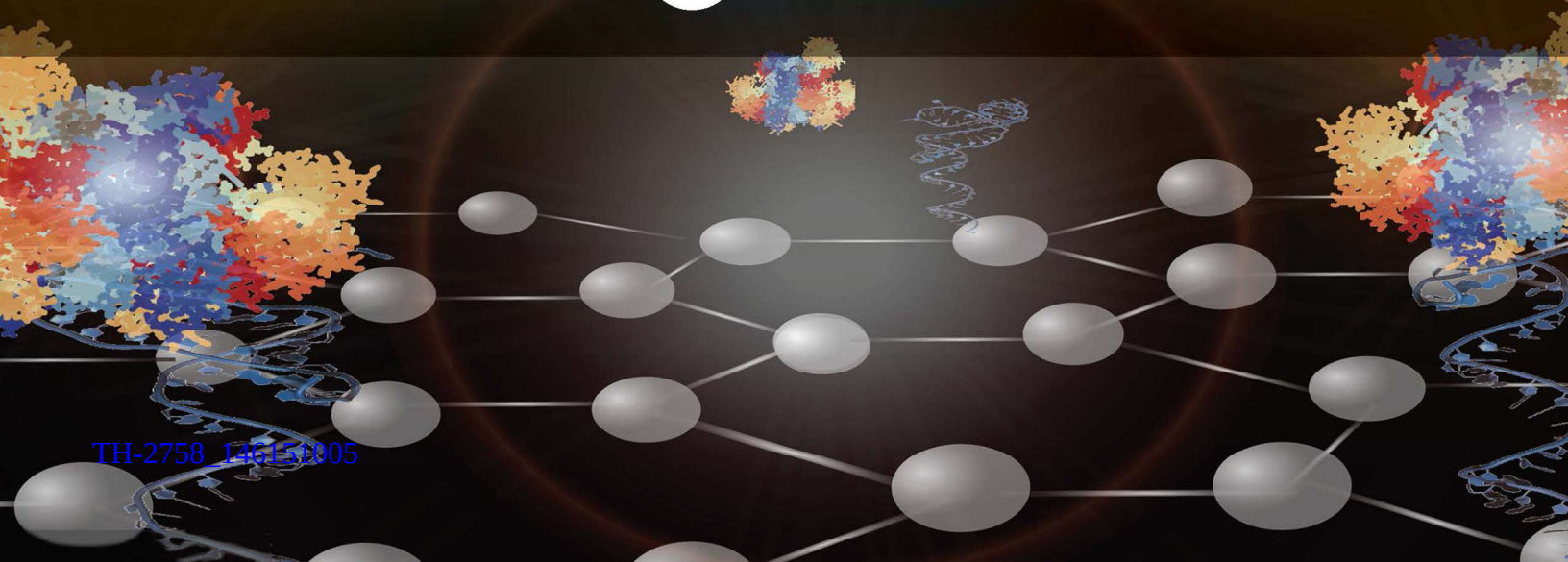

1 Fundamentals of Biosensors

Pooja Rani Kuri, Priyanki Das* and Pranab Goswami*
Indian Institute of Technology Guwahati, Assam, India (* equal contribution)

CONTENTS

1.1 Introduction to Biosensors 2
1.1.1 History of Biosensors 2
1.2 General Configuration of a Biosensor 3
1.3 Characteristics/Salient Features of a Biosensor 3
1.3.1 Selectivity 3
1.3.2 Sensitivity 3
1.3.3 Reproducibility 4
1.3.4 Stability 4
1.3.5 Response Time 4
1.3.6 Recovery Time 4
1.3.7 Linearity and Dynamic Range 4
1.3.8 Effect of Physical Parameters 4
1.3.9 Additional Factors 4
1.4 Classification of Biosensors 5
1.4.1 Classification of Biosensors Based on the Biorecognition Principle 5
1.4.2 Classification of Biosensors Based on the Biorecognition Element 5
1.4.2.1 Enzyme-Based Biosensors 5
1.4.2.2 Immunosensors 6
1.4.2.3 Nucleic Acid/DNA Biosensors 6
1.4.2.4 Cell-Based Biosensors 7
1.4.2.5 Biomimetic-Based Biosensors 7
1.4.3 Classification of Biosensors Based on the Transducer Elements 7
1.4.3.1 Electrochemical Biosensors 7
1.4.3.2 Optical Biosensors 12
1.4.3.3 Calorimetric Biosensors 16
1.4.3.4 Piezoelectric Biosensors 17
1.5 Bioreceptor Immobilization Strategies 18
1.5.1 Adsorption 18
1.5.2 Covalent Binding 19
1.5.3 Entrapment 20
1.5.4 Crosslinking 20
1.5.5 Affinity 20
1.6 Application of Biosensors 21
1.6.1 Application in the Food Industry 21
1.6.2 Application in the Fermentation Industry 21
1.6.3 Biomedical Applications 21
1.6.4 Environmental Applications 21
1.6.5 Applications in Biodefense 22
1.7 Recent Advances in Biosensor Technology 22
1.7.1 Wearable Biosensors 22
1.7.2 Implantable Biosensors 23
1.7.3 Engineered Enzymes for Biosensor Development 24
1.8 Market Potential for Biosensors 24
References 25

Copyright Permissions

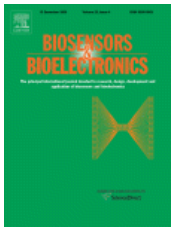

Paper electrodes for bioelectrochemistry: Biosensors and biofuel cells

Author: Cloé Desmet,Christophe A. Marquette,Loïc J. Blum,Bastien Doumèche

Publication: Biosensors and Bioelectronics

Publisher: Elsevier

Date: 15 February 2016

Order Completed

Thank you for your order.

This Agreement between Mrs. PRIYANKI DAS ("You") and Elsevier ("Elsevier") consists of your license details and the terms and conditions provided by Elsevier and Copyright Clearance Center.

Your confirmation email will contain your order number for future reference.

License Number	5065100911936
License date	May 09, 2021

Printable Details

Licensed Content

Licensed Content Publisher	Elsevier
Licensed Content Publication	Biosensors and Bioelectronics
Licensed Content Title	Paper electrodes for bioelectrochemistry: Biosensors and biofuel cells
Licensed Content Author	Cloé Desmet,Christophe A. Marquette,Loïc J. Blum,Bastien Doumèche
Licensed Content Date	Feb 15, 2016
Licensed Content Volume	76
Licensed Content Issue	n/a
Licensed Content Pages	19
Journal Type	S&T

Order Details

Type of Use	reuse in a thesis/dissertation
Portion	figures/tables/illustrations
Number of figures/tables/illustrations	1
Format	both print and electronic
Are you the author of this Elsevier article?	No
Will you be translating?	No

About Your Work

Title	Development of Small Scale Alcohol Biofuel Cells using Enzymes as Catalyst
Institution name	Indian Institute of Technology Guwahati
Expected presentation date	Jul 2021

Additional Data

Portions	Figure 3

TH-2758_146151005

Requestor Location

Mrs. PRIYANKI DAS
CENTRE FOR ENERGY, IIT GUWAHATI

Requestor Location

GUWAHATI, 781039
India
Attn: Mrs. PRIYANKI DAS

Tax Details

Publisher Tax ID GB 494 6272 12

Price

Total 0.00 USD

Total: 0.00 USD

CLOSE WINDOW ORDER MORE

TH-2758_146151005

Tackling the Challenges of Enzymatic (Bio)Fuel Cells

Author: Xinxin Xiao, Hong-qi Xia, Ranran Wu, et al
Publication: Chemical Reviews
Publisher: American Chemical Society
Date: Aug 1, 2019

PERMISSION/LICENSE IS GRANTED FOR YOUR ORDER AT NO CHARGE

This type of permission/license, instead of the standard Terms & Conditions, is sent to you because no fee is being charged for your order. Please note the following:

- Permission is granted for your request in both print and electronic formats, and translations.
- If figures and/or tables were requested, they may be adapted or used in part.
- Please print this page for your records and send a copy of it to your publisher/graduate school.
- Appropriate credit for the requested material should be given as follows: "Reprinted (adapted) with permission from (COMPLETE REFERENCE CITATION). Copyright (YEAR) American Chemical Society." Insert appropriate information in place of the capitalized words.
- One-time permission is granted only for the use specified in your request. No additional uses are granted (such as derivative works or other editions). For any other uses, please submit a new request.

If credit is given to another source for the material you requested, permission must be obtained from that source.

BACK CLOSE WINDOW

TH-2758_146151005